REFINEMENT OF INHIBITORY CIRCUITS DURING DEVELOPMENT OF THE MAMMALIAN AUDITORY BRAINSTEM

by

Gunsoo Kim

BS, Seoul National University, 1994

MS, Seoul National University, 1999

Submitted to the Graduate Faculty of

School of Medicine in partial fulfillment

of the requirements for the degree of

Doctor of Philosophy

University of Pittsburgh

2004

UNIVERSITY OF PITTSBURGH

SCHOOL OF MEDICINE

This dissertation was presented

by

Gunsoo Kim

It was defended on

November 30, 2004

and approved by

Committee Chair: Daniel J. Simons, Ph.D.

Elias Aizenman, Ph.D.

Guo-Qiang Bi, Ph.D.

Stephen D. Meriney, Ph.D.

Laurence O. Trussell, Ph.D.

Thesis Advisor: Karl Kandler, Ph.D.

REFINEMENT OF INHIBITORY CIRCUITS DURING DEVELOPMENT OF THE MAMMALIAN AUDITORY BRAINSTEM

Gunsoo Kim, Ph.D.

University of Pittsburgh, 2004

Establishing precise neuronal connections is crucial for normal brain function. In many parts of the brain, this is accomplished by refining initially diffuse neuronal connections during development. In contrast to our understanding of the mechanisms by which excitatory connections are refined, the refinement of inhibitory circuits is poorly understood.

In this thesis, I investigated the refinement of inhibitory connections in the lateral superior olive (LSO), a mammalian auditory brainstem nucleus involved in sound localization. The glycinergic, and during development also GABAergic, projection from the medial nucleus of the trapezoid body (MNTB) to the LSO is tonotopically organized with a single-cell-level precision in adults. I asked whether and by what mechanisms the precise organization emerges during development.

I found that the refinement of this inhibitory pathway is achieved by a large degree of functional elimination of exuberant inputs and strengthening of maintained inputs. Elimination of inputs occurred in a frequency-specific manner, resulting in a sharper inhibitory topography. The topographic refinement occurred while the MNTB inputs act excitatory, raising the possibility that depolarizing action of GABA and glycine is a mechanism underlying the rearrangement of inhibitory synaptic connections. In parallel with the elimination, synaptic responses elicited by the maintained MNTB inputs increased over 10-fold. This was due to a moderate increase in quantal size and a large increase in the number of release sites formed by each MNTB fiber.

I further investigated whether olivocochlear efferent neurons that project from the brainstem back to the cochlea play a role in the topographic sharpening. I found that the

refinement of the MNTB-LSO pathway is impaired in animals with compromised efferent projections. In both efferent-lesioned rats and mice lacking the α9 nicotinic acetylcholine receptor subunit, LSO neurons received a greater number of weak MNTB inputs than in control animals. These results indicate that normal olivocochlear efferent projections are necessary for the refinement of the MNTB-LSO pathway. I discuss the possibility that the effect of efferent manipulation could be due to altered levels or temporal patterns of spontaneous activity before hearing onset.

TABLE OF CONTENTS

LIST OF FIGURES

1. INTRODUCTION

1.1 OVERVIEW

Establishing precise neuronal circuitry is a prerequisite for normal brain function. In many parts of the brain, this is accomplished by refining initially diffuse neuronal connections during development (Purves and Lichtman, 1985; Hubel and Wiesel, 1977; Katz and Shatz, 1996). Over the past decades, much has been learned about the general principles underlying the refinement of excitatory synaptic connections (Lichtman and Colman, 2000; Katz and Shatz, 1996). Inhibition is equally important for normal brain function, and a growing body of evidence indicates that inhibition is critical not only for maintaining network stability, but also for plasticity of synaptic circuitry and information coding (Huang et al., 1999; Hensch et al., 1998; Brand et al., 2002). Despite the importance of inhibition, the question as to how precise inhibitory circuits are established in the developing brain is poorly understood. This is largely because inhibitory connections are typically intrinsic to local circuitry and lack the clear spatial organization of many internuclear or interlaminar pathways.

In this thesis, I investigated this question using a topographically organized inhibitory pathway found in a sound localization system. I found that the refinement of this inhibitory pathway is accomplished, with a remarkable similarity to excitatory systems, through elimination of exuberant inputs and strengthening of maintained ones. This elimination of inputs occurred in a frequency-specific manner, resulting in a sharpening of the topographic organization of this pathway. Furthermore, I found evidence that implicates early spontaneous activity in this refinement process.

1.2 REFINEMENT OF EXCITATORY CIRCUITRY THROUGH ACTIVITY-DEPENDENT COMPETITION

At early stages of neural development, neurons send out axons to their appropriate target regions under the guidance of various molecular cues. Once growing axons arrived at their target area they begin to form relatively crude functional connections. These initial connections undergo substantial synaptic rearrangements during development, which result in precise, mature neuronal circuitry. In many parts of the nervous system, elimination of exuberant inputs is a key process of developmental refinement, and this elimination is thought to occur via activity-dependent competition among inputs (Lichtman and Colman, 2000).

Activity-dependent competition has been especially well-studied in the primary visual cortex, where thalamic axon terminals carrying visual inputs from the two eyes segregate and form alternating bands, so-called ocular dominance stripes or columns (Hubel and Wiesel, 1977). Using extracellular recordings in kittens, Hubel and Wiesel (1963) found that if one eye is deprived of visual input, the number of neurons that respond to stimulation of the previously deprived eye dramatically decreased while neurons driven exclusively by the open eye increased. Transneuronal tracing of thalamic axons using intravitreal injection of radioactive amino acids revealed that the size of the bands in the cortex occupied by the thalamic afferents representing the deprived eye decreases while that for the other eye expands (Hubel et al., 1977; LeVay et al., 1978; LeVay, et al., 1980). These changes after monocular deprivation seem to be mediated by "neuronal competition," because closing both eyes had little effect on either the anatomical or functional organization of ocular dominance columns (Wiesel and Hubel, 1965). This phenomenon of ocular dominance plasticity occurred only during a restricted, "critical," developmental period. Together, observations gave rise to the idea that during development, presynaptic axons compete for the innervation of postsynaptic neuron in an activity-dependent manner.

Subsequently, studies at the neuromuscular junction (NMJ) provided more detailed insights into the cellular mechanisms of synapse elimination (Lichtman and Colman, 2000). In rodents, at birth each muscle fiber is innervated by multiple motor neuron axons. During the first 3 weeks of postnatal life, all except one of the initial inputs become eliminated and the winning axon elaborates its synaptic contact with the its postsynaptic muscle fiber. As a result, the

number of synaptic contacts within an endplate actually increases while the number of presynaptic axons innervating a given muscle fiber decreases. The observation that only one axon ends up taking over the entire NMJ suggested that there is a competition among the presynaptic inputs. Consistent with this idea, a reduced level of activity slowed the transition from multiple to single innervation of a muscle fiber, whereas an increased level of activity sped up the transition, indicating that neuronal activity can modulate the refinement process (Purves and Lichtman, 1980). In addition, focal blockade of synaptic transmission in a small region of an NMJ led to the weakening and subsequently withdrawal of the axons whose synaptic contacts were blocked (Balice-Gordon and Lichtman, 1994). Recent experiments using genetically engineered mice in which only a small subset of motor neurons are fluorescently labeled allowed researches to perform *in-vivo* long-term observation of the anatomical changes that occur at competing axon terminals. These studies revealed that the competition occurs locally (i.e., different branches of the single motor neuron in different region of the muscle can be either winners or losers), and axon branches from motor neurons with more extensive axonal branches had a competitive disadvantage as if each of their terminals had less resources for competition (Kasthuri and Lichtman, 2003). Indeed, axon branches of motor neurons in which production of neurotransmitter is genetically reduced had a clear disadvantage in the competition and, perhaps as a result of this, became eliminated (Buffelli et al., 2003). These findings provide compelling evidence that the postsynaptic target favors and selects inputs that are more efficient in driving the postsynaptic targets.

Although these studies have provided evidence that synaptic refinement occurs through activity-dependent competition, all were performed by blocking or reducing electrical activity. Therefore, these results could mean that a certain threshold level of activity is required to read pre-determined molecular cues rather than a genuine competition through activity in which the relatively more active inputs outcompete the weaker ones (‘permissive’ vs ‘instructive’ role of activity). The important question of whether neuronal activity can instructively guide the outcome of the competition has been recently addressed at the retinogeniculate synapse (Stellwagen and Shatz, 2002).

In the lateral geniculate nucleus (LGN), axonal branches of retinal ganglion cells of the two eyes are intermingled at early stages of development but then gradually segregate to form the eye-specific layers (Shatz, 1996). This segregation of inputs from the two eyes occurs before

vision, but still requires activity. In the immature retina, spontaneous bursts of action potentials among neighboring retinal ganglion cells are found to travel across the retina before the onset of vision ("retinal waves") (Meister et al., 1991; Wong et al., 1993). Blockade of this spontaneous activity prevents the formation of eye-specific layers, and blockade of activity of one eye shrinks the layer formed by the eye while the layer formed by the other active eye expands. Most importantly, in a more recent set of experiments, Stellwagen and Shatz increased the frequency of retinal waves by injecting drugs that elevated cAMP, which was shown to regulate spatiotemporal patterns of retinal waves (Stellwagen et al., 1999; Stellwagen and Shatz, 2002). They found that the LGN layer formed by the eye with more frequent retinal waves enlarged while the layer formed by the unmanipulated eye, despite its *normal* level of activity, became smaller. On the contrary, when the frequency of retinal waves was elevated in both eyes, both layers stayed normal. This result demonstrates that relative levels of activity among competing inputs can determine the outcome of the synaptic refinement.

Taken together, activity-dependent competition among presynaptic inputs has emerged as a central rule in the refinement of excitatory synapses. Stronger or more active inputs that can more efficiently drive the postsynaptic target gain advantage in establishing synaptic connections with the target cell, whereas weaker or less active inputs become weaker and eventually become eliminated.

However, while such competition-mediated refinement is a well-established mechanism for organizing excitatory synaptic circuits, very little is known about how developing inhibitory circuits are organized. What are the rules underlying the establishment of precise inhibitory connections? Do inhibitory connections start out with diffuse connectivity and the inputs compete in an activity-dependent manner? Do stronger inhibitory inputs that hyperpolarize the target cell more have a competitive advantage? In my thesis, I investigated the refinement of inhibitory connections as a first step towards answering these important questions.

1.3 NEURONAL ACTIVITY AND THE MODIFICATION OF INHIBITORY SYNAPSES

Evidence from a number of neuronal systems indicates that synaptic inhibition can be regulated by neuronal activity. Deprivation of vision decreases GABA immunoreactivity in the primary visual cortex (Hendry and Jones, 1988; Benevento et al., 1995). In the rodent barrel cortex, continuous trimming of whiskers from birth markedly reduces the number of GABAergic synapses and the GABA synthesizing enzyme glutamic acid decarboxylase (GAD) (Akhtar and Land, 1991; Micheva and Beaulieu, 1995, but see also Land et al., 1995 for a somewhat different result), whereas selective stimulation of a single whisker increases the number of GABAergic synapses in the corresponding barrel (Knott et al., 2002). In addition, activity-dependent, long-lasting changes in synaptic efficacy such as LTP and LTD have been observed in GABAergic synapses, and the molecular mechanisms underlying these changes are being actively investigated (Kano, 1995; Korn et al., 1992; Otis et al., 1994; Kittler and Mose, 2003; Woodin et al., 2002).

A growing body of evidence indicates that spontaneous or experience-elicited neuronal activity strongly influences the maturation of inhibitory synaptic transmission. In cultured neonatal cortical neurons, activity blockade weakens GABAergic synapses by a reduction in synaptic $GABA_A$ receptor number (Rutherford et al., 1997; Kilman et al., 2002). In the primary visual cortex, dark rearing during the critical period of ocular dominance plasticity prevented normal strengthening of GABAergic inputs that converge on individual cortical neurons (Morales et al., 2002). Finally, in the superior colliculus, chronic stimulation of the NMDA-type of glutamate receptors accelerated the maturation of inhibitory synaptic transmission (Aamodt et al., 2000).

There is also accumulating evidence that neuronal activity can modify the number of inhibitory synapses during development. In organotypic cultures of neonatal hippocampus, blockade of either GABAergic or glutamatergic synaptic transmission reduced the number of GABAergic synapses (Marty et al., 2000). In congenitally deaf mice (dn/dn), in which cochlear hair cells degenerate from birth on, miniature IPSCs measured around hearing onset were smaller in amplitude but significantly more frequent than in normal mice (Leao et al., 2003). In immature hippocampus, repeated application of depolarizing pulses induced long-lasting changes in

frequency of spontaneous GABAergic inputs, perhaps by activating 'silent' synapses, and this phenomenon was observed only during the first postnatal week (Guibellini et al., 2001). In summary, these data indicate that the number of inhibitory synapses is sensitive to the ongoing level of activity and can be dynamically regulated during development.

Recently, in the gerbil auditory brainstem, an experience-dependent, subcelluar redistribution of glycinergic synapses has been observed (Kapfer et al., 2002). Before hearing onset, neurons in the medial superior olive (MSO) receive a high density of glycinergic inputs onto the dendrites as well as the soma. In ~3 week old animals, however, glycinergic synapses are found primarily on the somata of MSO neurons, indicating that the synapses on the dendrites have been eliminated during development. This redistribution of glycinergic synapses was prevented by unilateral cochlear ablation and reduced by rearing animals in omnidirectional noise. Thus, it appears that subcellular reorganization of inhibitory synapses can also be regulated by neuronal activity.

The above examples illustrate that developing inhibitory synaptic connections are plastic and can be regulated by neuronal activity. However, most studies focused on changes of the overall levels of inhibition or of inhibitory synapses within a single cell without addressing how these changes affect the synaptic organization of a specific inhibitory network. How the dynamic properties of developing inhibitory synapses are operating in a defined functional inhibitory network has remained unclear. This is largely due to the fact that in most parts of the nervous system inhibitory neurons are local interneurons that lack clear spatial organization. Moreover, inhibitory interneurons come in many different types with diverse morphology and physiological characteristics, which makes it difficult to investigate how these circuits emerge during development and how they are regulated by activity (McBain and Fisahn, 2001; Maccaferri and Lacaille, 2003). To overcome these obstacles, I took advantage of an organized inhibitory pathway in which a homogeneous population of inhibitory neurons gives rise to a topographically organized pathway.

1.4 THE MNTB-LSO PATHWAY

The lateral superior olive (LSO) is one of the first binaural nuclei in the ascending auditory pathway. Neurons in the LSO compare the sound stimulus intensities at two ears and can encode the azimuthal location of a high frequency sound source (**Figure 1.1**). Neurons in the LSO receive excitatory, glutamatergic inputs from the ipsilateral cochlear nucleus (CN) and inhibitory, glycinergic inputs from the medial nucleus of the trapezoid body (MNTB). The MNTB conveys information from the contralateral CN to the LSO via powerful calyceal synapses. The projections from the MNTB to the LSO are tonotopically organized such that there is a gradual gradient of frequency representation from the low frequency lateral region to high frequency medial region (Friauf, 1992; Muller, 1990). The tonotopic organization is precise in that the ipsi- and contralateral inputs representing the same frequency converge onto a single LSO neuron (Sanes and Rubel, 1988).

Intracellular recordings in fetal rat LSO neurons demonstrated that both glutamatergic and glycinergic projections have formed functional synapses as early as at embryonic day 20 (E20) (Kandler and Friauf, 1995b). Synaptic transmission from the MNTB in young animals is partly mediated by GABA; this GABAergic response is replaced by glycine over the first three postnatal weeks (Kotak et al, 1998). Recent evidence suggests that this neurotransmitter switch may be occurring at the level of individual synaptic vesicles (Nabekura et al., 2004). Intracellular recordings from the LSO neurons at early stages of development with electrical stimulation of MNTB fibers revealed that MNTB inputs depolarized LSO neurons. Depolarizing MNTB responses gradually switch to hyperpolarizing responses and after postnatal day (P) 8, virtually

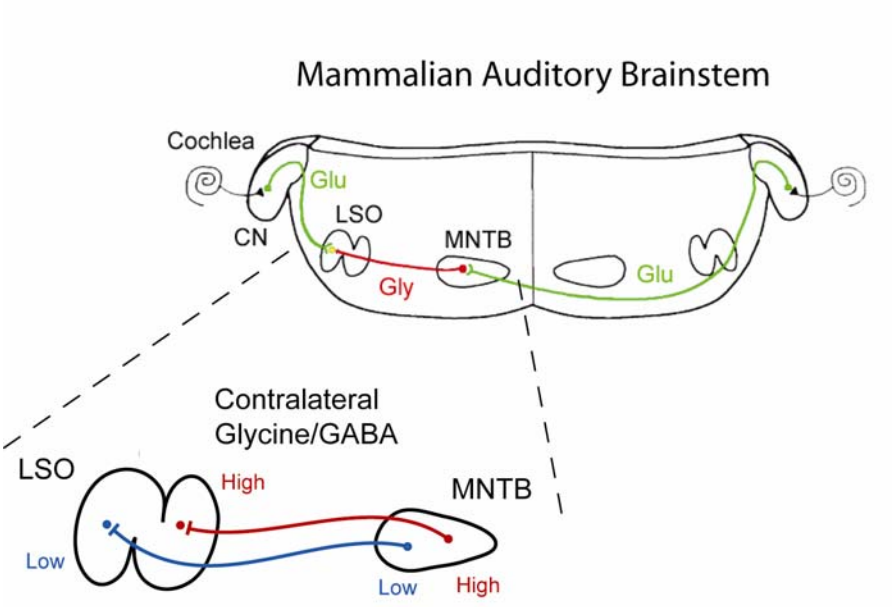

Figure 1.1 Schematic illustration of the LSO circuit. The LSO receives excitatory, glutamatergic afferents from the ipsilateral cochlear nucleus (CN) and inhibitory, glycinergic afferents from the medial nucleus of the trapezoid body (MNTB). The MNTB is innervated by the contralateral CN and, in neonatal animals, MNTB inputs also release GABA. Both inputs converge onto single LSO neurons in a precise tonotopic manner. MNTB neurons that encode low acoustic frequencies project to lateral parts of the LSO while high frequency axon terminals terminate in medial parts.

all of the MNTB responses were hyperpolarizing (Kandler and Friauf, 1995b). It has been shown that the depolarization induced by GABA and glycine is due to higher levels of intracellular Cl^- in immature LSO neurons (Ehrlich et al., 1999; Kakazu et al., 1999). The depolarizing GABA/glycinergic inputs can act as excitatory inputs because they can elevate the level of intracellular Ca^{2+} via activation of voltage-gated Ca^{2+} channels, independently from the glutamatergic inputs, and can elicit spikes in LSO neurons (Kullmann and Kandler, 2001; Kullmann et al., 2002). It has been suggested that the depolarizing GABAergic and glycinergic inputs exert a trophic effect on the dendritic arborization of LSO neurons through elevation of intracellular Ca^{2+} (Sanes and Friauf, 2000), or that they are involved in the development of the MNTB-LSO tonotopy (Kandler et al., 2002), but their role in LSO development remains to be determined.

The precise tonotopic organization of the MNTB-LSO pathway provides an opportunity to study the developmental refinement of inhibitory connections. Sanes and colleagues have shown that the axonal arbors of MNTB neurons are diffuse and occupy a relatively large area in the LSO in immature animals. Around P21, however, MNTB axon terminals are confined within a narrow frequency region in the LSO (Sanes and Siverls, 1991). The degree of refinement was the greatest in the medial part of the LSO, which corresponds to the high frequency region. This structural refinement seems to require normal neuronal activity from the cochlea because the developmental pruning of the aberrant branches or their stabilization was prevented when the cochlea contralateral to the MNTB was ablated (Sanes and Takacs, 1993). Similar to the refinement of MNTB axon terminals, the dendrites of LSO neurons also undergo a refinement; the dendritic field is wider in younger animals, and by ~P21 LSO dendrites are restricted to a narrow region along the frequency axis (Sanes and Chokshi, 1992; Rietzel and Friauf, 1998). This structural refinement of LSO dendrites was impaired in animals with unilateral cochlear ablation (at P7) as well as in the animals raised with systemic strychnine administration or in organotypic cultures incubated in strychnine (Sanes et al., 1992; Sanes and Chokshi, 1992; Sanes and Hafidi, 1996). These results suggest that the topographic sharpening of MNTB axon terminals and LSO dendrites requires normal neuronal activity. Both structural refinement processes occur primarily during the third postnatal week and there is no sign of pruning during the first postnatal week. Based on these observations, Sanes and Friauf proposed that the period

of depolarizing MNTB inputs is important for dendritic and axonal growth, whereas substantial refinement occurs during the hyperpolarizing period (Sanes and Friauf, 2000).

Long-term changes in synaptic efficacy are considered to be involved in the activity-dependent refinement of synaptic circuits (Katz and Shatz, 1996). Consistent with this, long-term depression (LTD) has also been shown in the MNTB-LSO pathway and it has been suggested to represent a cellular mechanism of MNTB-LSO refinement (Kotak and Sanes, 2000). LTD at hyperpolarizing MNTB-LSO synapses was induced by low frequency stimulation (1 Hz) and required the elevation of postsynaptic intracellular Ca^{2+}. The LTD was expressed postsynaptically and was mediated by activation of $GABA_B$ and Trk receptors (Kotak et al., 2001; Chang et al., 2003). LTD was developmentally regulated: The size of LTD was greater in P7-12 LSO neurons than in P17-19 neurons. Sanes and his colleagues argued that this long lasting change in synaptic efficacy may underlie the synaptic rearrangement in the MNTB-LSO pathway.

Taken together, there is considerable evidence that the GABA and glycinergic connections from the MNTB to LSO undergo a significant structural refinement during the first three weeks of postnatal development. Moreover, normal levels or patterns of spontaneous or sound-evoked activity seem to be necessary for this refinement process. Anatomical changes in axonal arbor and dendritic trees, however, do not necessarily correspond to changes in functional synaptic connections, and a direct demonstration that these apparent anatomical changes indeed represent modifications in functional connectivity is lacking. The observed impairments of refinement by manipulations that presumably interfere with normal activity could be due to the requirement of activity for general viability of the system (Lohmann et al., 1998), rather than a specific role of activity in constructing precise neuronal connections. If the level or spatiotemporal patterns of activity can indeed be transformed into specific connectivity patterns, potentially through competition among inputs, the diffuse MNTB inputs must first form functional synapses before the elimination process occurs.

In this thesis I addressed the question of whether the refinement of the MNBT-LSO pathway is accomplished by elimination of functional GABA/glycinergic synapses and what synaptic changes may accompany these processes. I also investigated the question as to whether these functional changes are influenced by spontaneous neuronal activity.

2. ELIMINATION AND STRENGTHENING OF GLYCINERGIC/GABAERGIC CONNECTIONS DURING TONOTOPIC MAP FORMATION

2.1 INTRODUCTION

Elimination and strengthening of excitatory synaptic connections by spontaneous or experience-evoked neuronal activity are critical steps in the developmental organization and fine-tuning of neuronal circuits (Purves and Lichtman, 1985; Lichtman and Colman, 2000; Goodman and Shatz, 1993; Jackson and Parks, 1982; Chen and Regehr, 2000; Stellwagen and Shatz, 2002; Hubel et al., 1977). However, direct evidence for the involvement of synapse elimination/strengthening in the formation of organized inhibitory circuits has remained largely elusive. Most cellular mechanisms and models thought to mediate synaptic plasticity and reorganization depend on the depolarizing and spike-eliciting effects of excitatory synapses, effects that generally are not associated with inhibitory synapses.

Compared with the clear organization that is present in topographically organized excitatory pathways, the detailed anatomical organization of most inhibitory circuits is obscure. In most brain areas, inhibition is generated by local inhibitory networks, which are composed of anatomically and functionally distinct local interneurons. This organization represents a major obstacle for specific experimental manipulation and the developmental analysis of inhibitory circuits. Thus, despite accumulating evidence for plasticity and developmental changes in global levels of inhibition (Kilman et al., 2002; Rico et al., 2002; Hendry ad Jones, 1986) and its further influence on excitatory plasticity (Hensch et al., 1998; Huang et al., 1999; Rozas et al., 2001) interpretation of these changes at the level of specific inhibitory connections has been difficult.

To date, perhaps the best evidence in support of spatial fine-tuning of inhibitory networks comes from studies of the developing auditory system (Knudsen, 2002; Kapfer et al., 2002; Sanes and Friauf, 2000). In mammals, evidence from two sound localization circuits has

demonstrated the presence of specific reorganization of inhibitory connectivity. In the medial superior olive of gerbils, anatomical analysis shows an activity-dependent cellular redistribution of glycinergic synapses, a process that is thought to be important for processing interaural time differences in this species (Kapfer et al., 2002). In the lateral superior olive (LSO), pruning of immature glycinergic/GABAergic axon terminals and refinement of LSO dendrites support the hypothesis that elimination of inhibitory synapses sharpens inhibitory connectivity (Rietzel and Friauf, 1998; Sanes and Siverls, 1991). It remains unclear, however, whether and to what degree these anatomical changes reflect the reorganization of an operative inhibitory network, rather than the structural elimination of exuberant (and perhaps non-functional) immature synaptic contacts or axonal processes.

Here I investigated the emergence of a precisely organized inhibitory circuit by analyzing functional connectivity and synaptic properties of MNTB-LSO connections in developing rats before hearing onset. Neurons in the MNTB are glycinergic in adult animals and glycinergic/GABAergic during development (Sanes and Friauf, 2000; Kotal et al., 1998), and give rise to a purely inhibitory and precisely tonotopically organized pathway to the LSO (**Figure 2.1**; Sanes and Siverls, 1991; Boudreau and Tsuchitani, 1968). The MNTB-LSO pathway carries auditory information from the contralateral cochlea. The frequency-specific alignment of this inhibitory pathway with excitatory inputs from the ipsilateral cochlea provides the neuronal basis for encoding the interaural intensity differences used for sound localization. My results indicate that the establishment of the functional topography of the MNTB-LSO pathway is accomplished by extensive, but specific, elimination of functional glycinergic/GABAergic synapses and by an increase in the synaptic conductance elicited by maintained connections. Notably, functional elimination of MNTB-LSO connections takes place while these connections are excitatory, lending support to the hypothesis that the transient excitatory action of immature inhibitory synapses is an important mechanism for organizing the development of inhibitory circuits.

2.2 METHODS

2.2.1 Animals and slice preparation

All experiments used slices from neonatal rats (P1-P14; Sprague-Dawley, Charles River Laboratories, Wilmington, MA). Experimental procedures were in accordance with NIH guidelines and were approved by the IACUC at the University of Pittsburgh. Rats were anesthetized by hypothermia (P1-P4) or isoflurane (P5-P14) before decapitation. Coronal slices (300-400 μm) were cut at 8-15 °C on a vibrating microtome (DTK-1500E, Ted Pella, Redding, CA, USA). Slices containing both the LSO and the MNTB were selected and allowed to recover in an interface-type chamber under 95%O_2/5%CO_2 atmosphere for 1~2 hours at RT (23°C) before recording. For slice preparation and incubation, 1 mM kynurenic acid was present in the ACSF (composition in mM: NaCl 124, $NaHCO_3$ 26, Glucose 10, KCl 5, KH_2PO_4 1.25, $MgSO_4$ 1.3, $CaCl_2$ 2, pH = 7.4 when bubbled with 95% O_2/5% CO_2). For recordings, slices were transferred to a submerged-type chamber and superfused with oxygenated ACSF at RT at a rate of ~3-4ml/min.

2.2.2 Electrophysiology

Whole-cell patch-clamp recordings were obtained from visualized principal-type LSO neurons (Olympus BX50, equipped with infrared contrast system, Luigs & Neumann, Ratingen, Germany, and CCD camera) identified by their bipolar morphology under IR illumination and post-hoc determination of their soma-dendritic structure. Location and morphology of neurons was confirmed by filling neurons with biocytin (0.5% in pipette solution) and post-hoc visualization with standard techniques (ABC kit, Vector). For reconstruction of axon terminals of MNTB neurons, neurons were filled for 30 min and given additional 2 h for transport of biocytin before fixation. Recordings were obtained from the medial part of the LSO, which corresponds to the tonotopic high-frequency region (Friauf, 1992). Mapping experiments were conducted in current clamp. Patch electrodes (5-6 MΩ) were filled with solution containing (in mM): 54 K-gluconate, 56 KCl, 1 $MgCl_2$, 1 $CaCl_2$, 5 Na_2-phosphocreatine, 10 Hepes, 11 EGTA, 0.3 Na-GTP, 2 Mg-ATP, 5 QX314, 0.5% biocytin (pH 7.2, 280 mOsm/l). The calculated reversal potential for

Cl^--mediated PSPs (E_{Cl}) was –20 mV. During mapping, the cell was held at –70 mV by manually adjusting the holding current. Amplitudes of postsynaptic potentials varied widely between cells, even in the same age group, perhaps due to the large differences in input resistance of immature LSO neurons (Kandler and Friauf, 1995a). Minimum stimulation data indicated that single input-evoked synaptic responses had amplitudes > 10 pA. Given the input resistance (measured by applying 10-30 pA negative current pulses) of LSO neurons of >> 100 MΩ (P1-P4: 751.7 ± 112.0 MΩ, n = 11; P11-P14: 214.8 ± 33.8 MΩ, n = 14) single fibers should elicit PSPs of > 1 mV, which is well above my detection threshold. Recordings were corrected for a liquid junction potential of –7 mV. Input resistance was monitored throughout the recording. Data were filtered at 1kHz (Bessel filter, Axoclamp 1D), digitized at 5kHz with an A/D board (National Instruments, Inc) and stored on a computer using custom-written Labview 5.0 software (National Instruments, Austin, Texas).

Recording in electrical stimulation experiments were made in voltage-clamp using patch electrodes (3-4 MΩ, coated with epoxy, Elementis Performance Polymers, NJ) filled with solution containing (in mM): 54 D-gluconic acid, 54 CsOH, 1 $MgCl_2$, 1 $CaCl_2$, 10 Hepes, 11 EGTA, 0.3 Na-GTP, 2 Mg-ATP, 5 QX314, 0.5% biocytin (pH 7.2, 280 mOsm/l). In some experiments, the pipette solution additionally contained 0.1 mM D600 (Sigma), an L-type calcium channel antagonist. Series resistance of 5-20 MΩ was compensated by 70-90% (Axopatch 1D) and was continuously monitored throughout recordings. The MNTB-LSO fiber bundle was stimulated by positioning a low resistance patch electrode (~2 MΩ, filled with ACSF) at the lateral end of the MNTB. Electrical stimuli were delivered at a rate of 0.033-0.067 Hz (Master 8 and Isoflex, AMPI, Israel).

For some experiments, cells were held at +30 mV (**Figure 2.8**). In these cells the quality of voltage control was confirmed by the presence of linear current-voltage relationships (r = 0.98) for synaptic current and average reversal potentials of –14.8 ± 0.76 mV (n = 4) close to the theoretical value (-20 mV). Analysis of electrophysiological data and statistical tests were performed with custom written Labview 5.0 and MatLab 6.0 (Mathworks) programs.

2.2.3 Functional mapping

The spatial distribution of presynaptic MNTB neurons was determined using focal photolysis of *p*-hydroxyphenacyl-glutamate ("caged glutamate", 150-200 μM). This approach can reveal the location of monosynaptically connected, presynaptic neurons with high spatial resolution as it avoids the stimulation of axons *en passant* (Callaway and Katz, 1993). The optical fiber for delivering UV-light (duration 50-100 ms; 100W mercury arc lamp) had a 20 μm diameter light-conducting core (Polymicro Technologies Inc, Phoenix, Az) that produced almost circular UV spots (diameter ~25 μm) on the surface of the slice. For mapping, the microscopic objective was switched to 4x, and 80-100 locations spaced ~45 μm apart, in and around the MNTB, were stimulated. To minimize variability in light spot size and uncaging resolution, at each location, the fiber was carefully lowered until it slightly touched the surface of the slice (**Figure 2.1b**). The location of the light spot on the slice was monitored with a CCD camera and guided by a grid placed on the video monitor. Grid size was ~45 μm, and the same grid was used in all experiments. Accuracy of fiber placement was estimated to be ~ ±10 μm. The location of each recorded neuron and each MNTB stimulation site were recorded with a frame grabber (Scion Corp.). Consistency of input maps was confirmed by rescanning in about half of the cases. Only one map was obtained per MNTB.

Spatial resolution of uncaging was determined by recording responses of MNTB neurons in current clamp. "Spike-eliciting distance" to an MNTB cell body was measured between the recording electrode tip and a line drawn between the farthest spike-eliciting light spot and the first subthreshold spot. While mapping subthreshold stimulation areas, the ability of the recorded neurons to generate spikes was confirmed by injecting suprathreshold positive currents after testing each stimulation site.

2.2.4 Construction and analysis of MNTB-LSO input maps

For each map, stimulation sites were marked by circles aligned to the center of each uncaging site, indicated by the position of the green light spot on the slice on digitized video frames (Adobe Photoshop; **Figure 2.1c** and **2.2**). Peak PSP amplitudes of corresponding PSPs elicited from each site were determined. For each LSO neuron, peak amplitudes were normalized to the

largest response and were color coded (**Figure 2.2**). Each successful stimulation site was assigned a filled circle (diameter ~50 μm), and the total area covered by all circles marking successful stimulation sites was defined as input area.

To normalize input areas to MNTB cross-sectional areas, MNTB boundaries were determined by three investigators (two of them were blind to the actual data) using video images taken from the slice. MNTB areas determined by the three independent observers were in close agreement (coefficient of variation, 9%), and the mean area was used for normalizing input maps. The width of input maps along the mediolateral axis (tonotopic axis in the MNTB) was determined by measuring the width of each horizontal row of stimulation sites and calculating the mean width of all rows. For normalization, the largest mediolateral width of the oval-shaped MNTB was used.

2.2.5 Calcium imaging

Slices were prepared from P2 rats and bulk-labeled with Fura-2 AM following standard protocols (Kullmann et al., 2002). Changes in intracellular calcium concentrations were measured using 340/380 nm ratio-imaging on an inverted microscope (Nikon Eclipse TE200) with a 10x objective (NA: 0.5) (Kullmann et al., 2002). The MNTB was stimulated electrically with bipolar stimulation electrodes (two pulses at 30 μA in A and 40 μA in B, 0.1 ms duration, separated by 20 ms). To increase spike activity and increase the detection of calcium responses, 10 mM TEA was included in the perfusion medium. Ionotropic glutamate receptors were blocked by CNQX (20 μM) and D,L-APV (100 μM) to isolate glycinergic/GABAergic calcium responses. Stimulus-induced calcium responses were detected by subtracting the ratio-image immediately taken before electrical stimulation from the first ratio-image taken after MNTB-stimulation. The resulting Δratio-image was smoothed by a 3 x 3 Gaussian filter (Adobe Photoshop), thresholded, and overlaid onto the corresponding bright-field image. To map the entire superior olivary complex, 4-6 areas in the superior olivary complex were sequentially imaged and assembled using the corresponding bright-filed images for orientation. At each position, responses to two stimulus trials were measured and all responses were overlaid over the composite image.

2.2.6 Stimulus–response relation experiments

During stimulus-response experiments, responses were considered to be maximal if further increase in stimulus intensities led to a decline in response amplitudes or if the responses remained unchanged over about 100 μA. The maximal stimulus intensities tested were 506.7 μA ± 35.8 at P1-P5 (n = 16) and 304.2 μA ± 48.4 at P9-P14 (n = 18). The lower values in older animals most likely reflect the lower thresholds of MNTB fibers at this age (intensities necessary for eliciting responses with >50% failure rates were 42.1 μA ± 5.5 at P9–P14, n = 19 vs. 60.4 μA ± 11.7 at P1–P5, n = 23). In additional experiments, I tested whether the lower stimulus intensities in P9-P14 animals indeed were sufficient to stimulate all intact connections. In 13 LSO neurons from P9-P14 animals, stimulation intensities were increased up to 1,000 μA. The maximum current elicited with these high stimulus intensities was 5.0 nA ± 0.56 nA (n = 13), which is very similar to the average current elicited during the stimulus response experiments (4.5 nA, P = 0.51, Student's ttest). In 4 cells, I further increased stimulus intensity to 2,000 μA and in no case did this elicit an additional increase in response amplitudes.

2.2.7 Minimal stimulation

Electrical stimulus intensity was adjusted to give a failure rate of > 50% (10-60 μA). At this intensity, 100-300 responses were evoked at 0.03-0.1 Hz. Identification of successful responses and failures was performed off-line by eye. Only responses that had latencies that fell within a 1 ms window were accepted, and the mean peak amplitude of those selected minimal PSCs was taken as the size of single-fiber inputs for the cell. As minimal stimulation cannot distinguish whether a given failure is due to a failure in neurotransmitter release or a failure in fiber excitation, all failures were excluded when calculating mean peak amplitudes. Therefore, at all ages, estimated single-fiber response amplitudes are probably biased toward higher values.

2.2.8 Cluster analysis

To achieve an objective estimate of the number of steps present in the stimulus-response curves, cluster analysis was used on PSC peak amplitudes (partitioning around medoids; S-Plus 2000,

MathSoft). This method uses an optimization algorithm in which a sum of dissimilarities is minimized through iterations of grouping. Numbers of suspected clusters for each sequence of iterations were assigned values from 1 to 25. After clustering, an optimal number of clusters was chosen by calculating the silhouette index (Kaufman and Rousseeuw, 1990). In neurons from neonatal animals, any number of potential clusters tested resulted in an equally low silhouette index, indicating the absence of identifiable clusters.

2.2.9 Statistical test

Student's t-tests and Kolmogorov-Smirnov tests were used. Data are expressed as mean ± standard error of the mean throughout the text.

2.3 RESULTS

Whole-cell patch-clamp recordings were obtained from visually identified principal neurons of the LSO in brainstem slices (**Figure 2.1**; Rietzel and Friauf, 1998; Helfert and Schwartz, 1986). To determine the spatial distribution of presynaptic MNTB neurons, 80-120 discrete locations spaced ~50 μm apart were stimulated in the MNTB using focal photolysis of caged glutamate (**Figure 2.1b** and **c**; Kandler et al., 1998). Detection of weak glycinergic/GABAergic connections was enhanced by increasing the driving force for Cl^- to about 50 mV while blocking postsynaptic action potentials (5 mM QX 314 in the pipette solution). Under these conditions, stimulation of glycinergic/GABAergic MNTB neurons evoked depolarizing postsynaptic potentials (PSPs, **Figure 2.1b**, inset) or inward postsynaptic currents (PSCs). Consistent with the glycinergic/GABAergic nature of the immature MNTB-LSO pathway (Kotak et al., 1998; Kullman et al., 2002), synaptic responses were abolished by bicuculline (10 μM) and strychnine (10 μM). At all ages, the reversal potential of MNTB-evoked responses was about –20 mV, close to the calculated value of the Cl^- reversal potential.

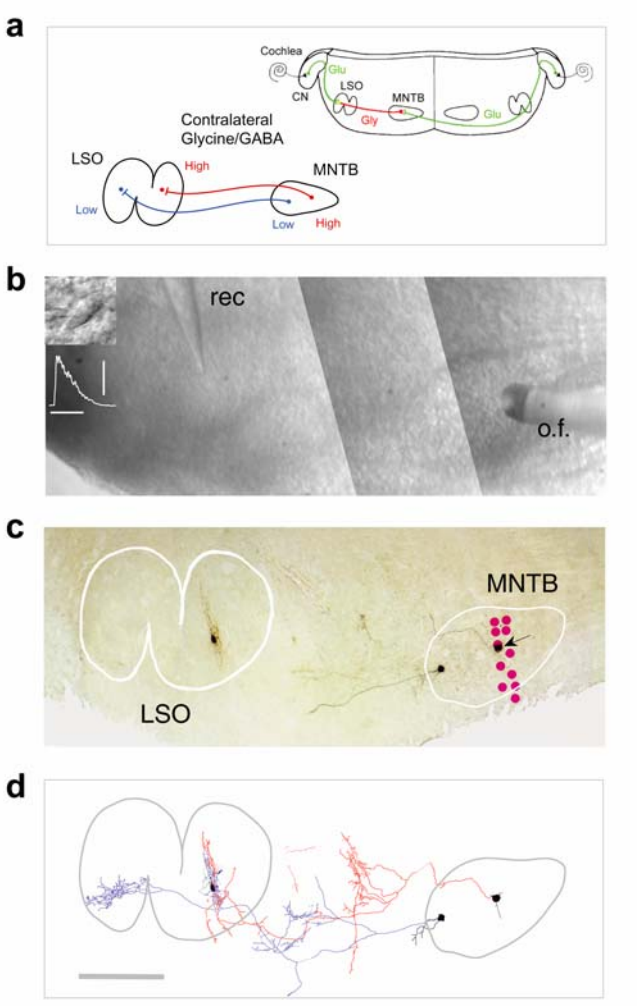
a
Cochlea
Glu
CN
LSO
MNTB
Gly
Glu
Contralateral
Glycine/GABA
LSO
High
MNTB
Low
Low
High
b
rec
o.f.
c
MNTB
LSO
d

Figure 2.1

Figure 2.1. Focal photolysis of caged glutamate in auditory brainstem slices reveals functional GABAergic/glycinergic connections in the MNTB-LSO pathway.

(**a**) Illustration of afferent connections to the lateral superior olive (LSO). In adult animals, both inputs converge on single LSO neurons in a presice tonotopic manner. The tonotopic organization of the MNTB-LSO pathway is shown in the enlargement. (**b**) Montage of video images taken during a mapping experiment. The recording electrode (rec) is positioned in the medial limb of the LSO, and the movable optical fiber (o.f.) is positioned above the MNTB. Photo inset shows an IR-image of a typical of LSO neuron with elongated cell body and two emerging primary dendrites. The trace inset shows a synaptic response elicited by uncaging glutamate in the MNTB of a P11 animal (flash duration 100 ms, indicated by horizontal bar). Vertical scale bar, 10 mV. (**c**) The location and morphology of the recorded LSO neuron in (**b**) is revealed by biocytin staining. Red circles in the MNTB mark uncaging sites from which PSPs could be elicited in the LSO neuron. For clarity, non-responding sites in and around the MNTB are excluded. Two MNTB neurons were filled with biocytin: one within the input map (arrow) and the other outside the input map. (**d**) Camera-lucida drawing of biocytin-filled neurons. Notice the close overlap of axonal terminals from the MNTB neuron located inside the input map (red) with the recorded LSO neuron (green). Additional MNTB axon collaterals are visible in several other auditory nuclei. Scale bar, 200 μm.

glycinergic/GABAergic nature of the immature MNTB-LSO pathway (Kotak et al., 1998; Kullman et al., 2002), synaptic responses were abolished by bicuculline (10 μM) and strychnine (10 μM). At all ages, the reversal potential of MNTB-evoked responses was about –20 mV, close to the calculated value of the Cl^- reversal potential.

To confirm that functional MNTB-LSO connectivity, as indicated by uncaging glutamate, indeed reveals direct anatomical MNTB-LSO projections, MNTB neurons were filled with biocytin and their axonal termination pattern in the LSO was determined (n = 10; **Figure 2.1c** and **d**). MNTB neurons located inside the functionally connected area formed axon terminals that closely intermingled with the dendritic tree of the postsynaptic LSO neuron. In contrast, axon terminals of the MNTB neurons residing in nonresponsive areas were completely segregated from the dendritic trees of recorded LSO neurons (**Figure 2.1d**, blue). Together, these results support the suitability of my approach to reveal functional MNTB-LSO connectivity (see also 2.3.1 below).

2.3.1 Spatial refinement of MNTB-LSO connectivity

To examine the development of spatial organization of functional MNTB-LSO connectivity, I determined MNTB-LSO input maps to individual LSO neurons in rats at P1 to P14. In all neonatal animals, PSPs could be elicited from a large number of MNTB sites that gave rise to wide, dorsoventrally oriented input areas (30579 ± 1739 μm^2, n = 8, P1-4; **Figures 2.2a**, **b**, and **2.3a**). On average, these input areas covered about 36% of the corresponding MNTB cross sectional areas (35.6 ± 2.2%, n = 8; **Figure 2.3a-c**). Input maps were always contiguous, however, suggesting that at birth, MNTB-LSO connections already show some degree of topographical organization (Sanes and Siverls, 1991; Lohmann et al., 1998).

MNTB-LSO input areas from animals around hearing onset were markedly smaller than those from neonatal animals (10988 ± 1668 μm^2, n = 15, P11-14, $P < 0.05$, Student's t-test; **Figures 2.2c**, **d**, and **2.3a**), and gave rise to narrow, generally dorsoventrally oriented maps that on average covered about 8% of the corresponding MNTB areas (8.3 ± 1.3%, n = 15; P11-14, $P < 0.05$, Student's t-test; **Figure 2.3a-c**). Thus, during the first two postnatal weeks, normalized MNTB input areas decreased by about 75%. Elongated input maps observed around the time of

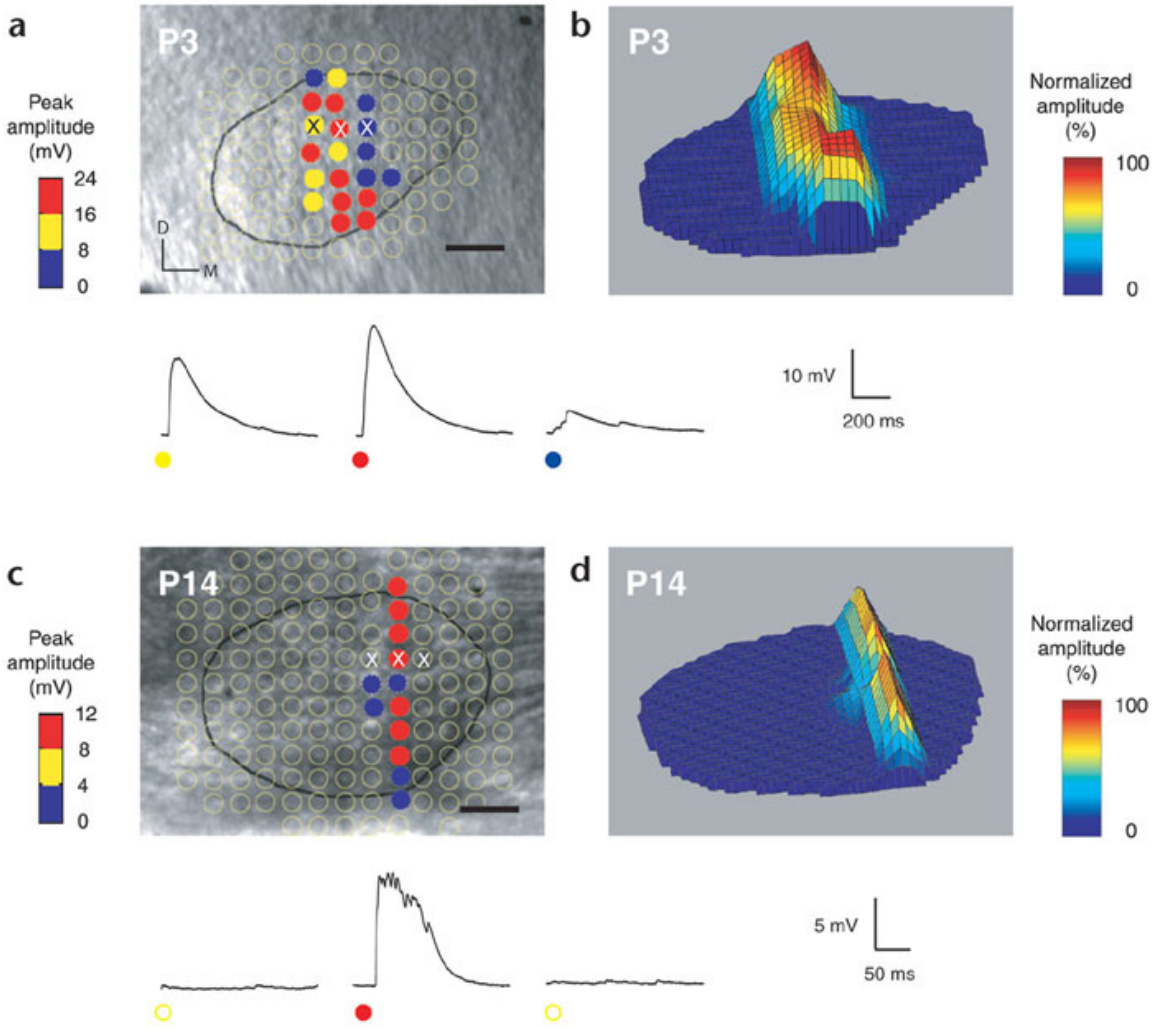

Figure 2.2. MNTB-LSO input maps from a P3 (**a**, **b**) and a P14 rats (**c**, **b**). (**a**) Location of unresponsive (open circles) and responsive (colored circles) stimulation sites are overlaid onto a video picture of the MNTB (outlined in black). Responsive areas are color-coded according to peak amplitudes of postsynaptic LSO responses. Examples of synaptic responses elicited from three locations (marked with x) are illustrated in the lower traces. (**b**) Interpolated 3-D plot of input areas. The size of the MNTB is scaled to match the size at P14 (**d**). (**c**, **d**) MNTB-LSO input map in a P14 rat. Scale bars in (**a**) and (**c**) are 100 µm.

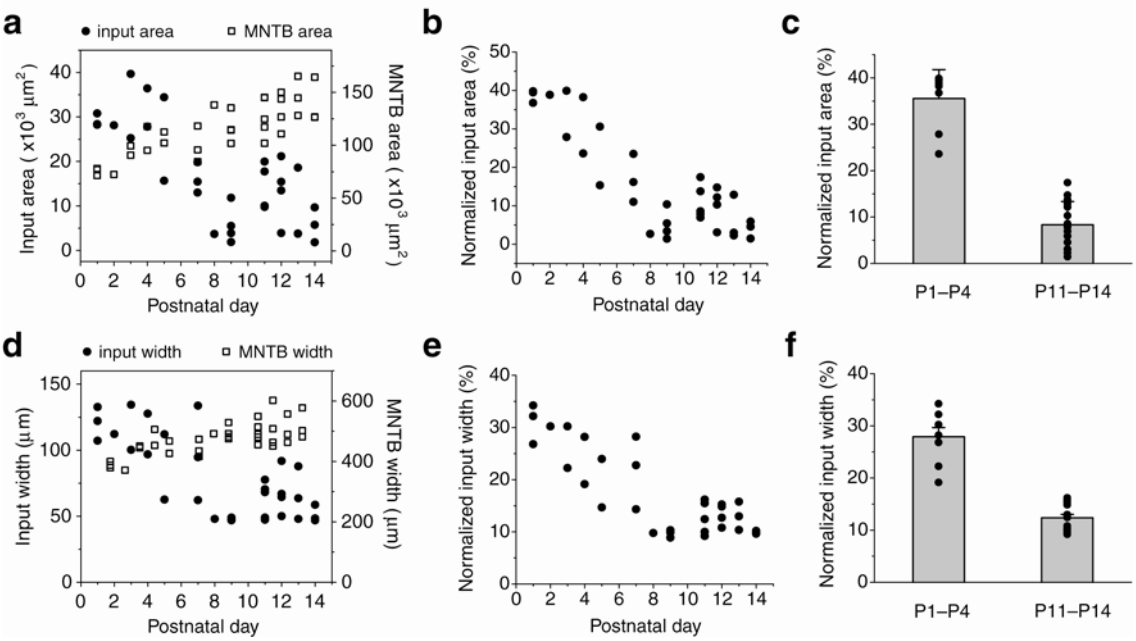

Figure 2.3. Age-dependent decrease in the size and width of MTNB-LSO input maps. (a-c) Age-dependent changes in input areas. (**a**) MNTB-LSO input areas (filled circles) and MNTB cross-sectional areas (open squares) as a function of age. (**b**) Input areas normalized to the corresponding MNTB cross-sectional area. (**c**) Normalized input areas in newborn and 2-week old animals (P1-4, n = 8; P11-14, n = 15; $P < 0.01$, Student's t-test). (**d-f**) Extent of input maps along the tonotopic axis in the MNTB (input width). (**d**) Absolute input width (filled circles) and mediolateral extension of the MNTB (open squares) as a function of age. (**e**) Input width normalized to corresponding MNTB width. (**f**) Normalized input width in newborn and 2-week-old animals (P1-4, n = 8; P11-14, n = 15; $P < 0.01$, Student's t-test).

hearing onset were oriented perpendicular to the mediolateral frequency axis in the MNTB (Friauf, 1992) and thus followed isofrequency contours (**Figure2. 2c** and **d**).

To quantify the sharpening of MNTB-LSO input maps in terms of refinement along the tonotopic axis, I measured the width of maps along the mediolateral MNTB axis (input width). During the first two postnatal weeks, absolute and MNTB-normalized input width decreased by about 50% (absolute width: P1-4, 113.7 ± 5.2 μm, n = 8; P11-14: 62.6 ± 3.8 μm, n = 15; $P < 0.05$, Student's t-test; normalized width: P1-4, 27.9%; P11-14, 12.4%; **Figure 2.3d-f**). Thus, spatial refinement of the MNTB-LSO pathway resulted in a two-fold sharpening of the topographic organization in the frequency domain, rather than a general reduction of connectivity over the entire map. This frequency-specific sharpening of functional MNTB-LSO connectivity occurred mainly between P3 and P8 and was essentially complete at P9, about 3-5 days before hearing onset (**Figure 2.3b** and **e**).

These conclusions depend on two premises: first, that uncaging glutamate at younger ages does not activate polysynaptic pathways from the MNTB to the LSO, and second, that the efficacy of uncaging glutamate remains constant from P1 to P14.

Three types of polysynaptic pathway are possible: 1) polysynaptic connections within the MNTB, 2) polysynaptic connections between the MNTB and LSO, and 3) polysynaptic connections within the LSO. Recurrent connections in the MNTB seem unlikely because, as shown in adult rats (Banks and Smith, 1992; Sommer et al., 1993), my labeled MNTB neurons in young animals never gave off recurrent collaterals in the MNTB (P1-4, n=8). In addition, in my uncaging-resolution experiments in the MNTB (**Figure 2.6** and see below), action potentials could only be elicited from stimulation sites very close the soma of recorded neurons but never from horizontally displaced sites. Thus, both anatomical and physiological data strongly argue against the possibility that recurrent, glycinergic/GABAergic connections in the MNTB are a source of polysynaptic MNTB-LSO connections that broadened the input maps in neonatal animals.

Next, to determine whether there are reliable relay stations between the MNTB and LSO, Ca^{2+} responses were recorded elicited by electrical stimulation of MNTB fibers in the superior olivary complex. MNTB stimulation elicited Ca^{2+} responses in neurons close to the simulation site and neurons in the LSO (**Figure 2.4**, P2, n = 2 slices). Outside the MNTB and LSO, however, very few Ca^{2+} responses were observed. These data are consistent with previous

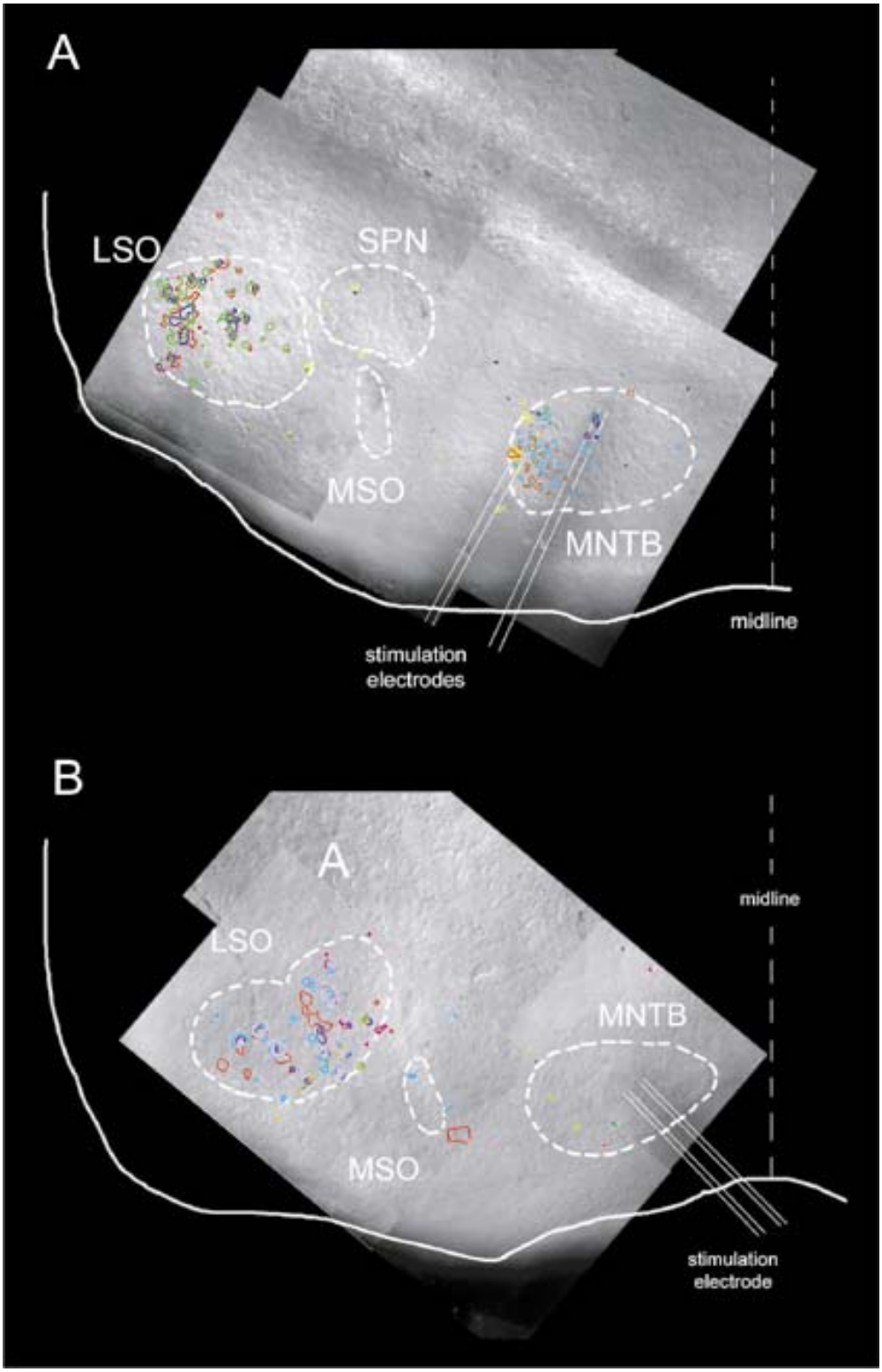
A
LSO
SPN
MSO
MNTB
midline
stimulation
electrodes
B
A
midline
LSO
MNTB
MSO
stimulation
electrode

Figure 2.4

Figure 2.4. MNTB-elicited calcium responses in the immature superior olivary complex. Areas of calcium responses are outlined (different colors represent different stimulation trials) and overlaid on corresponding bright-field images. Calcium responses occur consistently in the LSO and only on rare occasions also in a few other nuclei such as the medial superior olive (MSO) and superior paraolivary nucleus (SPN). The absence of consistent responses in areas outside the LSO indicates that calcium responses in the immature LSO are elicited by monosynaptic MNTB-LSO connections rather than by polysynaptic pathways between the MNTB and LSO.

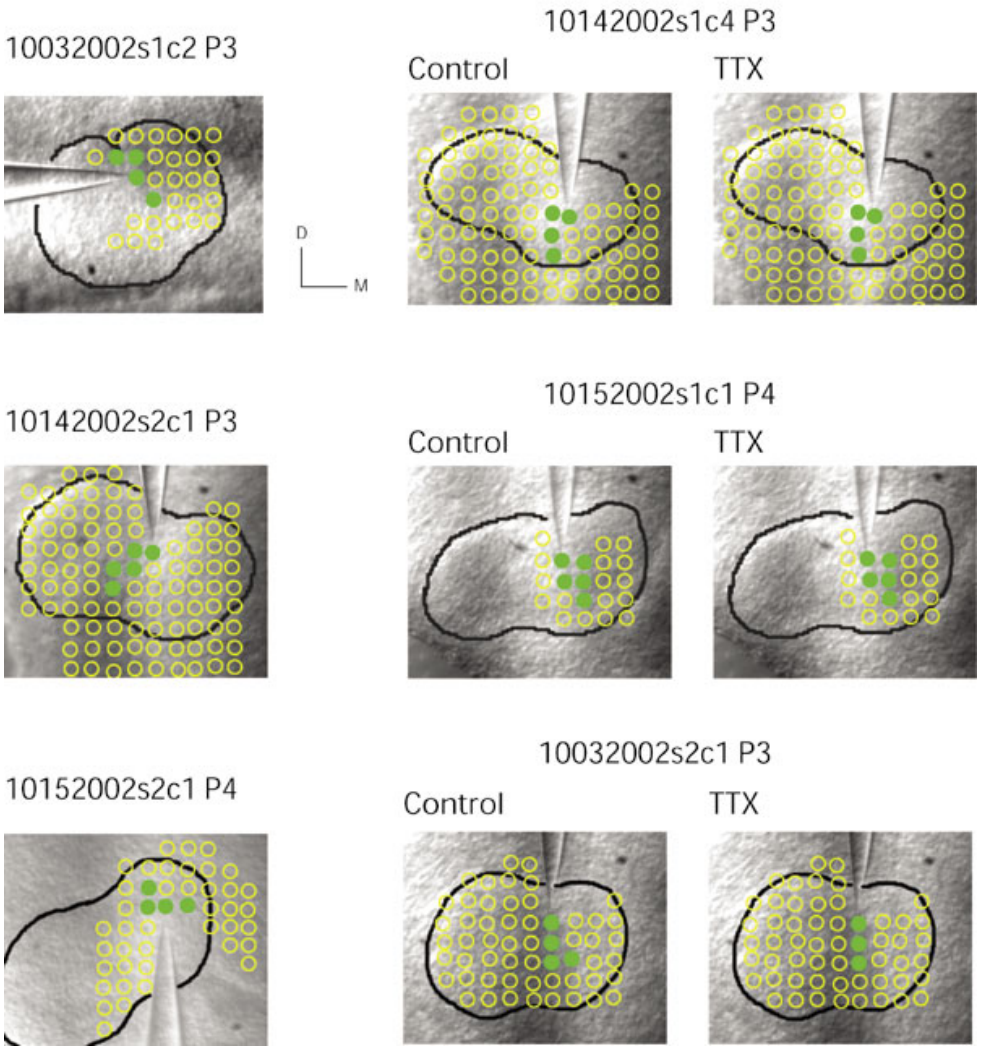

Figure 2.5. Absence of intra-nuclear synaptic connections between LSO neurons in neonatal rats as revealed by focal uncaging of glutamate. Locations of uncaging sites are indicated by circles and are overlaid on video pictures taken during the mapping experiments. LSO boundaries are outlined in black. Uncaging sites that failed to elicit currents in the recorded LSO neuron are marked in yellow; uncaging sites that elicited currents are marked in green. Slices were prepared from P3-P4 animals and recordings were performed in voltage clamp using a K-gluconate-based pipette solution.

anatomical studies in which the LSO in coronal slices of newborn rats was injected with biocytin and DiI and in which virtually no retrogradely labeled cell bodies were found outside the MNTB (Lohmann et al., 1998, 1999). Together, this indicates that in coronal slices of neonatal rats, LSO neurons receive input exclusively from the MNTB. Finally, to examine potential recurrent connections within the LSO, I uncaged glutamate around LSO neurons that are being recorded (**Figure 2.5**). In all 6 LSO neurons tested, responses could only be elicited from 4-5 stimulation sites located in close vicinity of LSO cell bodies (location of cell bodies indicated by the tip of the recording electrode). Successful stimulation sites formed elongated response areas (4.3 ± 0.2 locations, n = 6) and the long axis of these response areas matched the orientation of the bipolar dendrites of the recorded neurons as observed at 40x magnification during seal formation. Notably, responses were never elicited from medio-lateral ("tonotopically") distant stimulation sites. In 3 neurons (**Figure 2.5**, right columns), response areas were remapped after application of 1 μM TTX to block spike-elicited synaptic transmission. In two neurons, input patterns were completely unaffected by TTX, and in one neuron one single input site could not be reproduced in TTX (lower row). This TTX-insensitivity indicates that responses resulted from direct stimulation of LSO dendrites rather then the activation of local intranuclear connections between LSO neurons.

Taken together, the above results strongly argue against the possibility that the larger input maps observed in neonatal animals were caused by activation of exuberant polysynaptic pathways within or between the MNTB and LSO.

Another complication in interpreting the apparent shrinkage in input maps could arise if uncaging activates a larger MNTB area in neonatal animals than two–week old animals. Myelination of afferent and efferent fibers in the MNTB could increase scattering of UV light and thus affect the amount of free glutamate uncaged in the tissue. In addition, maturation of glutamate receptors and membrane properties of MNTB neurons (von Gersdorff and Borst, 2002) may alter the responses of MNTB neurons to a given concentration of uncaged glutamate. To address these issues, I determined the effective resolution of glutamate uncaging in the MNTB of neonatal (P2-3) and older animals (P12-13) by directly recording responses of MNTB neurons to uncaging glutamate nearby. UV flashes aimed directly at the cell body readily elicited action potentials at all ages (**Figure 2.6a**) In neonates, responses consisted of only one or two slow action potentials, whereas trains of fast action potentials occurred in older animals. The

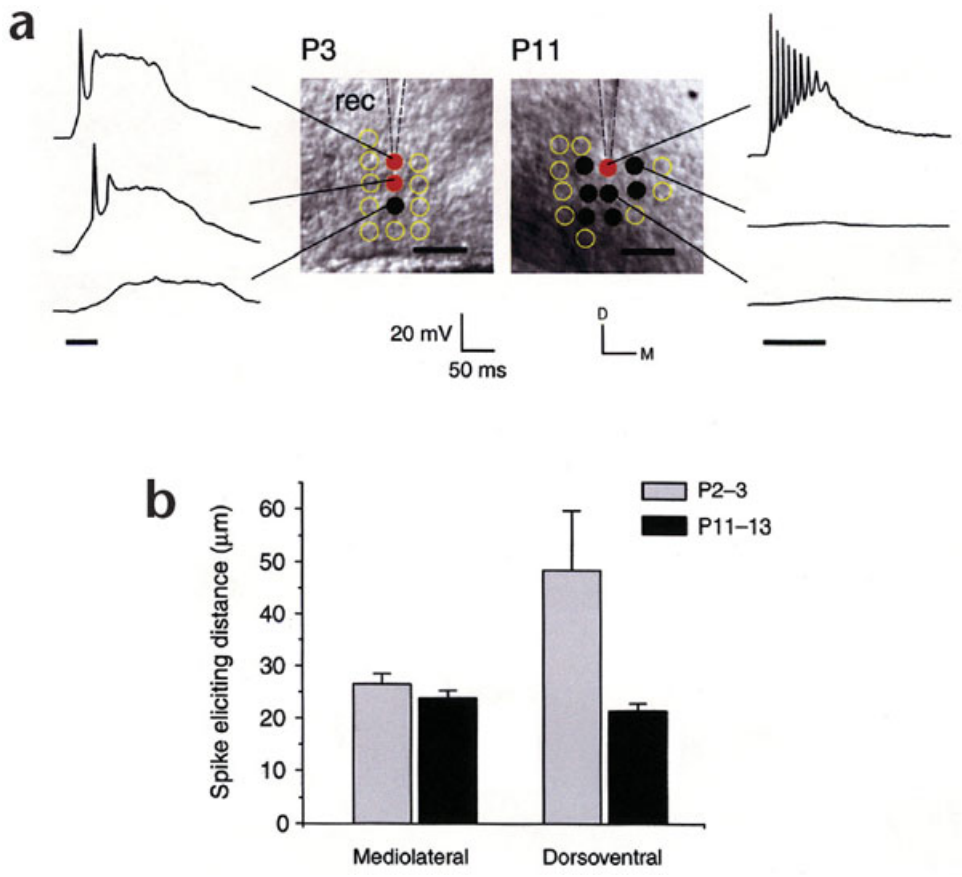

Figure 2.6. Spatial resolution of uncaging glutamate during MNTB maturation. (**a**) Responses of a P3 and a P11 MNTB neuron to photolysis of caged glutamate. At both ages, stimulation sites that elicit action potentials (filled red circles) are restricted to the immediate vicinity of the cell body at the tip of the recording electrode (rec). Stimulation sites at greater distances elicit subthreshold membrane depolarizations (black filled circles) or no responses (open yellow circles). D, dorsal; M, medial. Scale bar, 100 µm. (**b**) Maximal dorsoventral and mediolateral spike-eliciting distance (P2-3, n = 8; P11-13, n = 6).

burst of action potentials in older MNTB neurons should ease the detection of functional connection, tending to increase, rather than decrease, the size of input maps.

Uncaging glutamate at some distance from the cell body produced subthreshold depolarizations or no responses (**Figure 2.6**). Because only spiking MNTB neurons will generate synaptic responses in LSO neurons, I determined the effective uncaging resolution at the maximum distance from the cell body at which UV flashes elicited spikes. Along the mediolateral axis, this distance was about 25 μm and was equivalent in neonatal and older animals (P2-3: 26.5 ± 2.0 μm, n = 8; P11-13: 23.8 ± 1.5 μm, n = 6; $P > 0.3$, Student's t-test; **Figure 2.6b**). Along the dorsoventral axis, however, the distance was approximately twice as large in neonatal animals as in older animals (P2-3: 48.4 ± 11.2 μm, n = 8; P11-13: 21.4 ± 1.4 μm, n = 6; $P < 0.05$, Student's t-test). The decrease of spike-eliciting distance along the dorsoventral direction may reflect increasing myelination of horizontal fibers, which would restrict diffusion of glutamate in the dorsoventral direction, or it may reflect developmental changes in the physiological or morphological properties of dendrites of MNTB neurons.

The age-dependent change in resolution along the in the dorsoventral axis could produce an overestimation of input areas in younger animals because of the possible "filling in" of small MNTB areas that in fact are not connected to the recorded LSO neuron. However, because uncaging efficacy along the mediolateral axis remained stable, my measurements of input width are not affected by maturation of the MNTB. Using the 50% decrease in input width (**Figure 2.2** and **2.3d-f**) as a conservative estimate, I conclude that individual LSO neurons become functionally disconnected from at least 50% of their initial presynaptic MNTB partners.

2.3.2 Developmental changes in stimulus-response functions

A parsimonious explanation for the observed topographic sharpening is that it reflects the selective elimination of topographically exuberant connections. Alternatively, at these early developmental stages, topographic reorganization of MNTB-LSO connectivity might be caused by concentrating initially dispersed MNTB neurons with similar 'tonotopic identities' into LSO 'isofrequency stripes.' In addition, my mapping studies cannot address the question of whether elimination of inappropriate connections is counterbalanced by the formation of new connections from topographically appropriate areas.

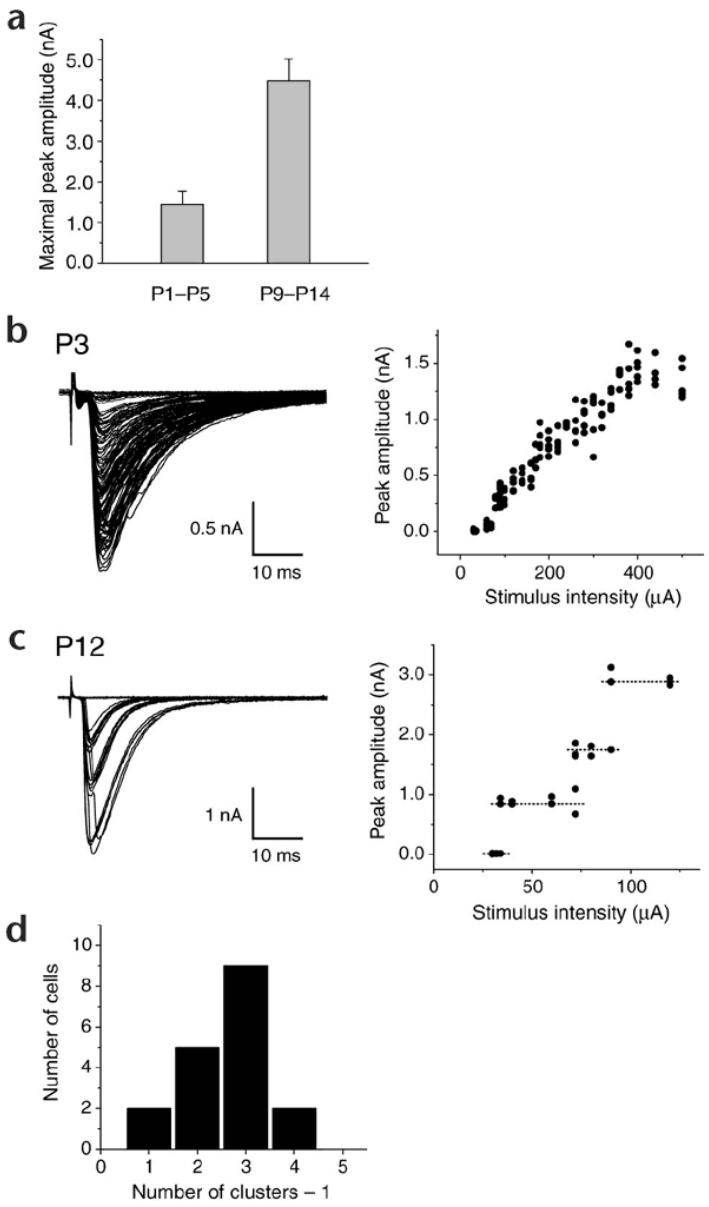
a
Maximal peak amplitude (nA)
5.0
4.0
3.0
2.0
1.0
0.0
P1–P5
P9–P14
b
P3
0.5 nA
10 ms
Peak amplitude (nA)
1.5
1.0
0.5
0.0
0
200
400
Stimulus intensity (μA)
c
P12
1 nA
10 ms
Peak amplitude (nA)
3.0
2.0
1.0
0.0
0
50
100
Stimulus intensity (μA)
d
Number of cells
10
8
6
4
2
0
0
1
2
3
4
5
Number of clusters – 1

Figure 2.7

Figure 2.7. Number of inputs to LSO neurons declines postnatally. (**a**) Maximal synaptic peak currents in P1-5 (n = 16) and P9-14 animals (n = 18). (**b**) Stimulus-response relationship in a P3 neuron. Left, superposition of synaptic currents elicited by electrical stimulation of the MNTB axon bundle with intensities between 30 μA and 500 μA. Right, plot of synaptic current peak amplitudes versus stimulus intensities reveals a smooth stimulus-response relation. (**c**) Stimulus-response relation in a P12 neuron. Left, superposition of synaptic currents elicited by electrical stimulation with intensities between 30 μA and 120 μA. Right, plot of synaptic current peak amplitudes versus stimulus intensities reveals three pronounced increments. Dotted lines indicate medians for each step as derived from cluster analysis. Recording solution contained the L-type calcium channel antagonist D600 (0.1 mM). (**d**) Histogram of number of response steps (number of non-zero clusters) identified in 18 neurons from P9-P14 animals.

To address these issues, I analyzed synaptic responses to electrical stimulation of MNTB inputs while blocking potential contamination of postsynaptic currents by glutamatergic inputs with kynurenic acid (1 mM). The maximal synaptic peak current at saturating stimulation intensities (see Methods) increased more than threefold during the first two postnatal weeks (P1-5: 1.4 ± 0.33 nA, n = 16; P9-14: 4.5 ± 0.54 nA, n = 18; $P < 0.01$, Student's t-test; **Figure 2.7a**). These results indicate that the elimination of MNTB-LSO connections is either outweighed by the formation of new connections or counteracted by an increase in the synaptic conductance elicited by maintained connections.

To distinguish between these possibilities, I estimated the number of MNTB axons that converge on individual LSO neurons by gradually increasing electrical stimulus intensities. Small increments in stimulus intensity gradually recruit more fibers, and the number of discrete response amplitude increments should provide a lower estimate of the number of converging fibers. In all LSO neurons from neonatal animals (P1-5, n = 16), PSC peak amplitudes smoothly increased as a function of stimulus intensity (**Figure 2.7b**). This is consistent with the idea that at this early age, LSO neurons are innervated by a large number of MNTB axons, each of which contributes only a small fraction to the total postsynaptic current. In contrast, in all neurons recorded from older animals (P9-14, n =18), PSC amplitudes increased in discreet steps in response to increasing stimulus intensities (**Figure 2.7c**). The beginning and end of response steps usually overlapped, consistent with the stochastic nature of fiber recruitment at threshold intensities. The number of amplitude steps, as determined by cluster analysis (Methods), varied between1 and 4 (average 2.6 ± 0.2, n = 18), with 50% of neurons showing three response steps (**Figure 2.8d**). These results are consistent with the idea that around the time of hearing onset, LSO neurons are contacted by only a few MNTB fibers, each of which generates large PSCs. It should be noted, however, that the number of converging fibers probably represents a lower bound due to the severance of some fibers during slice preparation. Nevertheless, these results support the idea that functional elimination of MNTB-LSO connections during topographic sharpening is paralleled by an increase in the synaptic conductances generated by single fibers.

During the first two postnatal weeks, LSO neurons undergo maturation both in dendritic complexity and in active and passive membrane properties (Rietzel and Friauf, 1998; Kandler and Friauf, 1995). This could complicate the interpretation of step-like responses in older LSO neurons if these steps resulted from the activation of dendritic voltage-gated currents that

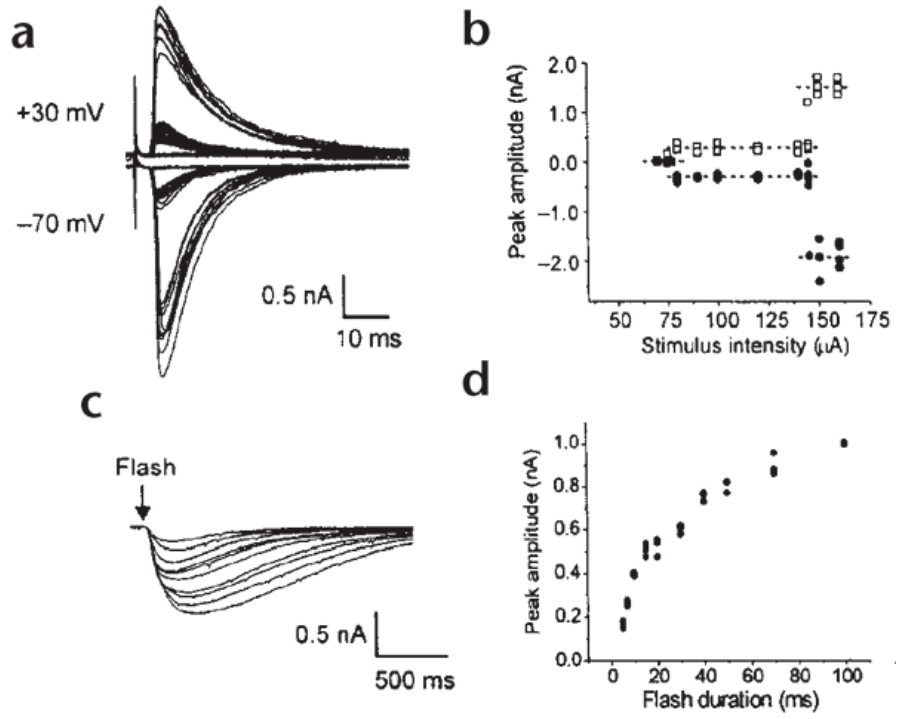

Figure 2.8. Response steps are not caused by activation of postsynaptic voltage-gated ion channels. (**a, b**) Response steps occur during voltage-inactivation of postsynaptic voltage-gated ion channels. (**a**) Synaptic currents in a P11 LSO neuron alternately held at –70 mV (inward currents) or +30 mV (outward currents). Membrane potential was changed to +30 mV 1.2 sec before electrical stimulation. (**b**) Corresponding stimulus-response curve. Notice the presence of response steps around 80 and 150 μA at each holding potential. Dotted lines indicate medians for each cluster. (**c, d**) Activation of postsynaptic GABA receptors by rapid photolysis of caged GABA produces smooth stimulus-response curves. (**c**) Overlaid postsynaptic currents elicited by gradually increasing UV flash durations from 5 ms to 100 ms. (**d**) Peak responses vary smoothly as a function of flash duration. V_{hold} = -70 mV.

escaped voltage-clamp. Several observations, however, argue against this possibility. First, discontinuous stimulus-response curves were readily observed when Na^+-channels and L-type Ca^{2+}-channels were blocked by the inclusion of QX314 (5 mM) and the L-type Ca^{2+}-channel antagonist D600 (0.1 mM) in the pipette solution (QX314: n = 18, QX314 + D600: n = 9; example shown **Figure 2.7c**), and there was no difference in the number of steps recorded in neurons with QX314+D600 (2.7 ± 0.3, n = 9) versus QX 314 alone (2.6 ± 0.3, n = 9). Second, discontinuous stimulus-response functions were also obtained when voltage-gated membrane currents were inactivated by holding neurons at positive membrane potentials (+30 mV, n = 4; **Figure 2.8a** and **b**) and all steps observed at –70 mV were also observed at +30 mV (2.5 ± 0.3 steps for both holding potentials, n = 4). Finally, direct dendritic application of GABA by focal photolysis of caged GABA (BC204, 200 μM) produced smooth stimulus-response curves despite the fact that the same neurons produced step-like response increments with synaptic stimulation (n = 2; **Figure 2.8c** and **d**). I therefore conclude that the step-like response increments observed at older ages reflect activation of additional fibers rather than activation of postsynaptic active membrane conductances.

2.3.3 Developmental increase of single-fiber inputs

Quantitative measurements of convergence based on stimulus-response increments critically depend on the ratio of increment size to variability, such that cluster analysis may not detect weak contributions. In young animals, all inputs were small relative to single-fiber response variability, making it impossible to count distinct inputs with cluster analysis.

I thus estimated the number of converging fibers in neonatal animals by estimating the strength of single MNTB fibers using minimal stimulation, an approach based on the idea that with stimulus intensities at threshold, only a single fiber is likely to be recruited (Stevens and Wang, 1994). In all neurons from neonatal animals (P1-5), minimal stimulation produced responses with variable amplitude (14-140 pA, n = 19 cells; **Figures 2.9a-c** and **10a**), even when stimulus intensities were decreased to result in failure rates > 70% (n = 3). A likely explanation for these variable amplitudes is that reponses are elicited by individual inputs that form multiple synapses on the recorded LSO neurons. Minimal stimulation responses in neurons from older animals (P9-14) were markedly larger (30 pA to 2400 pA, n = 23 cell; **Figures 2.9d-f** and

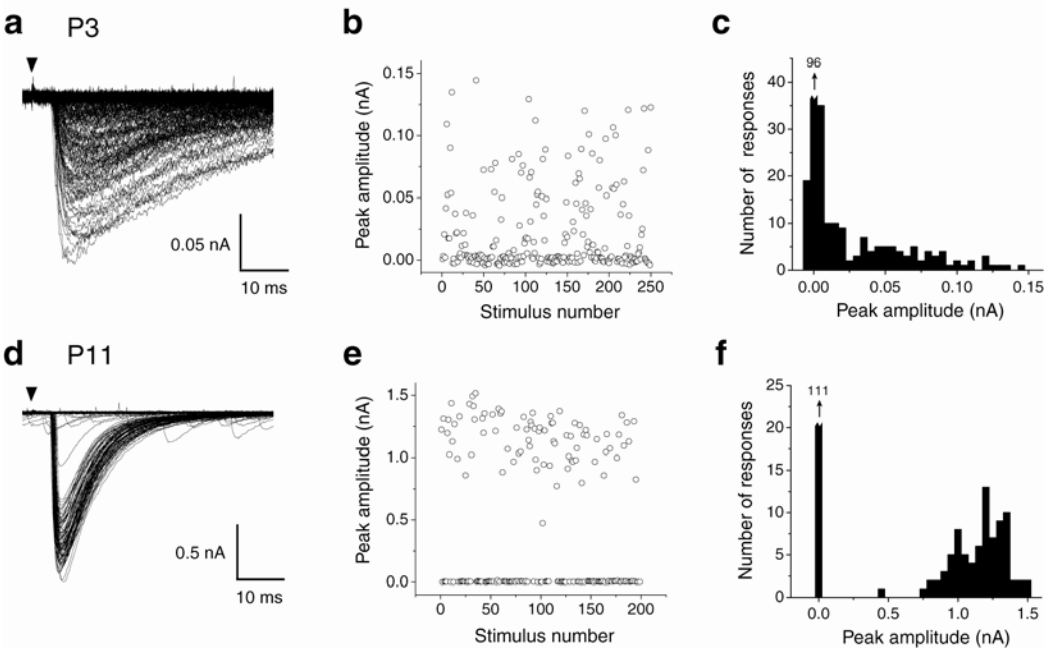

Figure 2.9. Minimal stimulation of MNTB inputs. (**a-c**) Synaptic responses in a P3 neuron. (**a**) Superposition of 250 consecutive currents. (**b**) Plot of peak amplitudes and (**c**) amplitude histogram of responses shown in (**a**). (**d-f**) Synaptic responses in a P11 neuron. Note different scales of abscissa in (**c**) and (**f**). For both neurons, the stimulus frequency was 0.067 Hz. Failure rates were about 60% and their frequency bars are trancated in (**c**) and (**f**). Arrowheads indicate stimulus.

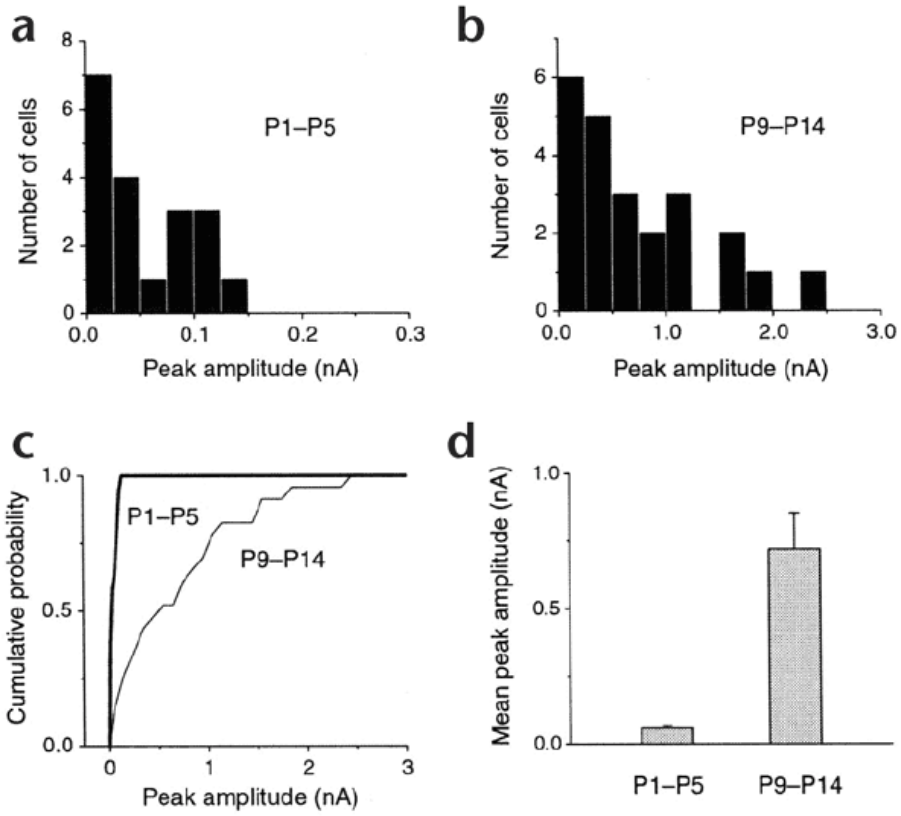

Figure 2.10. Age-dependent changes in single-fiber strength. (**a**) Amplitude histogram of average single-fiber responses in neonatal animals (P1-P5, n = 19). (**b**) Amplitude histogram of average single fiber responses in older animals (P9-P14, n = 23). Note different scale of abscissa between (**a**) and (**b**). (**c**) Cumulative amplitude histograms for the two age groups ($P < 0.01$, Kolmogorov-Smirnov test). (**d**) Mean amplitudes of single-fiber responses in P1-P5 and P9-14 animals ($P < 0.01$, Student's t-test).

2.10b). In addition, there was also a pronounced decrease in the decay times of synaptic currents, most likely reflecting the decrease in the GABAergic component over this developmental period. The average single fiber response was 57 ± 10 pA in P1-5 animals and 719 ± 134 pA in P9-14 animals ($P < 0.01$; Student's t-test). Thus, synaptic currents generated by single MNTB fibers increased more than 12-fold during the first two postnatal weeks. There was no correlation between rise-times and amplitudes of single fiber currents in older animals (10%-90% rise times: 0.71 ms to 1.47 ms, amplitudes: 30.6 pA to 2.4 nA; $n = 23$; $r = -0.08$), arguing against the possibility that the increase in synaptic currents was primarily due to selective somatodendritic relocalization of inhibitory synapses, as occurs in developing MSO neurons in gerbils.

Results from the electrical stimulation experiments allow me to estimate quantitative changes in the MNTB:LSO convergence ratio over the period of spatial refinement. In P1-5 animals, total synaptic currents generated by all MNTB axons converging on individual LSO neurons were 1.4 nA (**Figure 2.7a**), and the average single fiber response was about 57 pA (**Figure 2.10d**). Thus I estimated MNTB:LSO convergence ratio in neonatal animals to be ~25:1. In P9-14 animals, total synaptic currents generated by all converging MNTB inputs was 4.5 nA, and the average single fiber response was 719 pA, indicating that the estimated MNTB:LSO convergence ratio around hearing onset is ~6:1. These convergence ratios represent conservative estimates because some MNTB-LSO connections mostly likely were severed during slice preparation and because single-fiber responses are biased toward higher amplitudes by exclusion of all failures (Methods). In addition, because of the variable responses encountered in neonatal animals, some of the larger responses at this age could reflect the stimulation of more than one fiber, which would result in a bias toward higher fiber conductances and possible underestimation of convergence ratios at this age. Nevertheless, the reduction in the convergence ratio from 25:1 to 6:1 closely matches the ~75% reduction in the size of MNTB-LSO input maps. The difference between the 6:1 ratio obtained from minimal stimulation and the 3:1 ratio obtained from cluster analysis suggests that around hearing onset, LSO neurons on average receive inputs from about three MNTB fibers that generate large synaptic currents and three MNTB axons that generate very small synaptic currents (included in **Figure 2.10b**).

2.4 DISCUSSION

In the present study, I applied functional mapping with caged glutamate and electrical stimulation techniques to the developing MNTB-LSO pathway to shed more light on the events by which an inhibitory circuit in the mammalian brain becomes organized during normal development. My results indicate that specific elimination of functional connections and an increase in synaptic conductances elicited by the remaining connections are two prominent mechanisms involved in the formation of a tonotopic, inhibitory map. Synapse elimination is extensive and rapid, as individual LSO neurons become functionally disconnected from ~75% of their initial presynaptic MNTB partners, in only 5-6 days. Concomitant with this elimination process, synaptic currents generated by maintained connections increase ~12-fold.

A surprising finding of my functional mapping studies is that functional elimination of MNTB-LSO connections occurs primarily during the first postnatal week (**Figure 2.3a** and **e**), which is before the onset of hearing (around P12-14 in rats; Blatchley et al., 1987). This contrasts with previous anatomical data showing that tonotopic refinement in the MNTB-LSO pathway takes place primarily during the third postnatal week, which is after hearing onset (Rietzel and Friauf, 1998; Sanes and Siverls, 1991). The 50% functional sharpening along the tonotopic axis that I observed before P8 (**Figure 2.3f**) exceeds the degree of anatomical refinement that takes place after hearing onset (~35% sharpening of boutonal spread along tonotopic axis (Sanes and Siverls, 1991)). Thus, precise tonotopy of the MNTB-LSO pathway apparently emerges via two distinct processes: functional refinement during the first postnatal week and structural refinement during the third postnatal week. Delays between functional refinement and structural refinement have been observed previously in the developing neuromuscular junction (Colman et al., 1997) and visual cortex (Antonini and Stryker, 1993). In these excitatory systems, changes in synaptic transmission are followed by axonal rearrangement in only one or two days, whereas in the glycinergic/GABAergic MNTB-LSO pathway, synaptic silencing and axonal pruning are separated by about one week. As a consequence of this long delay, functional and structural refinement seems to take place during two distinct developmental periods during which the developing auditory system is in two fundamentally different physiological stages.

First, synaptic silencing takes place when glycinergic/GABAergic MNTB-LSO synapses are excitatory (Kandler and Friauf, 1995; Ehrlich et al., 1999), whereas structural synapse elimination occurs when MNTB-LSO synapses are inhibitory. As in many other brain areas (Ben-Ari, 2001) glycine and GABA in the LSO gradually change from being excitatory to being inhibitory. In the LSO of rats, this transition is completed by P8, the age after which functional MNTB-LSO connectivity is stable (**Figure 2.3**). Such a correlation is predicted by the hypothesis that the excitatory action of inhibitory synapses is crucial for the developmental organization of inhibitory networks (Ben-Ari, 2001). Consistent with this, depolarizing MNTB-LSO synapses increase postsynaptic calcium concentration (Kullman et al., 2002), which is an essential step for inducing plasticity in a variety of glycinergic and GABAergic synapses (Ben-Ari, 2001; Kotak and Sanes, 2000; Aizenman et al., 1998). This scenario predicts that formation of early functional topography in the MNTB-LSO depends on spontaneous activity and perhaps synaptic competition, as is the case in a number of excitatory systems (Stellwagen and Shatz, 2002; Katz and Shatz, 1996). The fact that spontaneous activity is necessary for sustaining functional MNTB-LSO connections before hearing onset (Kotak and Sanes, 1996) and that it is a critical factor in the formation and maintenance of glycinergic and GABAergic synapses in other systems (Kilman et al., 2002; Hendry and Jones, 1986; Kirsch and Betz, 1998) is consistent with this idea. Axonal pruning of MNTB axons during the hyperpolarizing phase (Sanes and Siverls, 1991; Kotak et al., 1998; Kandler and Friauf, 1995) most likely involves a different set of cellular mechanisms that is independent of depolarization-induced calcium influx (Kotak and Sanes, 2000; Aizenman et al., 1998).

Second, because functional elimination of MNTB-LSO synapses is essentially complete by P8, at least 4 days before hearing onset (**Figure 2.3**), sound-evoked neuronal activity is not involved in the initial steps of topographic sharpening. This differs from the prevalent view, based on anatomical observations, that tonotopic sharpening of the MNTB-LSO pathway takes place primarily in the presence of sound-evoked activity (Sanes and Friauf, 2000; Rietzel and Friauf, 1998; Sanes and Siverls, 1991). Although alteration of normal MNTB-LSO activity levels or patterns by cochlear ablation results in less precise MNTB-LSO connectivity, it is unknown whether these effects are due to changes in spontaneous or sound-evoked activity (Sanes and Takacs, 1993). For example, normal auditory experience may guide the structural manifestation of the functional tonotopic organization of the MNTB-LSO pathway that is present

at hearing onset, or it may reactivate 'silent' MNTB-LSO connections (Gubellini et al., 2001) to further fine-tune LSO circuits to the changing acoustic geometry of the growing head.

The roughly 4-fold decrease in convergence ratio before hearing onset is compensated by a roughly 12-fold increase in the synaptic conductance generated by individual MNTB axons. Developmental changes in receptor subunit composition (Sanes and Friauf, 2000) or neurotransmitter phenotype (Kotak et al., 1998) are unlikely to account for these changes because changes in subunit composition have relatively little effect on channel conductances, which tend to decrease rather than increase during development (Takahashi et al., 1992; Bormann et al., 1987). It is thus more likely that the increase in synaptic conductance reflects an increase in the number of release sites, postsynaptic receptors, and/or probability of release (Chen and Regehr, 2000; Gubellini et al., 2001; Grantyn et al., 1995). Homeostatic synaptic scaling, a process by which the strength of single synapses is regulated to counteract changes in overall neuronal activity (Kilman et al., 2002; Davis and Goodman, 1998) could provide a possible explanation for the increase in synaptic conductance during synapse elimination. However, additional mechanisms, such as age-dependent changes in the excitation set point of LSO neurons, would then be required to account for the excitation-inhibition switch. Finally, it remains to be shown how, during this excitation-inhibition switch, the pronounced increase in synaptic conductance influences postsynaptic responses to MNTB activity and integration of excitatory and inhibitory inputs in the LSO.

My results lend strong, albeit correlative, support for the long-standing hypothesis that the seemingly paradoxical excitatory effect of immature inhibitory synapses is crucially involved in the initial establishment of early developing inhibitory networks. Further detailed analysis of the developing MNTB-LSO system could uncover the cellular and molecular mechanisms guiding early specification of inhibitory circuits and their fine-tuning at later developmental stages (Hendry and Jones, 1986; Knudsen, 2002; Kapfer et al., 2002; Sanes and Friauf, 2000; Sanes and Siverls, 1991; Kotak and Sanes, 2000; Aizenman et al., 1998; Sanes and Takacs, 1993).

3. EFFECT OF UNILATERAL COCHLEAR ABLATION ON THE MNTB-LSO REFINEMENT

3.1 INTRODUCTION

In many systems, elimination of exuberant inputs and strengthening of the maintained ones occur in an activity-dependent manner (Lichtman and Colman, 2000; Katz and Shatz, 1996). Immature inputs compete for postsynaptic neurons such that the strong, correlated inputs that effectively drive postsynaptic neurons outcompete weak, uncorrelated ones (Weliky, 2000). It is not clear, however, whether neuronal activity is crucial in the selection process of immature inhibitory inputs as well. My functional mapping data in the MNTB-LSO pathway indicate a large degree of functional elimination of inputs well before hearing onset. The fact that the immature GABA/glycinergic inputs first form functional synapses before they become eliminated suggests that neuronal activity may play a role in this refinement process. Because the topographic sharpening of MNTB-LSO input maps occurred before hearing onset (**Figure 2.3b** and **e**), I hypothesized that spontaneous activity, known to exist in immature auditory pathway, is required for the functional refinement of the MNTB-LSO pathway.

Before hearing onset, immature hair cells and possibly spiral ganglion cells also spontaneously fire action potentials (Kros et al., 1998; Glowatzki and Fuchs, 2000; Beutner and Moser, 2001; Jones et al., 2001; Gummer and Mark, 1994). At birth, most synaptic connections in the auditory brainstem are functional (Kandler and Friauf, 1995b). The spontaneous activity generated in the cochlea is thought to travel along the central auditory pathway before hearing onset (Kotak and Sanes, 1995; Born and Rubel, 1988). For this reason, cochlear ablation is commonly used as a means to eliminate activity from the cochlea. Cochlear removal causes severe cell death in the antero-ventral cochlear nucleus (AVCN), which is the major source of calyceal inputs to the contralateral MNTB (Hashisaki and Rubel, 1989; Mostafapour et al., 2000). Thus, unilateral cochlea ablation would deprive the MNTB neurons of the source of

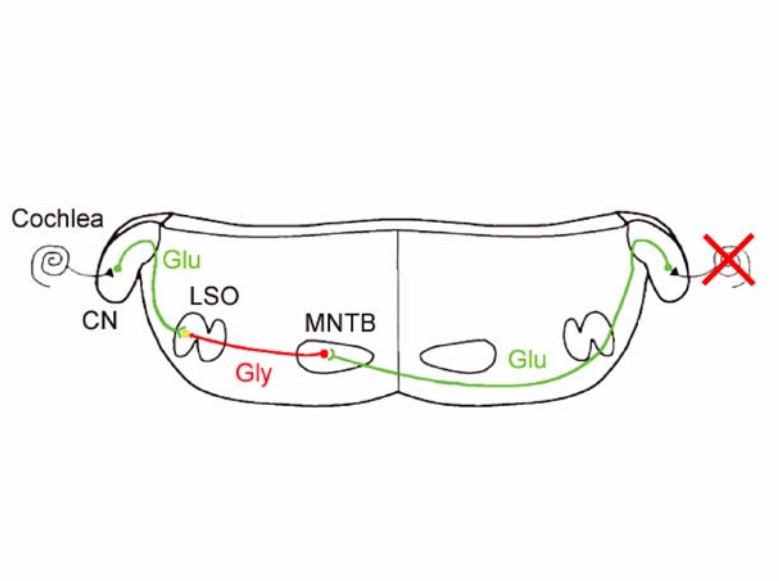

Figure 3.1. Unilateral cochlear ablation. The schematic diagram illustrates denervation of the left MNTB from their inputs by removal of the right cochlea. Lack of auditory nerve activity caused by cochlear removal induces cell death in the right CN. This degeneration of the right CN eliminates inputs to the left MNTB, thereby depriving the MNTB neurons of the afferent activity.

spontaneous activity (**Figure 3.1**). It has been shown that in animals with unilateral cochlear ablation (at P7), the developmental pruning of axonal arbors of MNTB neurons was impaired (assessed around P21) (Sanes and Takacs, 1993). These experiments indicate that normal activity or at least the intact cochlea is necessary for normal refinement of the MNTB-LSO pathway. In that experimental design, however, the authors could not distinguish the role of spontaneous activity before hearing onset and the potential involvement of sound-evoked activity after hearing onset. Also, as discussed in Chapter 2, quite different time courses suggest that the functional elimination and anatomical pruning of MNTB arbors may involve different sets of mechanisms. To determine whether spontaneous activity generated from the cochlea is necessary for the functional refinement of the MNTB-LSO pathway, I performed unilateral cochlear ablation in 2-day old rats, before the beginning of reduction of input maps (**Figure 2.3b** and **e**). In the operated animals, I mapped functional connectivity of the MNTB-LSO pathway around hearing onset when the input maps have become narrower (**Figure 2.3**).

3.2 METHODS

3.2.1 Electrophysiology and functional mapping

Same as in Chapter 2.

3.2.2 Cochlear ablation

P2 rat pups were anesthetized by hypothermia. A small incision was made ventral and posterior to the earflap. The tympanum was exposed, and the tympanic membrane was removed. The mesenchyme in the middle ear cavity was carefully removed using fine forceps and aspiration to expose the cochlea. The bony wall of the cochlea was gently broken and the structures inside the cochlea were aspirated. A small piece of gel foam was placed in the middle ear cavity, and the wound was closed. The pups were allowed to warm up and were returned to the mother. Body weight was monitored every other day until the day of mapping experiment. The operated

animals used for mapping experiments gained normal weight when compared with their normal littermates.

3.2.3 Nissl staining and biocytin tracing

During the preparation of slices for recording, the sections that contained the cochlear nucleus (CN) were selected and fixed in 4% paraformaldehyde (PFA). The slices were cut on a freezing microtome at 40 μm, and standard Nissl staining method was used to determine the degeneration of the CN ipsilateral to the ablated cochlea.

For biocytin tracing to visualize ectopic projections, unilateral cochlear ablation was performed at P2, and at P6-12, the animals were killed and the brain was removed. The brain was secured on a Petri dish with the ventral side up, and ACSF was temporarily removed with suction. The CN on the intact side was identified. With a pulled glass pipette small biocytin crystals were picked up and placed on the cochlear nucleus (CN). With the pipette tip, the CN was injured as an attempt to help biocytin to be taken up by the CN neurons more efficiently. The brain was washed to remove excess biocytin and was incubated in oxygenated ACSF at room temperature for ~3 hours before it was fixed (4 % PFA in PBS). The fixed brain was cryoprotected in 30% sucrose and cut at 80 μm on a freezing microtome. Biocytin was visualized using biotin-avidin binding (ABC kit) followed by diaminobenzidine (DAB)-peroxidase reaction.

3.3 RESULTS

3.3.1 Unilateral cochlear ablation does not alter input maps

For each animals that was recorded, the degeneration of the CN was confirmed by Nissl staining. As shown in **Figure 3.2a**, the CN on the ablated side is markedly degenerated compared with the intact side. In virtually all cases, 50 % or greater (judged by eye) AVCN degeneration was observed.

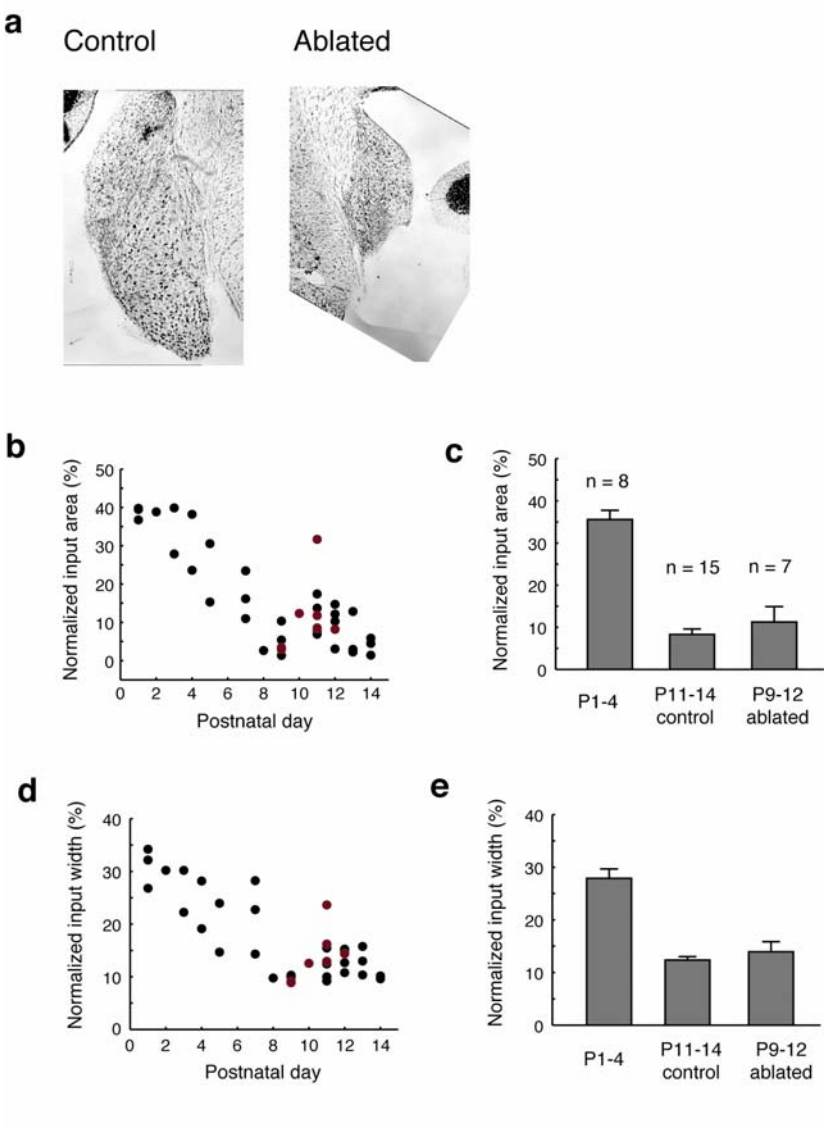
a
Control
Ablated
b
Normalized input area (%)
Postnatal day
c
Normalized input area (%)
n = 8
n = 15
n = 7
P1-4
P11-14 control
P9-12 ablated
d
Normalized input width (%)
Postnatal day
e
Normalized input width (%)
P1-4
P11-14 control
P9-12 ablated

Figure 3.2

Figure 3.2. Summary of MNTB-LSO input maps in cochlea-ablated animals. (**a**) Nissl stained CNs from a P11 animal that had unilateral cochlear ablation at P2. Degeneration of AVCN is apparent on the ablated side. (**b**) Normal age-dependent decrease of normalized input areas normalized (black) and normalized input areas in ablated animals (red). (**c**) Mean normalized input areas in normal P1-4 (n = 8), normal P11-14 (n = 15), and ablated P9-12 (n = 7) animals. The input areas in ablated animals were not significantly different from those in normal P11-14 animals (P = 0.35, Student's t-test). Errorbars = standard errors. (**d**) Normalized input widths in normal (black) and ablated animals (red). (**e**) Mean normalized input widths in normal P1-4 (n = 8), normal P11-14 (n = 15), and ablated P9-12 (n = 7) animals. Around hearing onset, normalized input widths were not significantly different between normal and ablated animals (P = 0.22, Student's t-test).

To determine the effects of cochlear ablation on functional connectivity in the MNTB-LSO pathway, I mapped the spatial distribution of the presynaptic MNTB neurons that converge onto a single LSO neuron using focal photolysis of caged glutamate. If spontaneous activity from the cochlea to the MNTB is necessary for the refinement, the MNTB-LSO input maps in ablated animals would remain broad around hearing onset as in newborn animals. Instead, I found that the size of the MNTB-LSO input maps decreased to the same degree as in normal animals (**Figure 3.2**). The average absolute input area was 13,293 ± 4,686 μm^2 (n = 7, P9-12) in the ablated animals and 10,988 ± 1,668 (n = 15) in the normal animals (P = 0.56, Student's t-test). The mean normalized input areas were 11.3 ± 3.7 % (ablated) and 8.3 ± 1.3 % (control), respectively and were not significantly different (P = 0.35, Student's t-test, **Figure 3.2b** and **c**). Both absolute (ablated: 73.0 ± 9.0 μm, n = 7, P9-12; normal: 62.6 ± 3.8 μm, n = 15, P11-14) and normalized tonotopic widths (14.0 ± 1.9 %, ablated; 12.4 ± 0.7 %, normal) in the ablated animals were also not different from the normal animals (absolute: P = 0.22, normalized: P = 0.33, Student's t-test, **Figure 3.2d** and **e**). These data indicate that unilateral cochlear ablation did not prevent the functional elimination of aberrant MNTB inputs to the LSO neurons.

3.3.2 Ectopic innervation of the denervated MNTB

The normal MNTB-LSO input maps in animals with unilateral cochlear ablation could indicate that the functional refinement of the MNTB-LSO does not require spontaneous activity generated in the cochlea. Alternatively, however, the data could have resulted from certain compensatory mechanisms induced by cochlear removal. In gerbils, it has been shown that neonatal cochlear ablation induces ectopic projections to the denervated MNTB from the intact CN within 24 hours (Kitzes et al., 1995; Russsell and Moore, 1995). To determine whether this ectopic sprouting also occurs in rats with unilateral cochlear ablation, I injected biocytin crystals into the intact CN (Methods). As shown in **Figure 3.3**, the axons from the CN that normally innervate only the contralateral MNTB sent out collaterals with calyx-like endings into the denervated ipsilateral MNTB (ablation at P2 and tracing at P6-12, n = 8). The density of ectopic sprouting appeared substantial. I further tested whether this ectopic sprouting still occurs if ablation is performed at later stages. Cochlear ablation at P6 still caused substantial sprouting (tracing at P12, n = 3, data not shown). This is consistent with the data in gerbils that the

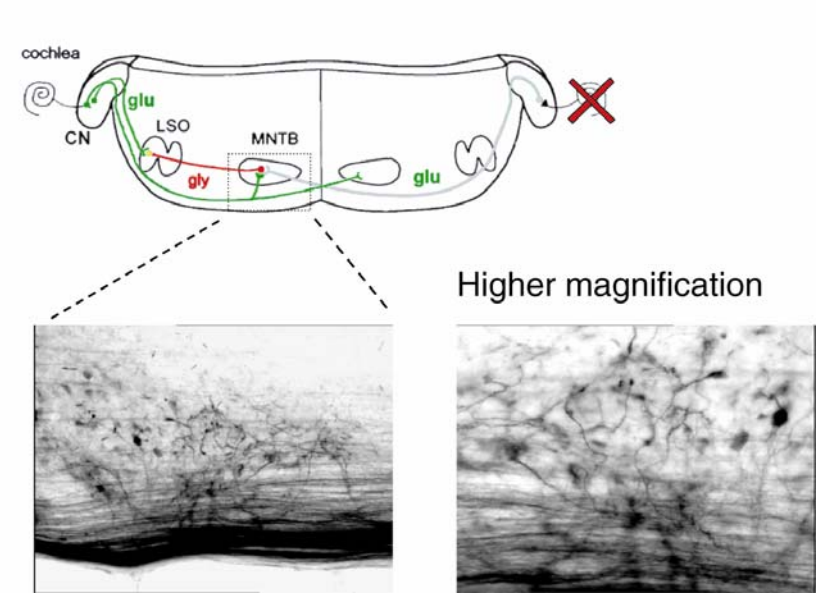

Figure 3.3. Ectopic sprouting of calyces into the denervated MNTB. Illustrated in the schema is denervation of the left MNTB from their normal inputs (light gray) by removal of the right cochlea. Axons from the left (intact) CN, on their way to the right MNTB, send out ectopic projections into the left MNTB. In the high magnification photomicrograph, normal-looking, immature calyces formed by ectopic projections are shown. In this example, CA was performed at P2 and biocytin tracing was done at P6.

induction of ectopic sprouting was still heavy with ablation at P5, but was negligible when ablation was performed at P10 (Russell and Moore, 1995). Taken together, my data raise the possibility that the ectopic innervation of the denervated MNTB by the intact CN could have provided the level or temporal pattern of spontaneous activity necessary to drive refinement.

3.4 DISCUSSION

I performed unilateral cochlear ablation to determine the role of cochlea-generated activity in the MNTB-LSO refinement by eliminating contralateral afferent inputs to the MNTB. The MNTB neurons, however, regained afferent inputs from the compensatory projections from the intact CN. These ectopic inputs have shown to form functional synapses and appear to be tonotopically organized (Kitzes et al., 1995). Thus, it is possible that although the MNTB neurons were transiently deprived of normal afferent inputs, the ectopic projections restored afferent activity similar to that of normal afferents. It is also possible that the functional refinement of the MNTB-LSO pathway is an activity-independent process while the structural pruning of MNTB axon is an activity-dependent process. At this point, however, I cannot distinguish between these two possibilities, and thus, with unilateral cochlear ablation, I cannot address my hypothesis that the functional refinement of MNTB-LSO pathway requires spontaneous activity.

To address my hypothesis, alternative ways to deprive the MNTB neurons of afferent activity will be required. Chronic TTX treatment to the cochlea has been shown to silence spontaneous activity (Lippe, 1994). Deprivation of auditory nerve activity to the CN, however, also causes cell death in the CN (Born and Rubel, 1988). Thus, I expect that chronic TTX treatment to the cochlea would also induce ectopic sprouting. Another possibility to eliminate CN-driven activity in the MNTB is bilateral cochlear ablation. Because the ectopic projection stems from the fibers from the intact CN, removing both cochleae should deprive the MNTB neurons of all afferent inputs from both CNs. Although it has been suggested that some LSO neurons die when they are deprived of glutamatergic inputs from the ipsilateral CN, one should still be able to determine whether topographic sharpening still occurs in the MNTB-LSO pathway, lacking cochlea-generated spontaneous activity before hearing onset.

I have shown that PSCs elicited by single MNTB fibers are 12-fold larger in P9-14 than in P1-4 (**Figure 2.10**). In the current cochlear ablation study, I did not measure synaptic currents elicited by stimulation of MNTB fibers. It is possible that despite the normal input maps, strengthening of MNTB fibers is impaired in ablated animals. It has been shown that unilateral cochlear ablation at P7 weakens IPSPs evoked by MNTB stimulation in P8-14 gerbils (Kotak and Sanes, 1996). The reversal potential for the IPSPs was also slightly elevated in ablated animals. It will be important to determine whether uni- or bilateral cochlea ablation at P2 rats influences strengthening of MNTB fibers and/or the developmental shift in Cl^- reversal potential in the LSO neurons (Kandler and Friauf, 1995b; Ehrlich et al, 1999). If in ablated animals, MNTB inputs do not become strengthened while input maps sharpens normally, it would indicate that distinct mechanisms operate in elimination and strengthening. Also, in my previous study, the period of refinement tightly correlated with the period of depolarization, implicating depolarizing GABA/glycinergic MNTB inputs in organizing MNTB-LSO pathway (**Figure 2.3b** and **e**). Determining whether normal shift in Cl^- reversal potentials towards lower values occurs in ablated animals will help us to correlate the depolarizing MNTB inputs with either functional elimination or strengthening or both.

Normally, the MNTB inputs to LSO neurons are driven by the CN contralateral to the LSO. With unilateral cochlear ablation and the following ectopic projections, now the MNTB inputs to the LSO (left LSO in **Figure 3.3**) are driven by the CN ipsilateral to the LSO. Thus, in ablated animals, both glutamatergic inputs (from CN) and GABA/glycinergic inputs (from MNTB) are driven by the same CN. In this situation, I expect that patterns of afferent activity to LSO neurons might be more correlated than in the normal situation where LSO neurons are driven by two CNs. My data indicate that this ‘monauralization’ did not prevent the refinement of the MNTB-LSO pathway. This could mean that normally there is a mechanism to coordinate activity in the two cochleae and cochlear nuclei (Needham and Paolini, 2003).

4. REFINEMENT OF THE MOUSE MNTB-LSO PATHWAY

4.1 INTRODUCTION

In chapter 2, I presented evidence for the functional refinement of the MNTB-LSO pathway in pre-hearing rats. The topographic sharpening of the pathway was accomplished by functional elimination and strengthening of GABA/glycinergic inputs converging onto single LSO neurons (Kim and Kandler, 2003). This finding prompted important hypotheses about the role of spontaneous activity and depolarizing GABA/glycinergic inputs in organizing developing inhibitory circuits. Addressing these hypotheses requires technically challenging manipulations of neuronal activity in vivo for a prolonged period in neonatal rats. Thus, genetically engineered animals would provide crucial means to address these questions. As a first step, I decided to determine whether similar functional refinement also occurs in the developing mouse MNTB-LSO pathway.

In rats, I observed ~12-fold increase in the amplitudes of peak PSCs elicited by the MNTB inputs that were maintained during the period of refinement (**Figure 2.10d**). The synaptic changes underlying this large increase in PSC amplitudes are poorly understood. Therefore, in addition to examining the refinement of the mouse MNTB-LSO pathway, I investigated in more detail developmental changes in synaptic properties of MNTB inputs in mice. Increases in the amplitude of GABA/glycinergic PSCs elicited by a single axon can be achieved by an increase in quantal amplitude (Awatramani et al., 2004b), in the number of release sites (Morales et al., 2002), or in presynaptic release probability. To investigate relative contributions from these different pre- and postsynaptic synaptic mechanisms, I measured evoked miniature PSCs (mPSCs) from the MNTB and paired-pulse ratios (PPRs) in mice shortly after birth (P1-3) and around hearing onset (P10-12). My data indicate that the refinement of the mouse MNTB-LSO pathway highly resembles the refinement observed in the rat. My data further indicate that the

strengthening of the maintained MNTB inputs is achieved by an increase in quantal amplitude and the number of release sites.

4.2 METHODS

4.2.1 Slice preparation and electrophysiology

Acute brainstem slices (300 μm thick) were prepared from 129S6/SvEv mice aged P1-12 as described in Chapter 2. Whole-cell voltage clamp recordings at room temperature (22 degrees C) were obtained from visually identified LSO principal neurons in the medial half of the LSO using an Axopatch 1D amplifier. Recording electrodes (2-3 MΩ) contained (in mM): 76 Cs-methanesulfonate, 56 CsCl, 10 EGTA, 1 $MgCl_2$, 1 $CaCl_2$, 2 ATP-Mg, 0.3 GTP-Na, 5 Na_2-phosphocreatine, and 10 HEPES (pH = 7.3, 290 mOsm). During the recording, oxygenated ACSF was continuously circulated at 3-4 ml/min (composition in mM: NaCl 124, $NaHCO_3$ 26, Glucose 10, KCl 5, KH_2PO_4 1.25, $MgSO_4$ 1.3, $CaCl_2$ 2, 1 Kynurenic acid, pH = 7.4 when bubbled with 95% O_2/5% CO_2, 310 mOsm). With this configuration of internal and external solutions, E_{Cl} was -20 mV and LSO neurons were held at -70 mV (corrected for -5 mV liquid junction potential), resulting in -50 mV driving force for Cl^--mediated currents. Patch electrodes with a larger tip size (~ 1MΩ) were used for electrical stimulation. The stimulation electrode was placed at the lateral edge of the MNTB as an attempt to gain access to as many MNTB fibers as possible. Constant current pulse (0.2 ms) was delivered using a stimulation isolation unit (IsoFlex). Data were filtered at 2 kHz (Axopatch 1D) and acquired at 10 kHz using custom-made Labview data acquisition software.

4.2.2 Minimal stimulation

To record responses elicited by a single MNTB axons, minimal stimulation technique was used (Stevens and Wang, 1994; Gil et al., 1999). A stimulus-response relation was obtained and the first plateau was determined at which the failure rate decreased without increasing the mean amplitude of successful responses (**Figure 4.2b** and **d**). Within this range of stimulus intensities,

a stimulus intensity was chosen that resulted in failures 30 to 40% of the time. Under these conditions, it is likely that only one fiber is activated. At stimulus intensities of 10-40 μA, 20-100 responses were evoked at 0.2 Hz. Only responses with latencies that fell into a 1 ms window were accepted.

4.3.3 Evoked mPSC experiments

To examine mPSCs specifically from MNTB terminals, MNTB fibers were electrically stimulated in 2 mM Sr^{2+} / 0 mM Ca^{2+}. It is generally thought that in this condition, asynchronous release is promoted, and those asynchronous events represent quantal events (Goda and Stevens, 1994; Behrends and ten Bruggengate, 1998). In 2mM Sr^{2+} / 0 mM Ca^{2+}, PSCs evoked by electrical stimulation were markedly smaller than in normal 2 mM Ca^{2+} bath solution, and asynchronous events were observed. However, especially in P1-3 animals, single stimuli were not efficient at inducing asynchronous events. To more efficiently induce asynchronous quantal events, 2-10 pulses of stimulus trains (100 Hz) were used. These train stimuli effectively induced asynchronous events in both age groups (**Figure 4.3a** and **b**). A one-second long base line was recorded prior to the stimulus train and another 1 second long trace was recorded after the train. In some cells, the frequency of spontaneous synaptic inputs recorded before the stimulus train was as high as the frequency of asynchronous events. These cells were excluded from the analysis.

4.3.4 Data analysis

Synaptic responses were analyzed using custom written Labview and MatLab programs. Evoked mPSCs were identified and collected from a 3-400 msec window after the stimulus train using a sliding template method (Clements and Bekkers, 1997) or a derivative threshold crossing technique implemented in MatLab. For both methods, detection thresholds were set low, and false positives (events that did not exhibit a rapid rise followed by a typical decay time) were rejected by visual inspection. In P1-3 animals, asynchronous events often appeared only during the decay phase of the synchronous, stimulus-locked responses (data not shown). For these

events, peak amplitude was measured after the baseline was adjusted by fitting a straight line to the baseline immediately before the peak (Lu and Trussell, 2000).

Paired pulse ratios were computed from the paired PSCs evoked by two stimuli with intervals of 10, 20, 50, 100, 200, and 500 ms. At least 20 trials were averaged and then the mean second PSC peak amplitude was divided by the first (Kim and Alger, 2001). When there was a significant overlap between the two PSCs due to short inter-pulse intervals (10, 20, and 50 ms in P1-3; 10 and 20 ms in P10-12), the second PSC peak was measured after subtracting the first response obtained from longer intervals. Throughout the text and figures, errors are expressed in standard error.

4.3 RESULTS

4.3.1 Developmental changes in single-fiber and maximal MNTB responses

Synaptic currents evoked by electrical stimulation of MNTB fibers were recorded from visually identified mouse LSO neurons using whole-cell voltage clamp technique. Recording electrodes contained Cs^+-based internal solution with a high Cl^- concentration, resulting in inward PSCs. To isolate PSCs mediated by GABA and glycine receptors, all recordings were performed in the presence of Kynurenic acid (1mM). The MNTB-evoked PSCs in P1-3 animals were relatively small and slow, and exhibited both bicuculline sensitive (10 μM) and strychinine sensitive (1 μM) components, indicating mixed release of GABA and glycine as previously described in rats and gerbils (n = 2; **Figure 4.1a**, P2; Kotak et al., 1998; Nabekura et al., 2004). Around hearing onset, PSCs were larger and faster and in the LSO neurons tested, were entirely blocked by 1 μM strychnine (n = 5; **Figure 4.1a**, P11). Shown in **Figure 4.1b** is an example of a P11 LSO neuron in which MNTB-evoked PSCs were recorded at different holding potentials. A linear current-voltage relationship was observed (r = 0.998), and the measured reversal potential for the PSCs (-19.5 mV) was in good agreement with the theoretical value (E_{Cl} = -20 mV) (P10-12, n = 3, reversal potential = -17.6 ± 1.1 mV, r = 0.999, corrected for -5 mV junction potential). This indicates that I had a good control of membrane voltage.

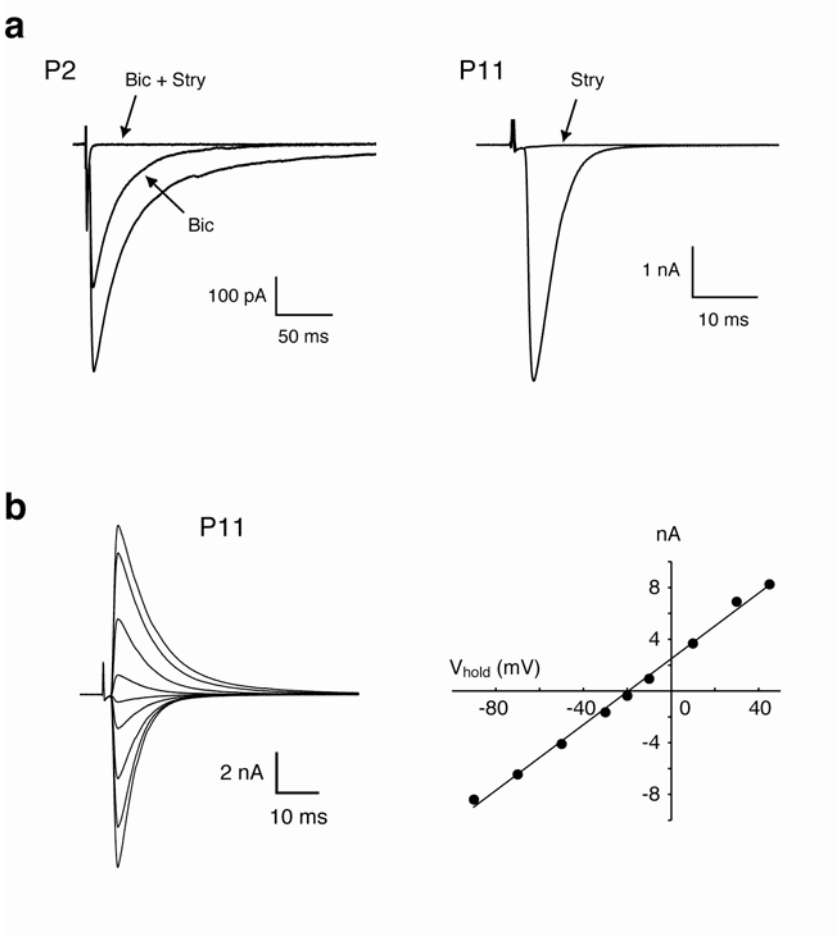

Figure 4.1. MNTB responses in the mouse LSO. (**a**) Shown are two PSCs recorded from a P2 and a P11 LSO neuron. In the P2 PSC shown, peak amplitude was reduced by 36.7% by 10 μM bicuculline (Bic) and the rest was blocked by 1 μM strychnine (Stry). In P11 example, the response was completely blocked by 1 μM strchinine. (**b**) Reversal potential of large MNTB responses in a P11 LSO neuron. Linear current-voltage relationship was observed (r = 0.998) and the reversal potential was -19.5 mV (calculated E_{Cl}= -20 mV).

I first investigated how the maximal MNTB responses onto a single LSO neuron change during this developmental period. As shown in the example traces and stimulus-response curves from P2 and P10 animals (**Figure 4.2a-d**), the peak amplitudes of MNTB-evoked PSCs increased with increasing stimulus intensity. The stimulus intensity was increased up to 1 mA, and the maximal peak PSC amplitude was regarded as the maximal MNTB response the LSO neuron received. Typically, PSC amplitudes peaked at the stimulus intensity of 200 to 400 μA. The maximal MNTB responses increased ~6-fold from 0.84 ± 0.12 nA in the neonates (P1-3, n = 25) to 4.79 ± 0.64 nA in the hearing onset group (P10-12, n = 31) (**Figure 4.2e-h**). Given the -50 mV of driving force, the maximal synaptic conductance (peak current divided by driving force) increased from 17 nS (1-42 nS, P1-3) to 95 nS (7-313 nS). These data demonstrate a large increase in the maximal synaptic conductance activated by the GABA/glycinergic inputs from the MNTB before hearing onset.

My previous data from rats indicated that the increase in maximal PSCs is achieved by strengthening of the maintained MNTB inputs while the number of MNTB inputs decreases significantly. To determine whether this is also true in mice, I recorded PSCs elicited by activation of single MNTB fibers using minimal stimulation technique (see Methods). As shown in **Figure 4.3a-d**, the first responses that emerged from the failures were taken as single-fiber PSCs. These single-fiber PSC amplitudes increased 16-fold from 30.0 ± 4.4 pA (P1-3, n = 21) to 470.2 ± 93.4 pA (P10-12, n = 34) (**Figure 4.3e-h**). By dividing the mean maximal amplitude by that of single input, I estimate that about 28 weak MNTB fibers innervate an LSO neuron in the neonates, whereas about 10 strong fibers converge onto an LSO neuron around hearing onset. Thus I estimate that about two thirds of the initial presynaptic MNTB inputs are functionally eliminated from an LSO neuron during this period.

4.3.2 Evoked MNTB mPSCs

An increase in the amplitude of PSCs can be achieved by an increase in quantal amplitude, release probability, and number of release sites. To determine the contribution of quantal size to the 16-fold increase in single-fiber PSCs, I recorded evoked mPSCs from the MNTB. To specifically obtain mPSCs from MNTB axon terminals, I electrically stimulated

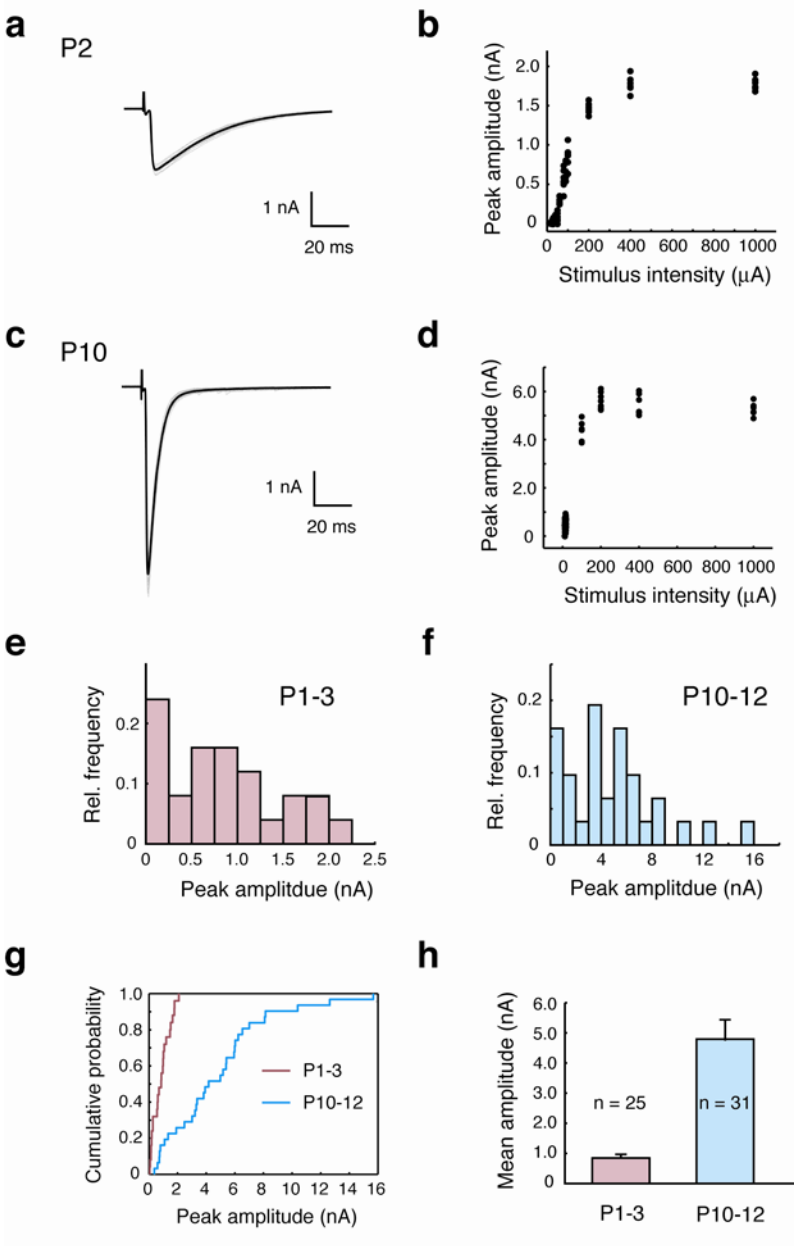

Figure 4.2. Maximal MNTB responses. (**a**) Example of a maximal PSC elicited by MNTB stimulation in a P2 LSO neuron and (**b**) the corresponding stimulus-response relationship. (**c-d**) Example of a maximal PSC in a P10 neurons and the stimulus-response relationship. (**e-f**) Histograms of maximal PSC amplitudes in P1-3 animals and P10-12 animals. (**g**) Cumulative probability distribution of maximal PSC amplitudes. (**h**) Mean maximal PSC amplitudes.

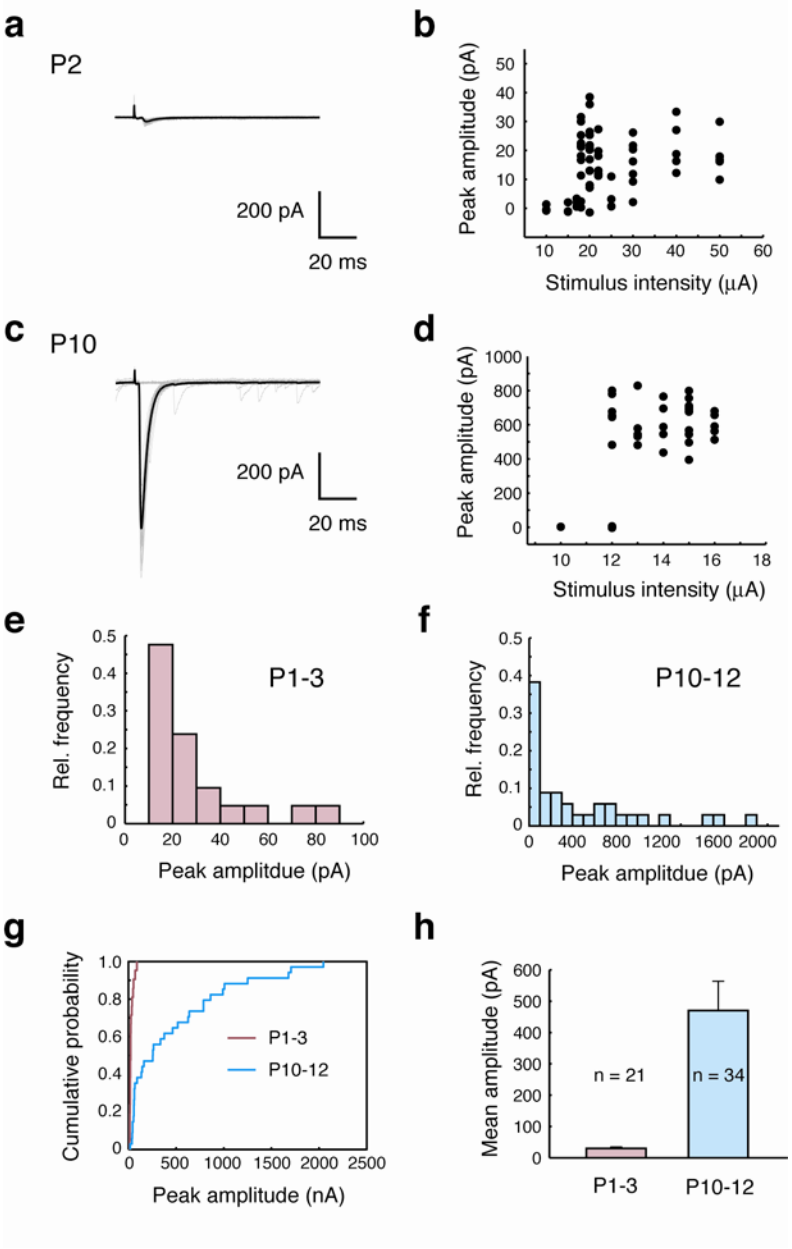

Figure 4.3. Single-fiber MNTB responses. (**a-d**) Example traces and stimulus-response relationships of single-fiber PSCs elicited by minimal stimulation in P2 (**a** and **b**) and P10 (**c** and **d**) LSO neuron. (**e-f**) Histograms of single-fiber PSC amplitudes in P1-3 animals (e) and P10-12 animals (**f**). (**g**) Cumulative probability distribution of single-fiber PSC amplitudes. (**h**) Mean single-fiber PSC amplitudes.

MNTB fibers in the extracellular solution containing 2 mM Sr^{2+} / 0 mM Ca^{2+}. Under this condition, asynchronous release followed by the stimulus-locked responses are promoted, allowing individual quantal events to be resolved. (Goda and Stvens, 1994; Xu-Friedman and Regehr, 1999). In the mouse MNTB-LSO, however, with single stimuli, the frequency of asynchronous events was quite low. To more effectively induce asynchronous events, a train of electrical stimuli at 100 Hz (2 to 10 shocks) was delivered to MNTB axons (**Figure 4.4a** and **b**). The evoked mPSCs were collected from a 3-400 ms window after the stimulus train, and their peak amplitudes were determined (Methods). Mean peak amplitudes of the evoked mPSCs increased 2.5-fold from 29.1 ± 5.1 pA (P1-3, n = 6) to 73.3 ± 6.4 pA (P10-12, n = 4) (**Figure 4.4c**, **d**, and **h**). Histograms (**Figure 4.4e** and **f**) and cumulative histograms (**Figure 4.4g**) of mPSC amplitudes for the two age groups show a clear shift towards larger amplitudes. These data indicate that there is a significant increase in quantal size in the MNTB-LSO pathway. However, this ~2-fold increase in quantal size alone cannot account for the 16-fold increase in single fiber PSC.

4.3.3 Paired-pulse responses of MNTB inputs

Greater PSC amplitudes can also be caused by higher release probabilities via an increased number of vesicles released per action potential. PPRs are commonly used to probe changes in release probability (Debanne et al., 1996; von Gersdorff and Borst, 2002; Davies et al., 1990). Paired-pulse facilitation (PPF; PPR > 1), for example, is thought to occur because the residual Ca^{2+} from the first stimulus results in a higher level of Ca^{2+} in the synaptic terminal upon arrival of the second stimulus and is generally accepted as an indication of low release probability. On the other hand, a high release probability would lead to a paired pulse depression (PPD; PPR < 1) because a large fraction of vesicles are released at the first stimulus and fewer synaptic vesicles will be available at the second stimulus. Thus, a developmental switch from PPF to PPD, for example, would indicate an increase in release probability. To examine whether increased release probability contributes to the increase in MNTB PSC amplitudes, I measured PPRs at different ages.

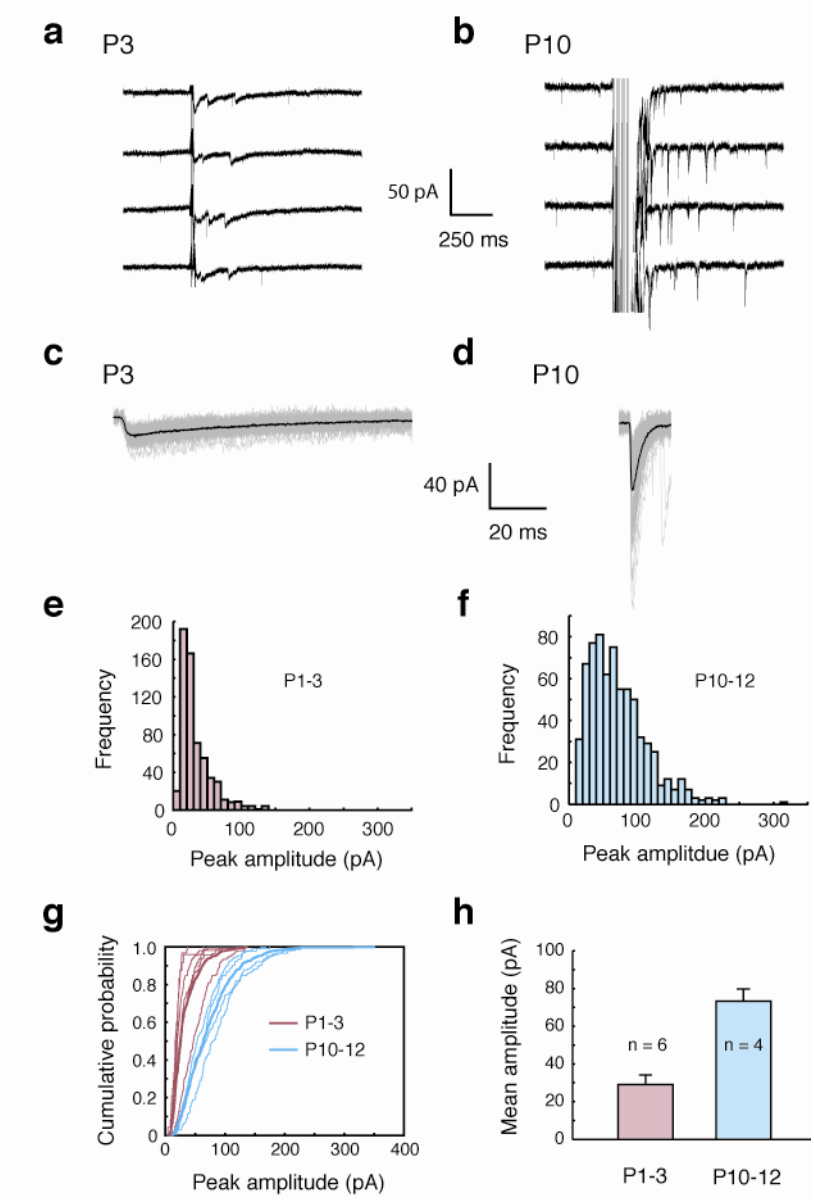

Figure 4.4. Evoked mPSCs by MNTB stimulation in Sr^{2+} (**a-b**) Example traces from a P3 (**a**) and P10 (**b**) LSO neuron. In (**a**) a train of stimuli at 100 Hz with two pulses was used, and in (b) 10 pulses at 100 Hz was used to induce asynchronous events. (**c-d**) Example of evoked mPSCs obtained from a P3 and P10 neurons (same cells as (**a**) and (**b**)). Black traces are the averages of 50 (P3) and 70 (P10) events aligned at the maximal rise (shown in grey). (**e-f**) Amplitude histograms of evoked mPSCs. Total of 609 (P1-3) and 701(P10-12) events from 6 and 4 cells, respectively, were analyzed. (**g**) Cumulative histogram of evoked mPSCs from individual neurons (thin lines) and pooled across the cells (thick lines). (**h**) Mean amplitudes of evoked mPSCs.

Paired-pulse responses at varying intervals were recorded at stimulus intensities at which PSC amplitudes were maximal (200-400 μA, **Figure 4.2b** and **d**) to minimize fluctuations in the number of fibers activated between two pulses. At 10 and 20 ms intervals, the response to the second pulse was significantly more depressed in the younger animals (PPR = 0.71 and 0.79, P1-3, n = 4) than in the older animals (PPR = 0.93 and 0.95, P10-12, n = 9) (**Figure 4.5a** and **b**). At 50 ms or longer intervals, PPRs were 0.9 or greater in both age groups, and there was no statistical difference between the two age groups (**Figure 4.5b**). This could indicate a higher release probability in younger animals (Pouzat and Hestrin, 1997; Brenowitz and Trussell, 2001).

PPD, however, can be caused not only by a reduction in presynaptic release, but also by postsynaptic mechanisms such as receptor desensitization and saturation. (Jones and Westbrook, 1995; Chen et al., 2002). To examine the locus of depression I analyzed the coefficient of variation (CV = std / mean) for the paired-pulse responses. In a binomial model, if PPD occurs due to a postsynaptic mechanism, the mean and standard deviation of the second PSC amplitude will decrease to the same extent, resulting in points above the diagonal in $1/CV^2$ vs. mean plot. On the other hand, if PPD is caused by reduced presynaptic release, points will fall below or on the diagonal because the standard deviation remains relatively unaffected while the mean decreases (Malinow and Tsien, 1990; Kraushaar and Jonas, 2000; Pedroarena and Schwarz, 2003). CVs were computed from individual paired-pulse responses at 10 and 20 ms intervals in P1-3 LSO neurons (n = 4), in which significant PPD was observed, and $1/CV^2$ and mean of the second PSCs normalized to those of the first PSCs were plotted (**Figure 4.5c**). Most points in this plot fell below the diagonal, suggesting a presynaptic origin of the observed PPD. If PPD occurs due to a high release probability such that at a large fraction of release sites vesicle release occurs at the first stimulus, resulting in fewer vesicles available for the second pulse, the second PSC amplitude should be inversely related to the first PSC. As shown in **Figure 4.5d**, there was a strong negative correlation between the second PSC amplitudes and the first (**Figure 4.5d**; $r = -0.47$, $P < 0.05$). Together, my PPR data suggest that release probability might be slightly higher in younger animals. Thus, it is unlikely that increased release probability is responsible for the dramatic increase in MNTB PSC amplitudes.

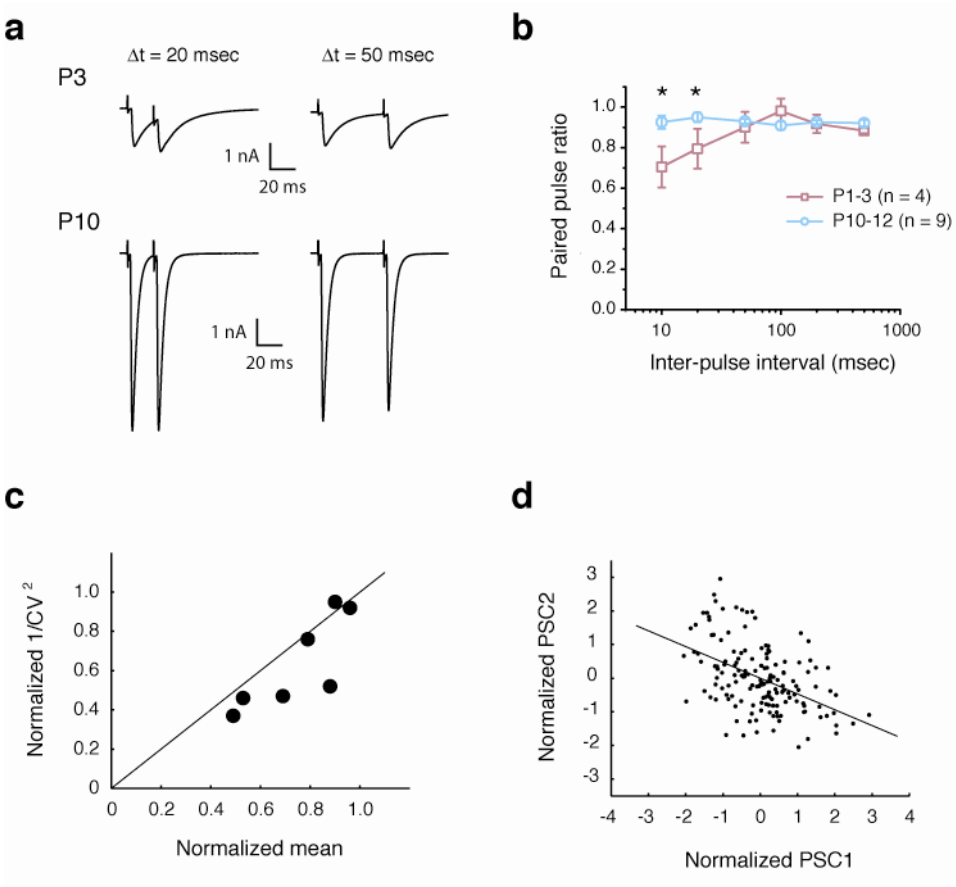

Figure 4.5. Paired-pulse responses of maximal MNTB inputs. (**a**) Example traces of paired-pulse responses from a P3 and P10 LSO neurons at 20 and 50 msec inter-pulse intervals. (**b**) Summary of PPRs at inter-pulse intervals of 10, 20, 50, 100, 200, and 500 msec shown in semi-logarithmic scale. Differences in PPR values at 10 and 20 msec intervals were statistically significant ($P < 0.05$, Student's t-test). (**c**) CV analysis of paired pulse responses. $1/CV^2$ for the PSCs normalized to $1/CV^2$ for PSC1 is plotted against the mean PSC2 amplitude normalized to the mean PSC1 amplitude. Paired-pulse responses at 10 and 20 msec intervals from 4 different cells in the P1-3 group were analyzed. (**d**) Both PSC1 and PSC2 were scaled ([peak amplitude of single trial – mean amplitude for the cell] / [standard deviation of peak amplitude for the cell]) and pooled across cells and intervals. PSC2 and PSC1 were negatively correlated ($r = -0.47$, $P < 0.05$).

4.3.4 Potential contribution of subcellular location of inputs

Principal neurons of the LSO have a bipolar shape with substantial dendritic trees. Because all my recordings were made at the soma, soma-dendritic location of synaptic inputs could also influence my recorded PSC amplitudes (Stuart et al., 2001). An age-dependent shift of synapse location towards the soma has been shown in the MSO (Kapfer et al., 2002). Whether a similar subcellular redistribution of synapses also occurs in the LSO neurons is not known. Even if there is relocation, PSC amplitude change due to the dendritic filtering cannot exceed the changes in quantal amplitudes. Thus, the observed 2.5-fold increase in quantal size provides the upper limit of the contribution of synapse redistribution.

The mean rise time of single-fiber PSC was 1.6 ± 0.08 msec in younger animals (P1-3, n = 19, **Figure 4.6a**) and 0.7 ± 0.04 msec in older animals (P10-12, n = 33, **Figure 4.6b**). This 2-fold reduction in rise time could indicate a synapse relocation toward the soma in the older animals. The rise time of synaptic responses, however, can also be influenced by other factors such as neurotransmitter concentration in the synaptic cleft and postsynaptic receptor distribution (Ali et al., 2000). In addition, in both age groups, the rise time of single-fiber PSCs was not correlated with amplitudes (**Figure 4.6a** and **b**; r = -0.09, P = 0.70, P1-3; r = -0.21, P = 0.24, P10-12). In older animals, most of the small-amplitude inputs (< 100 pA) exhibited rise times indistinguishable from those of large-amplitude inputs (**Figure 4.6b**). This indicates that at least in the older animals, the differences in PSC amplitudes are not largely due to different degree of dendritic filtering. Thus, although it can contribute to some degree, it seems highly unlikely that synapse redistribution is a major mechanism underlying the 16-fold increase in single-fiber PSCs.

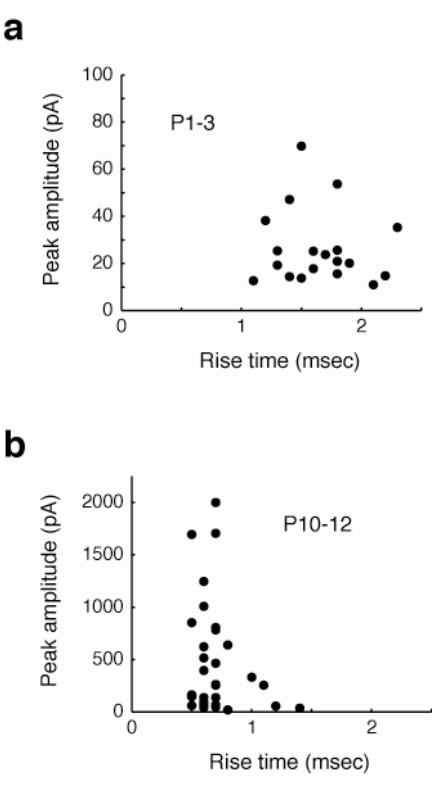

Figure 4.6. Rise times of single-fiber PSCs. 10-90% rise times from single-fiber PSCs from P1-3 animals (**a**) and P10-12 animals (**b**).

4.4 DISCUSSION

4.4.1 Refinement of MNTB-LSO pathway in mice

Based on the single-fiber and maximal MNTB responses, I estimate that the number of MNTB inputs converging onto a single LSO neuron decreases from approximately 28 to 10. During this period, a substantial strengthening of the maintained fibers occurs and outweighs the loss of inputs. There are several potential sources of error in this estimation. First, all my experiments were conducted in slice. Thus, my convergence estimation for both ages is likely to underestimate the actual number of converging inputs in vivo. Second, my estimation of single-fiber PSCs relies on the assumption that the individual MNTB fibers with various strengths are recruited randomly. This, however, may not be true and thus I cannot exclude the possibility that the potential correlation between the activation threshold and the strength of a fiber could have biased my measurements. Finally, especially in the older group, both maximal and single-fiber PSCs exhibited a wide range of amplitude values (**Figure 4.2f** and **4.3f**). This large variation in PSC amplitudes may introduce uncertainty in the exact number of converging inputs. Nevertheless, my data indicate a substantial degree of reduction in the convergence ratio during the developmental period. In addition, the similarities between the data from the two species are remarkable as shown in the reduction in convergence ratio (76 % in the rat vs. 64% in the mouse) and strengthening of individual fibers (12 fold in the rat vs.16 fold in the mouse). Because in this mouse study, the spatial distribution of MNTB neurons that innervate a single LSO neuron was not determined, it remains to be shown whether this substantial reduction in convergence ratio reflects a frequency specific sharpening of topography. In conclusion, these results strongly indicate that mice can be used as a model system to study cellular mechanisms underlying the refinement and maturation of tonotopically organized GABA/glycinergic synapses of the MNTB-LSO pathway.

4.4.2 Synaptic mechanisms underlying the strengthening of MNTB inputs

My measurements of amplitudes of evoked mPSCs from MNTB terminals showed that increase in quantal size can account for about 16% of the observed increase in single-fiber PSC amplitude. The absolute evoked mPSC amplitudes at the two age groups as well as the percent increase are comparable to the GABA/glycinergic mPSC amplitudes recorded in the dissociated rat LSO neurons in TTX over a similar time span (Nabekura et al., 2004): 29 to 73 pA vs. ~25 to ~55 pA (same driving force for Cl^- current). Quantal amplitudes can be increased by a number of mechanisms including increased number of receptors, greater single-channel conductance, and reduced dendiritic filtering (Stuart et al., 2001; Otis et al., 1994). Further analysis will be required to determine in more detail the contributions of these different mechanisms.

My CV analysis, together with the negative correlation between the first and second PSC amplitudes, indicated that the observed greater PPDs in younger animals are likely to be due to reduced transmitter release at the second pulse (**Figure 4.5c**). Decreased release can occur due a depletion of vesicles (von Gersdorff and Borst, 2002) or a reduction in release probability at the second pulse (Waldeck et al., 2000). In any case, it seems highly unlikely that greater release probability in the older animals is a mechanism underlying the increase in synaptic conductance.

The results from quantal size and PPRs strongly indicate that addition of release sites for each axon is a major mechanism underlying the large increase of single-finer inputs. Consistent with this idea, the quantal content of single-fiber PSCs rose from 1 to 6.4. Although it is difficult to determine the actual number of release sites, a quantal content of 1 in the younger animals suggests that at this age individual MNTB fibers may have only one or a few functional release sites (Also note the similarity between the histogram of single-fiber inputs (**Figure 4.3e**) and mPSCs (**Figure 4.4e**)). In older animals, however, considering PPD of less than 10% even at a 10 ms interval, it is likely that each MNTB fiber has more than 10 functional release sites. In conclusion, the strengthening of the maintained MNTB inputs is achieved by an increase in quantal amplitudes and a large increase in the number of release sites per axon.

A developmental increase in inhibitory postsynaptic currents has been reported in other neighboring nuclei of superior olivary complex (Smith et al., 2000; Awatramani et al., 2004a and b). In MNTB principal neurons, for example, synaptic currents elicited by GABA/glycinergic inputs increased from during the first four postnatal weeks and this increase was primarily

mediated by glycinergic transmission (Awatramani et al., 2004b). Around hearing onset, the mean peak PSC amplitude was ~430 pA (adjusted to –50 mV driving force for comparison with my data) and single-fiber peak amplitude was ~170 pA with mean the quantal amplitude of 87 pA. In the LSO, mean PSC amplitude was 4.8 nA (maximal) and 470 pA (single-fiber) with quantal amplitude of 73 pA. Thus around hearing onset, the maximal PSC amplitude was ~10 times as large in the LSO as in the MNTB while the quantal amplitude was comparable. The 10-fold difference in maximal PSC seems to be due to 3-fold larger single-fiber PSC and a greater number of inputs (~10 vs. ~3). In animals older than P20, the maximal and single-fiber PSC amplitudes in the MNTB were much larger than those in younger animals (6.2 nA and 1.3 nA, respectively), without much change in the number of inputs (~3 inputs). The quantal amplitude also greatly increased to be 275 pA in the older animals. Thus, in the MNTB, glycinergic synaptic currents significantly increase after hearing onset and this is primarily due to the increase in quantal amplitude. Because I did not record from animals older than P12, it is possible that there is a further increase in the LSO as well after hearing onset. It is also possible, however, that the two systems have different developmental time courses.

5. ROLE OF OLIVOCOCHLEAR EFFERENTS IN THE MNTB-LSO REFINEMENT

5.1 INTRODUCTION

During the development of excitatory synapses, immature exuberant inputs become eliminated via activity-dependent mechanisms (Lichtman and Colman, 2000; Katz and Shatz, 1996). Furthermore, there is evidence that neuronal activity is not only required, but also can play an instructive role in the circuit refinement (Stellwagen and Shatz, 2002). In Chapter 2 and 4, I presented evidence that GABA/glycinergic MNTB-LSO pathway become organized by a large degree of functional elimination of aberrant inputs and strengthening of the maintained ones. A key hypothesis is that this refinement process of neuronal circuits that use GABA and glycine as neurotransmitters also require neuronal activity or can be instructively shaped by activity as shown in excitatory systems. In my previous study, I have found that functional elimination of the GABA/glycinergic inputs to the LSO occurs before hearing onset, raising the possibility that spontaneous activity in the auditory pathway prior to hearing (Kros et al., 1998) may play a role in organizing the MNTB-LSO circuitry.

Olivocochlear efferent neurons reside in the superior olivary complex, receive afferent inputs from the cochlear nucleus, and project back to the cochlea (**Figure 5.1**; Warr, 1992). In adults, medial olivocochlear (MOC) neurons, which are primarily cholinergic, innervate outer hair cells (OHCs) and are thought to protect the cochlea from acoustic injury by providing inhibitory feedback (Maison, et al., 2002; Luebke and Foster, 2002). During development, however, these cholinergic efferents innervate inner hair cells (IHCs) and have formed functional synapses by birth (Bruce et al., 2000; Cole and Robertson, 1992; Glowatzki and Fuchs, 2000). Direct electrophysiological recordings from IHCs in neonatal rats showed that the cholinergic inputs hyperpolarize IHCs by activating Ca^{2+}-activated potassium channels (Glowatzki and Fuchs, 2000). The authors suggested that this hyperpolarization could impose rhythmicity on spontaneous activity. Interestingly, in neonatal cats, in which rhythmic spontaneous firing of

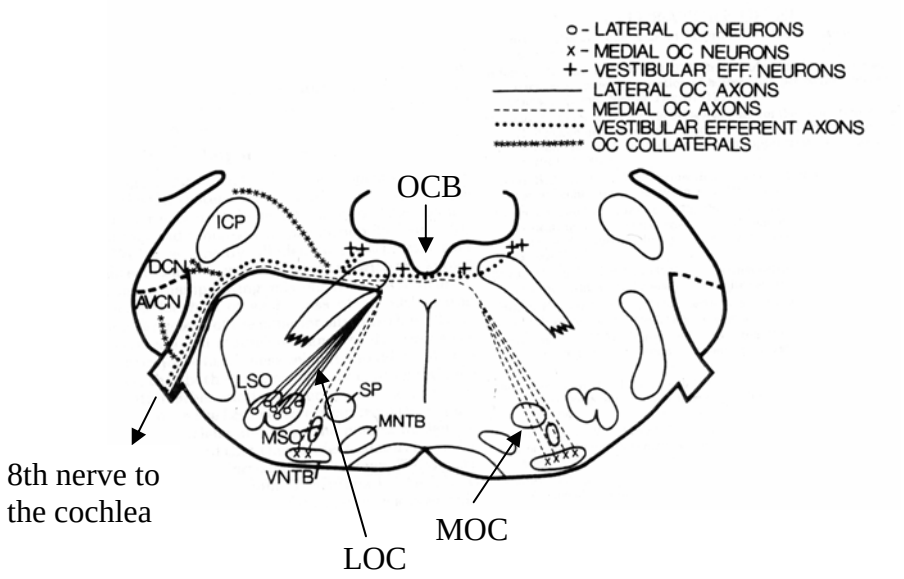

Figure 5.1. A schematic illustration of the olivocochlear efferent systems to illustrate origins and courses of olivocochlear efferent fibers. Lateral olivocochlear (LOC) neurons are located in the LSO whereas medial (MOC) neurons are found in the ventral nucleus of the trapezoid body (VNTB). In the rat, about a half of the olivocochlear efferent neurons are MOC neurons, and about two thirds of the MOC fibers cross the midline just beneath the 4th ventricle to project to the contralateral cochlea. In the rat, the LOC neurons exclusively project to the ipsilateral cochlea. OCB: olivocochlear bumdle. (Adopted from White and Warr, 1983.)

auditory nerve is observed, the rhythmic firing was abolished upon sectioning of the olivocochlear bundle (OCB) (Walsh and McGee, 1997; **Figure 5.1**). Therefore, it is likely that eliminating the cholinergic inputs from the MOC efferent neurons will alter the level or temporal patterns of spontaneous activity in the auditory pathway before hearing onset.

If the early cholinergic inputs from the olivocochlear neurons are an important component of spontaneous activity, eliminating these inputs would allows us to address the hypothesis that spontaneous activity is important for organizing brainstem circuit. To explore this possibility, I took two approaches. First, I lesioned the OCB in P2 rats (**Figure 5.1**). The medial olivocochlear neurons send out their axons dorsally and, in rats, about two thirds of these axons cross the midline as a fiber bundle right below the floor of the 4th ventricle (White and Warr, 1983). Sectioning the OCB would eliminate this cholinergic innervation. My second approach was using mice lacking α9 nicotinic acetylcholine receptor (nAChR) subunit (α9 KOs). Mammalian IHCs express unique nAChR subunits, α9 and α10. Because α10 subunits alone do not form functional receptors, in α9 KOs the cholinergic transmission via nicotinic receptors should be absent (Vetter et al., 1999; Elgoyhen et al., 2001). Vetter et al. have demonstrated that in α9 KOs although the MOC fibers are still present, electrical stimulation of MOC fibers did not have an effect on auditory nerve responses or distortion product otoacoustic emission (Vetter et al., 1999). Using the above two approaches, I asked whether the cholinergic feedback to the cochlea is crucial in refining the GABA/glycinergic connections of the MNTB-LSO pathway.

5.2 METHODS

5.2.1 Animals and slice preparation

Acute brainstem slices were prepared from P10-12 control (129S6/SvEv) or α9 KO mice as described previously. α9 KO founder mice were kindly provided by Dr. D. Vetter at Tufts University.

5.2.2 OCB section and acetylcholinesterase (AChE) staining

P2 rat pups were anesthetized by hypothermia and placed on a stereotaxic device with an adapter for small animals. An incision was made on the posterior dorsal surface of the head along the midline to the back of the neck. The skull was exposed and two rostrocaudal lesions were made in the occipital bone between the lamda and foramen magnum and medial to the lateral sinuses using cauterization. The bone flap was opened, still attached to the dura toward the spinal cord. Dura mater was carefully removed to expose the immature cerebellum. Using fine forceps, the cerebellum was lifted up to expose the floor of the 4th ventricle. The choroid plexus on the floor of the 4th ventricle was carefully removed using a tissue wick. OCB was lesioned either by a cut made by a knife custom made using steel wire or by electrolytic lesion. In the case of the knife cut, the knife (~1 mm) was positioned along the midline on the floor of the 4th ventricle at the beginning of the cerebral aqueduct. The knife was vertically lowered 2 mm to sever OCB. For electrolytic lesion, a tungsten electrode was placed the same way and lowered by 2 mm. A positive current pulse of 300 μA was passed using a stimulation isolation unit for 5 seconds to electrolytically lesion the OCB bundle. Two more lesions were made at positions slightly rostral and caudal to the initial penetration position along the midline. A piece of gelfoam was gently placed in the posterior fossa, the bone flap was placed back to cover the brain, and the incision was sutured. The animals were allowed to recover on a heatblock before they were returned to their mother.

To confirm OCB lesion, AChE staining was done following the protocol in Adams (1995). Brain slices obtained during slice preparation for physiology were fixed and sectioned at 80 μm. Sections obtained from brain slices were washed in distilled water and placed in a medium containing: 12.5 ml 0.1 M acetate buffer (pH = 5.0), 1.7 ml 30 mM cupric sulfate, 2.5 ml 0.1 M glycine, 0.03 g acetylthiocholine, 8.5 ml water. Sections were gently agitated in the medium for 20 minutes, washed, and placed in 0.1 M sodium ferricyanide for 3 min. Sections were washed again, and the staining was visualized using a reduced silver-reaction product: 1.0 % sliver nitrate (1 min), wash, reduced in 1 % hydroquinone/ 1 % sodium sulfite (3 min), wash, 3 % sodium thiosulfate (3 min). AChE reaction product appeared as dark staining (**Figure 5.2a**).

5.2.3 Electrophysiology and data analysis

For mouse experiments, except during initial preliminary recordings, the experimenter was blind to the genotype of the animals until the analysis was finished. Minimal and maximal responses were obtained as described in Chapter 4 using electrical stimulation. Only1 or 2 LSO neurons were recorded per MNTB-LSO pathway to avoid bias introduced by slicing.

5.3 RESULTS

5.3.1 Refinement of MNTB inputs in OCB-sectioned rats

To determine whether olivocochlear efferents are important for the refinement of MNTB-LSO pathway, I measured single-fiber and maximal PSCs (Chapter 2 Methods) in P11-14 rats whose OCB was lesioned at P2. The lesion was assessed by AChE staining (Methods). In control animals, OCB was visualized as a strong dark staining whereas it was missing in lesioned animals using a knife cut or electrolytic lesion (**Figure 5.2a**). In **Figure 5.2b**, mean peak amplitudes of the maximal MNTB PSCs at P10-14 are shown for three experimental groups: 1) control (data from Chapter 2), 2) animals with successful OCB (OCB), and 3) animals in which lesion was not successful (uncut). Although the maximal MNTB PSCs were somewhat larger in OCB and uncut group (4.5 ± 0.5 nA (normal, n = 18), 6.3 ± 1.5 nA (OCB, n = 12), 8.5 ± 1.5 (uncut, n = 7)), the differences were not statistically significant (**Figure 5.2b**, P = 0.09, ANOVA).

Single-fiber PSCs from OCB-lesioned animals were, however, significantly smaller than those in control animals (**Figure 5.2c**, 720 ± 135 pA, n = 23 (control), 198 ± 66 pA, n = 12 (OCB), bonferroni post-hoc test following ANOVA). These results indicate that the medial olivocochlear efferent fibers are important in the developmental strengthening of MNTB inputs. Moreover, the smaller single-fiber PSC amplitudes in OCB-lesioned animals in the presence of unchanged maximal PSC amplitudes suggest a higher convergence of MNTB inputs in lesioned

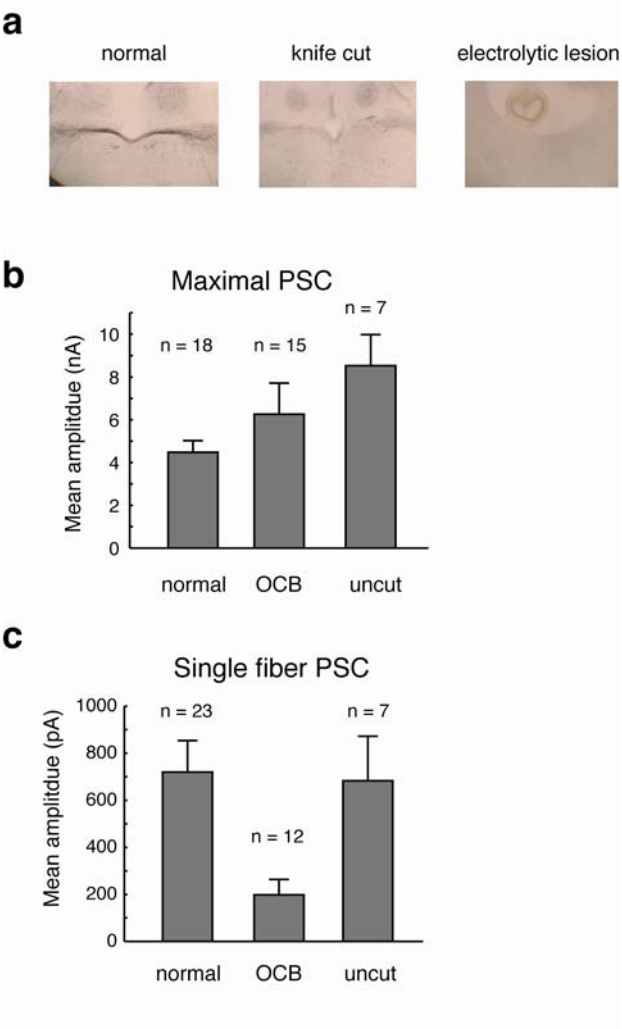

Figure 5.2. Strengthening of MNTB inputs in OCB-lesioned rats. (**a**) OCB lesion was assessed by AChE reaction procedure. Shown are OCB staining where it crosses midline in normals animals, and absence of staining in the lesioned animals with either knife cut or electrolytic lesion. Sections are from the animals in which recordings were made. (**b**) Mean maximal MNTB PSCs amplitudes in P10-14 normal, OCB-lesioned, and animals in which the lesion was attempted, but OCB was missed. The PSC amplitudes between groups were not statistically significant (P = 0.09, ANOVA) (**c**) Mean single-fiber PSC amplitudes. The mean amplitude in the OCB-lesioned animals was significantly different from the normal animals (ANOVA followed by bonferroni post-hoc test).

animals. I estimated that ~6 MNTB inputs innervate a single LSO neuron in the normal group, whereas ~32 inputs innervate an LSO neuron in OCB-lesioned animals.

5.3.2 Refinement of MNTB inputs in α9 nAChR KO mice

My OCB lesion experiments in rats suggest that the medial olivocochlear efferents might be crucial in the refinement of MNTB inputs. It is possible, however, that cutting or lesioning the OCB also injured nearby structures (e.g., Raphe nucleus) of other unidentified components of the brainstem development. To avoid these shortcomings, I took another independent approach to address the question using α9 KO mice in which cholinergic efferent inputs are specifically silenced.

To determine whether the refinement of the mouse MNTB-LSO pathway (Chapter 4) occurs normally in the absence of cholinergic feedback to the cochlea, I measured maximal and single MNTB fiber responses in LSO neurons of α9 KO. The results in these experiments are summarized in **Figure 5.3** along with the data from control animals. In α9 KO animals, the amplitudes of maximal MNTB PSCs increased from 0.87 ± 0.26 (P1-3, n = 6, 4 animals) to 3.93 ± 0.36 nA (P10-12, n = 57, 26 animals) (**Figure 5.3a**, α9 KO). These amplitudes did not differ from those in age-matched control animals (P1-3: 0.84 ± 0.12 nA, n = 25, P = 0.91; P10-12: 4.79 ± 0.64 nA, n = 31, P = 0.21, Student's t-test). In α9 KOs, there was also a significant increase in single-fiber PSC amplitudes from 29 ± 9 pA (P1-3, n = 6) to 200 ± 52 pA (P10-12, n = 57) (**Figure 5.3b**). However, this increase was significantly less than the increase in single-fiber PSCs in control animals (α9KO: 29 ± 9 pA to 200 ± 52 pA, P1-3, n = 6; control: 30 ± 4 pA to 470 ± 93 pA, P1-3, n = 34) (**Figure 5.3b**).

The amplitude distributions of single-fiber PSCs reveal that the smaller mean value in α9 KO animals is due to a higher fraction of weak inputs (**Figure 5.4**). As compared in the amplitude histograms in **Figure 5.4a** and **b**, in α9 KOs, approximately twice as many inputs had amplitudes smaller than 100 pA and inputs greater than 500 pA were rarely observed. This difference is clearly demonstrated in cumulative distributions of single-fiber PSC amplitudes (**Figure 5.4c**, $P < 0.05$, Kolmogorov-Smirnov test).

The higher fraction of weak fibers could represent a higher fraction of distal dendritic inputs in α9 KOs. To examine this possibility, I measured rise times of single-fiber PSCs in both groups at P10-12 (**Figure 5.5**). In both groups, however, there was no significant correlation between amplitude and rise time (control: r = -0.21, P = 0.24; α9 KO: r = -0.14, P = 0.24, linear regression). In addition, the distributions of rise times from the two groups were not different (mean rise time, control: 0.7 msec, KO: 0.8 msec; P = 0.14, Kolmogorov-Smirnov test). Thus, it is unlikely that the higher fraction of small PSC amplitudes in α9 KOs represent a difference in soma-dendritic distribution in the two groups. Taken together, my data indicate that strengthening of individual MNTB inputs are impaired in the mice lacking α9 nAChR subunit.

Based on the mean single-fiber and maximal MNTB PSC amplitudes, I estimate that in α9 KOs, each LSO neuron receive ~30 MNTB inputs in neonates, similar to control neonates, but around hearing onset, each LSO neuron still receives ~20 MNTB inputs instead of ~10 (controls). These results suggest that in α9 KOs, each LSO neuron receives twice as many MNTB inputs as in controls, and most of these exuberant fibers are weak inputs.

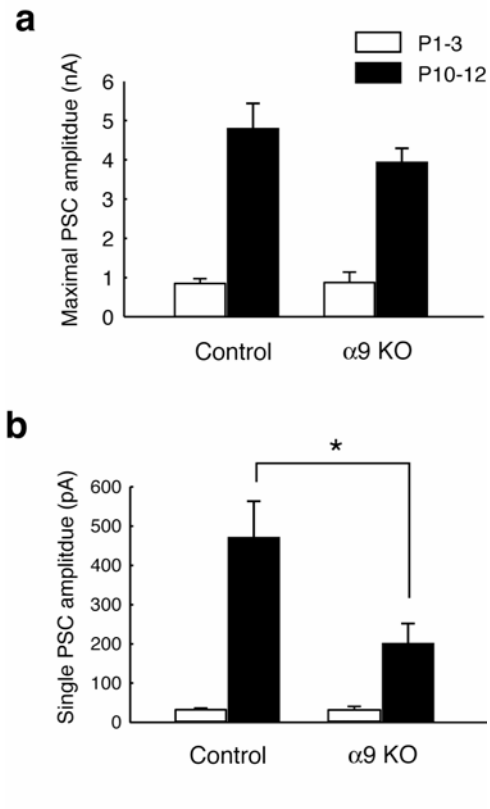

Figure 5.3. Strengthening of MNTB inputs in α9 KO mice. (**a-b**) Developmental changes in mean amplitudes of maximal PSCs (**a**) and single-fiber PSCs (**b**) are shown for both control and KOs. For both (**a**) and (**b**), white bars: P1-3 and black bars: P10-12. Asterisk in (**b**) indicates statistical significance in mean single-fiber PSC amplitude between controls and KOs in the P10-12 group ($P < 0.05$, Student's t-test).

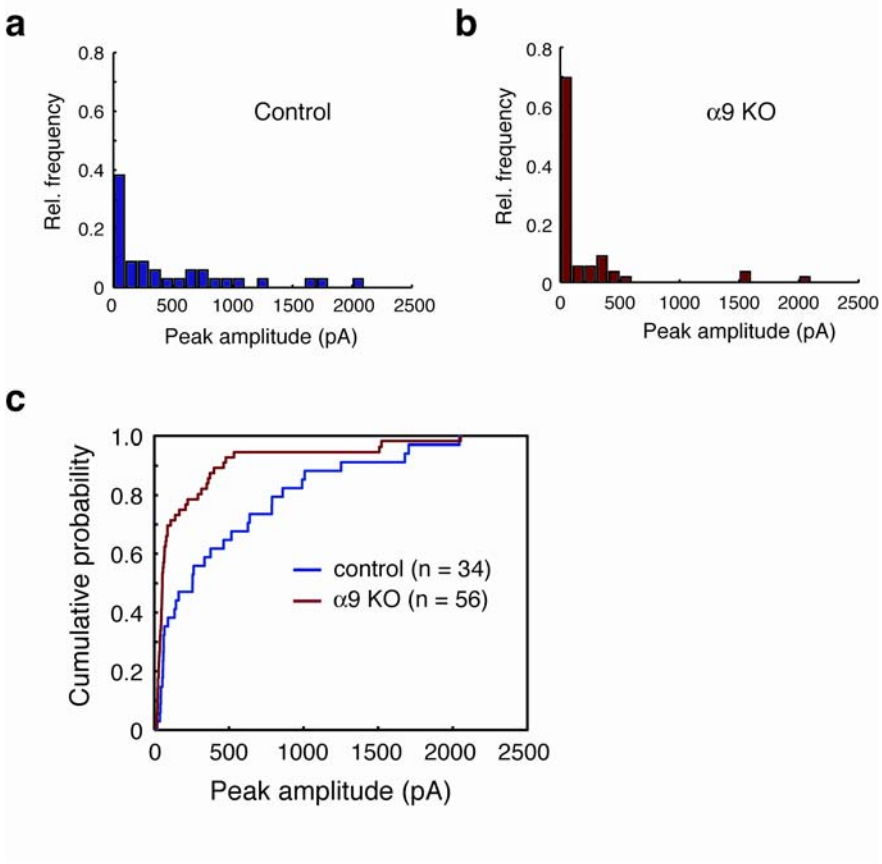

Figure 5.4. Amplitude distribution of single-fiber PSCs in α9 KO mice. (**a-b**) Amplitude histograms for single-fiber PSCs for control (**a**) and KO (**b**) animals. (**c**) Cumulative distribution of single-fiber PSCs amplitudes were significantly different ($P < 0.05$, Kolmogorov-Smirnov test).

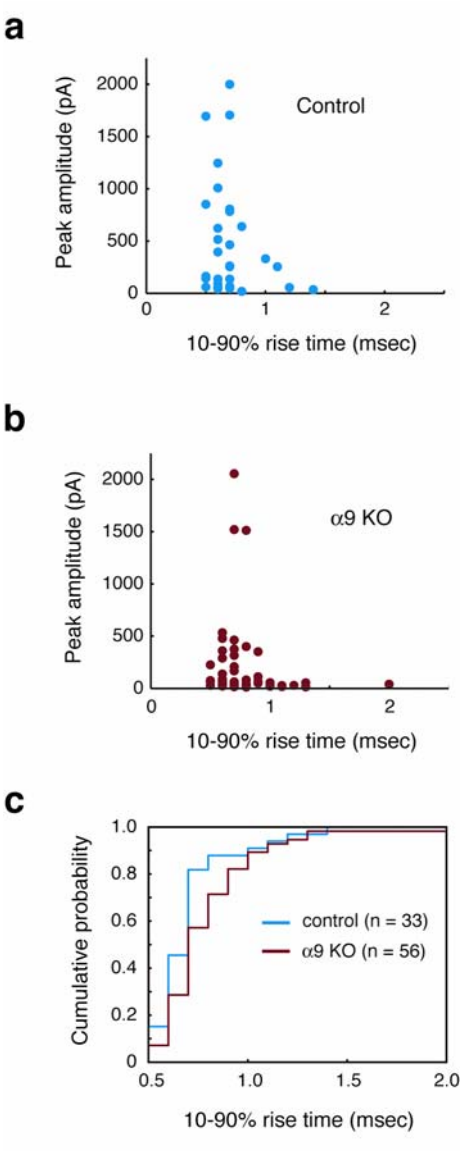

Figure 5.5. Rise times of single-fiber PSCs in control and α9 KO mice. (**a**-**b**) Peak amplitudes of single-fiber PSCs are plotted against 10-90% rise time. (**c**) Cumulative distribution of rise times were not significantly different (P = 0.14, Kolmogorov-Smirnov test).

5.4 DISCUSSION

My lesion experiments showed that in OCB-lesioned rats individual MNTB inputs were weaker than normal animals. The data from α9 KO mice also indicated that strengthening of MNTB inputs is impaired such that there are more weak fibers (< 100 pA) and fewer strong (> 500 pA) fibers around hearing onset. In both cases, maximal PSC amplitude did not significantly differ from controls. Thus, two independent approaches in two different species yielded similar results, strongly indicating that normal function of cholinergic innervation of IHC by MOC neurons is necessary for MNTB-LSO development.

It remains to be shown that through what mechanisms the MOC inputs influenced the refinement of the MNTB-LSO pathway. In addition to changing spontaneous activity in the cochlea, other mechanisms are possible. For example, since the cell bodies of MOC neurons are in the SOC, the observed effect could be due to some kind of local interactions within the brainstem. It is possible that MOC neurons normally exert trophic effects on MNTB and LSO neurons by local release of acetylcholine acting on receptors that do not require α9 subunit for their functioning. Indeed several studies indicate that acetylcholine is involved in inducing neuronal plasticity in the auditory system (Ji et al., 2001; Hsieh et al., 2000). It is likely, however, that the effect originates in the cochlea because the α9 nAChR subunit is not expressed elsewhere in the brain and thus in α9 KOs cholinergic inputs are silenced *only* in the cochlea (Elgoyhen et al, 1994). If the MOC neurons die in OCB-lesioned or α9 KO animals, this could affect the circuit refinement. The presence of MOC fibers in the brainstem and cholinergic terminals in the cochlea in α9 KOs, however, indicates that MOC neurons maintain their central projections despite the compromised cholinergic transmission in the cochlea (Vetter et al., 1999). Also, in my recordings, there was no obvious abnormality in morphology of the LSO and MNTB, and the neurons in the nuclei, as judged by IR images during recordings. As a way of more carefully examining whether there are changes in cellular properties in KOs, it will be useful to examine in more detail morphology and membrane properties of LSO neurons in the manipulated animals.

If the impaired refinement is due to some changes in the cochlea, the changes influenced the MNTB-LSO connections that are 2-3 synapses away. The most likely explanation is that

levels and/or temporal patterns of activity are altered in the cochlea and the difference in activity propagated down to the MNTB and LSO. Consistent with this idea, it has been shown that the cholinergic inputs can hyperpolarize the IHCs and counteract spontaneous Ca^{2+} action potentials before hearing onset (Glowatzki and Fuchs, 2000). Because the spontaneous firing of immature IHCs is thought to be a major source of spontaneous activity before hearing onset, I expect that MOC inputs participate in shaping spontaneous activity. Direct measurement of spontaneous activity in vivo from wild types and α9 KOs will be required to determine whether it is indeed the case.

It is not straightforward to predict in which direction the silencing of MOC inputs would bring the activity level. In the absence of hyperpolarizing MOC inputs, IHCs may fire without interruptions at an increased mean firing rate. This could mean the absence of burst-like activity, which has been shown to cause synaptic plasticity in other systems (McLean et al., 1996). On the other hand, it is also possible that certain level of inhibition by cholinergic inputs is required for maintaining the firing of IHCs. In that case, silencing of MOC inputs could decrease the firing rate of IHCs.

The MOC efferents not only innervate the cochlea but also send out collaterals to the CN (Mulders et al., 2003). The MOC inputs in the CN seem to have an excitatory effect on a subset of neurons called stellate cells (Fujino and Oertel, 2001; Mulders et al., 2003). Although these neurons do not provide major inputs to the LSO or MNTB, they could have an indirect effect on activity by interacting with other neurons in the CN that project to the MNTB and LSO. The degree of impairment in strengthening of single inputs seemed larger in the OCB-lesioned rats than in α9 KOs (73% vs. 57%). This difference could perhaps be due to the fact that in OCB-lesioned animals MOC inputs both to the cochlea and the CN are removed whereas in α9 KOs cholinergic inputs are removed only in the cochlea.

Even if altered activity in the efferent-manipulated animals is responsible for the effect, it does not necessarily mean that activity played an instructive role in the refinement. Afferent activity is crucial for the survival of young CN neurons (Born and Rubel, 1988). Blockade of auditory nerve activity inhibits protein synthesis and leads to cell death. It is thus possible that altered activity could have an effect on the viability of CN neurons that project to the SOC. If this were the case, there would have been indications such as smaller CNs; however, in my observations, there was no obvious change in CN morphology in the efferent-manipulated

animals. Also, α9 KO animals exhibit normal overall auditory function except the specific effect by MOC efferents (Vetter et al., 1999; May et al., 2002).

It could also be that activity played a permissive role in that a threshold level of activity is required to read out certain molecular cues. Or neurons may need a range of activity level, below or above which synaptic reorganization is impaired. An instructive role by activity is also possible. It may be that certain frequency of bursting activity may be required to sort out different inputs or that certain spatial pattern or certain degree of correlation among the inputs are important for establishing the correct connectivity.

The developmental innervation of IHCs by the MOC efferents has been hypothesized as a "waiting period" in which the efferent axons innervate IHCs because their final target, OHCs have not matured yet (Simmons et al., 1996). In this hypothesis, no functional implication of the transient innervation has been recognized. Neonatal lesioning of the OCB in cats permanently impaired tuning properties of the auditory nerve most likely by reducing basilar membrane tuning by OHCs (Walsh et al., 1998). However, in that study the effect of removing olivocochlear efferent inputs on the development of auditory brainstem circuitry has not been examined. Thus abnormal organization of central circuits could have also contributed to the impaired tuning.

In Chapter 2, by mapping functional connectivity of the MNTB-LSO, I have shown that the elimination of exuberant inputs is frequency specific, resulting in a sharper topography. In the current study, I did not investigate this aspect of refinement. It will be important to determine whether the smaller degree of elimination in OCB-lesioned animals or α9 KOs results in broader input maps in the MNTB.

In conclusion, my results from both OCB-lesion in rats and α9 KO mice suggest that the developmentally temporary innervation of IHCs by cholinergic MOC efferents may be a crucial step in organizing the central brainstem circuits. I further propose that this is due to changes in spontaneous activity before hearing onset.

6. DISCUSSION

6.1 TOPOGRAPHIC SHARPENING OF A DEFINED INHIBITORY NETWORK

In my mapping experiments, I found that the functional elimination of immature GABA/glycinergic inputs results in a sharper topographic organization during the refinement of a tonotopic map. To my knowledge this is the first demonstration of a functional refinement of a defined inhibitory circuit in the mammalian brain. The existence of transient functional connections suggests that neuronal activity and synaptic interactions may influence or guide the reorganization of the inhibitory connections. The topographic refinement occurred while the MNTB inputs are excitatory, raising the possibility that depolarizing action of GABA and glycine could be a mechanism underlying the activity-dependent rearrangement of inhibitory synaptic connections.

Hebbian plasticity such as LTP and LTD is thought to underlie the activity-dependent competition of excitatory connections during development (Katz and Shatz, 1996). As shown in the context of learning and memory, NMDA receptors play a pivotal role as a coincidence detector of pre- and postsynaptic activity. Correlated presynaptic inputs strongly activate postsynaptic NMDA receptors and cause Ca^{2+} influx. This Ca^{2+} entry through NMDA receptors leads to LTP and perhaps to a stabilization of the inputs via some kind of retrograde signaling (Constantine-Paton and Cline, 1998). Likewise, uncorrelated inputs may undergo LTD and be subsequently eliminated. The stabilization of correlated inputs by itself could also lead to concomitant destabilization of the other uncorrelated inputs (Ruthazer and Cline, 2004).

How would inhibitory inputs that *hyperpolarize* postsynaptic cells compete? My data suggest that competition mostly occurs while the MNTB inputs are depolarizing. The GABA/glycinergic MNTB inputs alone, without the activation of glutamatergic synapses from the ipsilateral CN, can increase intracellular Ca^{2+} in LSO neurons (Kullmann et al., 2002). In the absence of glutamatergic transmission, GABA/glycine-induced Ca^{2+} responses were mediated by

voltage-gated Ca^{2+} channels. This elevation of Ca^{2+} could then trigger signaling pathways that lead to strengthening or weakening of GABA/glycinergic synapses (Gaiarsa et al., 2002). In cultured hippocampal neurons, coincident activation of pre- and postsynaptic neurons caused long-lasting modifications of GABAergic responses (Woodin et al., 2003). This plasticity required activation of L-type Ca^{2+} channels, and coincident activity resulted in a long-term decrease in the activity of K^+-Cl^- cotransporters, resulting in an elevation of intracellular Cl^- level.

If GABA/glycinergic inputs are activated simultaneously with the ipsilateral glutamatergic inputs, the depolarization elicited by the GABA/glycinergic inputs may facilitate the removal of Mg^{2+} block of the NMDA receptors at glutamatergic synapses (Ben Ari, 1997; Caillard et al., 1999). In this scenario, the GABA/glycinergic synapses could be modified by Ca^{2+} entry through the NMDA receptors at glutamatergic synapses caused by a concurrent activation of glutamatergic inputs. Since this kind of interaction can occur at a subthreshold level depolarization, the ipsi- and contralateral synapses that are spatially close would have greater chances to influence each other.

Recently, it has been shown that MNTB inputs release glutamate in addition to GABA and glycine (Gillespie and Kandler, 2003). Physiological and anatomical evidence suggested that individual MNTB neurons can release all three neurotransmitters. The glutamate response had a large NMDA component and was most pronounced during the first postnatal week. It is plausible that the depolarization induced by GABA and glycine and the release of glutamate together could activate NMDA receptors. This finding opens the possibility that NMDA receptor-dependent modification of GABA/glycinergic synapses underlies the reorganization of inhibitory connections.

LTD has been has been implicated as a step toward input elimination (Allen et al., 2003; Celikel et al., 2004). Silencing of a subset of MNTB inputs could occur via LTD-like mechanisms triggered by various cellular mechanisms suggested above. However, a question remains how an LSO neuron distinguishes the inputs from different topographic regions and selectively silences the topographically “wrong” inputs. Let’s say in young animals an LSO neuron receives inputs from three future isofrequency bands in the MNTB. At hearing onset, only the inputs from the middle band are maintained and those from the side bands become silenced. One possibility is that from the outset the inputs from the side bands are weaker;

therefore, assuming excitatory action by GABA and glycine, the inputs from the middle band can drive the LSO neurons more efficiently. According to Hebbian rules, the middle band inputs are potentiated while the side band inputs become weakened. In this scenario, the selection of inputs is largely dictated by an initial bias in synaptic weights.

In addition to the initial bias, LSO neurons may be able to distinguish inputs from different topographic regions because of a higher correlation of activity within a band than across bands. This implies a mechanism that coordinates activation of MNTB neurons within a similar topographic region. One potential source of correlation could simply be a sharing of common inputs by neighboring neurons. In the projections from a row of IHCs to the CN and from the CN to the LSO and other higher nuclei, a single presynaptic neuron provides divergent inputs into a frequency lamina. This connectivity by itself could increase the chances of activating nearby neurons. There could also be local networks within an isofrequency lamina that coordinates firing of neighboring neurons.

In the visual system, retinal waves sweeping across the retina before eye opening play an important role in circuit development. Currently it is not known whether there is any spatial pattern in spontaneous activity either in the organ of Corti or in the auditory brainstem. Hypothetically one could think of a sequential activation of neighboring frequency bands with certain delays. For a postsynaptic neuron, the sequential activation of groups of inputs could create relative temporal relationships among pre- and postsynaptic activations. Temporal relationships between pre- and postsynaptic neurons have been shown to be important in spike timing-dependent synaptic plasticity and could play a role in sculpting the connectivity patterns (Bi and Poo, 2001).

In addition to spatiotemporal activation patterns among MNTB inputs, coincident activation of frequency-matching ipsi- and contralateral inputs to the LSO may also be a mechanism for organizing MNTB-LSO pathway. MNTB inputs may undergo LTP or LTD depending on their temporal relationship with excitatory CN inputs. It is not known whether ipsilateral inputs also undergo a refinement process. If they do, it will be important to know the relative time course of the refinement of CN and MNTB inputs. If the refinement of CN inputs precedes that of MNTB inputs, for example, the former may serve a template for organizing the latter. In the mature LSO, not only the inputs from the either side are tonotopically organized but also those two inputs are aligned so that frequencies are matched at a single LSO neuron level.

Therefore, interactions between the two inputs during the fine-tuning are highly likely and could be an important mechanism achieving both sharpening of topography and frequency-alignment.

6.2 STRENGTHENING OF THE GABA/GLYCINERGIC INPUTS

I found that the refinement of the MNTB-LSO pathway was accompanied by a large increase in synaptic conductance elicited by individual MNTB fibers. This was due to a moderate increase in quantal size and a larger increase in the number of release sites formed by each MNTB fiber. These changes are similar to what has been described in the glutamatergic retinogeniculate synapse during the period of substantial input elimination (Chen and Regehr, 2000). Since my study focused on the period before hearing onset, it is unclear whether the strength of inhibitory inputs to LSO neurons would continue to increase after hearing onset. Recordings from MNTB neurons in 3-4 week old animals have demonstrated that the major increase occurs after hearing onset (Awatramani et al., 2004a and b). However, since the observed increase in the LSO by hearing onset is quite large (the largest conductance was comparable to the value described in the MNTB), I speculate that the major increase in synaptic conductance may be achieved before hearing onset.

Is the observed increase in synaptic conductance the result of LTP-like mechanisms? Formation of new spines after induction of LTP has been shown in the hippocampus (Engert and Bonhoeffer, 1999). It is possible that new synaptic release sites form as a result of LTP. There is no example of LTP in which synaptic conductance increases over 10 fold, however. If the strengthening is achieved by LTP, LTP should be repeatedly induced over several stages of development. Alternatively, LTP-like changes occur only at the initial stages of competition and a quite distinct cellular mechanism may begin to function afterwards.

The strengthening of MNTB inputs might be a result of a compensation for the loss of initial inputs. Such homeostatic regulation of synaptic efficacy has been observed in several excitatory systems. For example, when muscle innervation was reduced in the Drosophila neuromuscular junction, motorneuron synapses were strengthened, whereas an increased innervation decreased synaptic efficacy (Davis and Goodman, 1998). It was suggested that this regulation of total synaptic gain ensures proper function of the muscle preventing tetanus or

paralysis. Homeostatic plasticity has also been demonstrated in central neurons. Pharmacological blockade of spike activity in cultured cortical neurons led to a scaling-up of the strength of excitatory synapses and a scaling down of inhibitory synapses. This synaptic scaling was a neuron-wide phenomenon and maintained a stable firing rate (Turrigiano and Nelson, 2004). During development, homeostatic mechanisms would be critical for maintaining a stable level of postsynaptic activation in response to dynamic formation and elimination of synapses.

Although it appears plausible that homeostatic mechanisms contribute to the strengthening of the MNTB inputs during synapse elimination, the switch from the depolarizing to hyperpolarizing action precludes a simple compensatory mechanism. During the depolarizing phase, both CN and MNTB inputs excite the LSO neurons. An important question is then how the young LSO neurons receiving only excitation maintain a desirable range of firing rate. On e possibility is that unlike highly recurrent cortical networks the LSO circuits may not be so prone to over-excitation and instability. It is also possible that there may be hyperpolarization caused by metabotrophic receptors coupled with K^+ channels. In addition, although depolarizing MNTB inputs can elicit action potentials by themselves (Kullmann and Kandler, 2001), when activated together with CN inputs, MNTB inputs may not always work synergistically causing greater excitation. In the nucleus magnocellularis of the chick, it has been shown that GABAergic inputs that are excitatory when activated alone can actually inhibit postsynaptic firing when activated together with other glutamatergic inputs (Lu and Trussell, 2001).

As MNTB inputs begin to hyperpolarize, LSO neurons would integrate the excitation from the CN and inhibition from the MNTB. In this phase, LSO neurons may need a new level of overall synaptic gain. Therefore, it is possible that the large increase in MNTB-elicited synaptic conductance could be in response to the increased excitation from the CN. The developmental time course of strengthening of CN inputs to the LSO is not known. In the MNTB inhibition continues to be stronger well after the calyceal excitatory inputs have reached their mature strength (Taschenberger and von Gersdorff**,** 2000**;** Awatramani et al., 2004b). This mismatch in the developmental time course of excitation and inhibition suggests that optimal firing rates may gradually become adjusted as the system matures. Comparing the developmental time course of CN and MNTB inputs to the LSO will shed light on this question. Another aspect that should be considered, however, is that in vivo it is unlikely that all the converging inputs are

activated simultaneously. If only a subset of inputs is activated at a time, it could add additional level of complexity to the homeostatic adjustment of total synaptic gain.

6.3 CHOLINERGIC EFFERENTS, SPONTANEOUS ACTIVITY, AND REORGANIZATIONS OF INHIBITORY CONNECTIONS

I found that in both OCB-lesioned rats and α9 KO mice, LSO neurons had higher numbers of converging MNTB inputs with smaller synaptic conductances. These results indicate that normal olivocochlear efferent inputs are necessary for the refinement of the MNTB-LSO pathway. The effect of the efferent manipulations could be due to the altered levels or temporal patterns of spontaneous activity before hearing onset.

The cholinergic efferents could potentially influence activity in a number of ways. They could increase or decrease the overall level of activity through their innervation of IHCs or CN neurons. Instead cholinergic inputs may be more important for temporal patterns such as periodic bursting. Because the efferent neurons are driven by auditory afferent inputs, certain spatial activity pattern that might exist in afferent activity could generate a corresponding efferent feedback back to the periphery. Direct measurements of ongoing spontaneous activity in vivo before hearing onset would allow us to examine some of these possibilities.

A line of evidence suggests that neuronal activity is important for the proper development and/or maintenance of central brainstem pathway. Sanes and colleagues have shown that cochlear ablation disrupts the structural refinement and synaptic transmission in the LSO (Sanes and Friauf, 2000). Cochlear ablation also altered synaptic transmission in the auditory midbrain, the inferior colliculus (IC) (Vale and Sanes, 2002; Vale et al., 2004). In all of these studies, however, the experimental design did not distinguish between the role of early spontaneously generated activity and sound-evoked activity.

A role for spontaneous activity in auditory brainstem development is suggested by a study on inhibitory projections from the dorsal nucleus of the lateral lemniscus (DNLL) to the IC (Gabriele et al., 2000). In the IC, inhibitory projections from the DNLL exhibit diffuse axonal arborization patterns in neonatal animals. At hearing onset, however, the ipsi- and contralateral DNLL axon terminals form alternating stripe-like termination patterns (“aural dominance

bands") through a refinement process. Unilateral cochlear ablation at P2 prevents the formation of aural dominance bands, presumably due to the changes in relative levels of activity between the two DNLLs. Recently it was also shown that in the CN of congenitally deaf mouse, the frequency and amplitude of inhibitory miniature currents were altered around hearing onset, suggesting a role of spontaneous activity in the maturation of synapses before hearing onset (Leao et al., 2004).

Spontaneously generated network activity in the absence of interactions with the outside world is in fact a common phenomenon in the immature nervous systems including the hippocampus, spinal cord, and retina (Feller, 1999) and there is ample evidence that early self-generated activity is crucial in organizing neuronal circuitry. Interestingly, as in the cochlea, in the spinal cord and the retina, cholinergic inputs are an important component of early spontaneous network activity (O'Donovan 1999; Hanson and Landmesser**,** 2003; Feller, 2002). Mice lacking the β2 nAChR subunit, for example, do not exhibit early retinal waves and the eye-specific layer formation in the LGN is disrupted. Moreover, the retinotopic organization was also disrupted in the superior colliculus in β2 KO mice (McLauglin et al., 2003).

Recently, in the spinal cord it has been shown that blockade of spontaneous activity by strychnine has a profound effect on even earlier developmental events such as motor axon guidance and expression of specific guidance molecules (Hanson and Landmesser, 2004).

Since I did not examine the topographic organization in efferent manipulated animals, we currently do not know whether the apparent alteration in the connectivity patterns is accompanied by an impaired topography. However, results from higher auditory circuits provided evidence that sensory experience in young animals can have a profound impact on the organization of auditory sensory maps. In the barn owl, early visual experience shapes the auditory space map in the inferior colliculus. This experience-dependent shift of space map is achieved by the formation of new axonal projections and specific changes in excitatory and inhibitory connections (Knudsen, 2002). In the developing auditory cortex, abnormal early auditory experience can dramatically alter the tonotopic representation in the primary auditory cortex (Zhang et al., 2001; Chang and Merzenich, 2003).

If MNTB-LSO input maps are topographically broader and if spontaneous activity patterns are abnormal in the efferent-manipulated animals, it would suggest that early spontaneous activity, in the absence of any sensory input, is critical for the establishment of a

tonotopic map. Moreover, it would suggest a novel developmental mechanism that central auditory neurons participate (through efferent feedback) in shaping the activity patterns at the sensory periphery, which in turn influences their own organization.

BIBLIOGRAPHY

Aamodt SM, Shi J, Colonnese MT, Veras W, and Constantine-Paton M (2000) Chronic NMDA exposure accelerates development of GABAergic inhibition in the superior colliculus. *J. Neurophysiol.* 83:1580-1591.

Adams JC (1995) Sound stimulation induces Fos-related antigens in cells with common morphological properties throughout the auditory brainstem. *J. Comp. Neurol.* 361:645-68.

Aizenman CD, Manis PB, and Linden DJ (1998) Polarity of long-term synaptic gain change is related to postsynaptic spike firing at a cerebellar inhibitory synapse. *Neuron* 21:827-835.

Akhtar ND and Land PW (1991) Activity-dependent regulation of glutamic acid decarboxylase in the rat barrel cortex: effects of neonatal versus adult sensory deprivation. *J. Comp. Neurol.* 307:200-13.

Ali DW, Drapeau P, and Legendre P (2000) Development of spontaneous glycinergic currents in the Mauthner neuron of the zebrafish embryo. *J. Neurophysiol.* 84:1726-36.

Allen CB, Celikel T, and Feldman DE. (2003) Long-term depression induced by sensory deprivation during cortical map plasticity in vivo. *Nat. Neurosci.* 6:291-9.

Antonini A and Stryker MP (1993) Rapid remodeling of axonal arbors in the visual cortex. *Science* 260:1819-1821.

Awatramani GB, Turecek R, and Trussell LO (2004a) Inhibitory control at a synaptic relay. *J. Neurosci.* 24:2643-7.

Awatramani GB, Turecek R, and Trussell LO (2004b) Staggered development of GABAergic and glycinergic transmission in the MNTB. *J. Neurophysiol.* Sep 29 [Epub ahead of print]

Balice-Gordon RJ and Lichtman JW (1994) Long-term synapse loss induced by focal blockade of postsynaptic receptors. *Nature* 372:519-524.

Bekkers JM and Stevens CF (1990) Presynaptic mechanism for long-term potentiation in the hippocampus. *Nature* 346:724-729.

Ben-Ari Y (2001) Developing networks play a similar melody. *TINS* 24:353–360.

Ben-Ari Y, Khazipov R, Leinekugel X, Caillard O, and Gaiarsa JL (1997) $GABA_A$, NMDA and AMPA receptors: a developmentally regulated 'menage a trois'. *TINS* 20:523-9.

Beutner D and Moser T (2001) The presynaptic function of mouse cochlear inner hair cells during development of hearing. *J. Neurosci.* 21:4593–4599.

Bi G and Poo M. (2001) Synaptic modification by correlated activity: Hebb's postulate revisited. *Annu. Rev. Neurosci.* 24:139-66.

Blatchley BJ, Cooper WA, and Coleman JR (1987) Development of auditory brainstem response to tone pip stimuli in the rat. *Brain Res.* 429:75-84.

Bormann J, Hamill OP, and Sakmann B (1987) Mechanism of anion permeation through channels gated by glycine and -aminobutyric acid in mouse cultured spinal neurones. *J. Physiol-London.* 385:243-286.

Born DE and Rubel EW (1988) Afferent influences on brain stem auditory nuclei of the chicken: presynaptic action potentials regulate protein synthesis in nucleus magnocellularis neurons. *J. Neurosci.* 8:901–919.

Boudreau JC and Tsuchitani C (1968) Binaural interaction in the cat superior olive S segment. *J. Neurophysiol.* 31:442-454.

Brand A, Behrend O, Marquardt T, McAlpine D, and Grothe B (2002) Precise inhibition is essential for microsecond interaural time difference coding. *Nature* 417:543-547.

Brenowitz S and Trussell LO (2001) Maturation of synaptic transmission at end-bulb synapses of the cochlear nucleus. *J. Neurosci.* 21: 9487-9498.

Bruce LL, Christensen MA, and Warr WB. (2000) Postnatal development of efferent synapses in the rat cochlea. *J. Comp. Neurol.* 423:532–548.

Buffelli M, Burgess RW, Feng G, Lobe CG, Lichtman JW, and Sanes JR (2003) Genetic evidence that relative synaptic efficacy biases the outcome of synaptic competition. *Nature* 424:430-434.

Caillard O, Ben-Ari Y, and Gaiarsa JL (1999) Mechanisms of induction and expression of long-term depression at GABAergic synapses in the neonatal rat hippocampus. *J. Neurosci.* 19:7568-77.

Callaway EM and Katz LC (1993) Photostimulation using caged glutamate reveals functional circuitry in living brain slices. *PNAS.* 90:7661-7665.

Celikel T, Szostak VA, and Feldman DE. (2004) Modulation of spike timing by sensory deprivation during induction of cortical map plasticity. *Nat. Neurosci.* 7:534-41.

Chang EF and Merzenich MM (2003) Environmental noise retards auditory cortical development. *Science* 300:498-502.

Chang EH, Kotak VC, and Sanes DH (2003) Long-term depression of synaptic inhibition is expressed postsynaptically in the developing auditory system. *J. Neurophysiol.* 90:1479-1488.

Chen C and Regehr WG (2000) Developmental remodeling of the retinogeniculate synapse. *Neuron* 28:955-966.

Chen C, Blitz DM, and Regehr WG (2002) Contributions of receptor desensitization and saturation to plasticity at the retinogeniculate synapse. *Neuron* 33:779-88.

Cherubini E, Gaiarsa JL, and Ben Ari Y (1991) GABA: an excitatory transmitter in early postnatal life. TINS 14:515-519.

Christopher Kirk E and Smith DW (2003) Protection from acoustic trauma is not a primary function of the medial olivocochlear efferent system. *J. Assoc. Res. Otolaryngol.* 4:445-465.

Clements JD and Bekkers JM (1997) Detection of spontaneous synaptic events with an optimally scaled template. *Biophys. J.* 73:220-9.

Cole KS and Robertson D (1992) Early efferent innervation of the developing rat cochlea studied with a carbocyanine dye. *Brain Res.* 575:223–230.

Colman H, Nabekura J, and Lichtman JW (1997) Alterations in synaptic strength preceding axon withdrawal. *Science* 275:356-361.

Constantine-Paton M and Cline HT (1998) LTP and activity-dependent synaptogenesis: the more alike they are, the more different they become. *Curr. Opin. Neurobiol.* 8:139-48.

Davies CH, Davies SN, and Collingridge GL (1990) Paired-pulse depression of monosynaptic GABA-mediated inhibitory postsynaptic responses in rat hippocampus. *J. Physiol.* 424: 513-531.

Davis GW and Goodman CS (1998) Synapse-specific control of synaptic efficacy at the terminals of a single neuron. *Nature* 392:82-86.

Debanne D, Guerineau NC, Gahwiler BH, and Thompson SM (1996) Paired-pulse facilitation and depression at unitary synapses in rat hippocampus: quantal fluctuation affects subsequent release. *J Physiol.* 491:163-76.

Ehrlich I, Lohrke S, and Friauf E (1999) Shift from depolarizing to hyperpolarizing glycine action in rat auditory neurones is due to age-dependent Cl- regulation. *J. Physiol* 520:121-137.

Elgoyhen AB, Johnson DS, Boulter J, Vetter DE, and Heinemann S. (1994) Alpha 9: an acetylcholine receptor with novel pharmacological properties expressed in rat cochlear hair cells. *Cell* 79:705-15.

Elgoyhen AB, Vetter DE, Katz E, Rothlin CV, Heinemann, SF, and Boulter J (2001) α10: A determinant of nicotinic cholinergic receptor function in mammalian vestibular and cochlear mechanosensory hair cells. *PNAS* 98:3501–3506.

Engert F and Bonhoeffer T (1999) Dendritic spine changes associated with hippocampal long-term synaptic plasticity. *Nature* 399:66-70.

Feldman DE, Nicoll RA, and Malenka RC (1999) Synaptic plasticity at thalamocortical synapses in developing rat somatosensory cortex: LTP, LTD, and silent synapses. *J Neurobiol.* 41:92-101.

Feldman DE, Nicoll RA, and Malenka RC (1999) Synaptic plasticity at thalamocortical synapses in developing rat somatosensory cortex: LTP, LTD, and silent synapses. *J. Neurobiol.* 41:92-101.

Feller MB (1999) Spontaneous correlated activity in developing neural circuits. *Neuron* 22:653-6.

Feller MB (2002) The role of nAChR-mediated spontaneous retinal activity in visual system development. *J. Neurobiol.* 53:556-67.

Friauf E (1992) Tonotopic order in the adult and developing auditory system of the rat as shown by c-fos immunocytochemistry. *Eur. J. Neurosci.* 4:798-812.

Gabriele ML, Brunso-Bechtold JK, and Henkel CK (2000) Plasticity in the development of afferent patterns in the inferior colliculus of the rat after unilateral cochlear ablation. *J. Neurosci.* 20:6939–6949.

Gaiarsa JL, Caillard O, and Ben-Ari Y (2002) Long-term plasticity at GABAergic and glycinergic synapses: mechanisms and functional significance. *TINS* 25:564-70.

Gil Z, Connors BW, and Amitai Y (1999) Efficacy of thalamocortical and intracortical synaptic connections: quanta, innervation, and reliability. *Neuron* 23:385-397.

Gillespie DG and Kandler K (2003) Glutamate release in the glycinergic/GABAergic MNTB-LSO pathway during early postnatal development. *Soc. Neurosci. Abs.*148.10.

Glowatzki E and Fuchs PA (2000) Cholinergic synaptic inhibition of inner hair cells in the neonatal mammalian cochlea. *Science* 288:2366–2368.

Goda Y and Stevens CF (1994) Two components of transmitter release at a central synapse. *PNAS* 91: 12942-12946.

Goodman CS and Shatz CJ (1993) Developmental mechanisms that generate precise patterns of neuronal connectivity. *Cell* 72 Suppl, 77-98.

Grantyn R, Kraszewski K, Melnick I, Taschenberger H, and Warton SS (1995) In vitro development of vertebrate central synapses. *Perspect. Dev. Neurobiol.* 2:387-397.

Gubellini P, Ben Ari Y, and Gaiarsa JL (2001) Activity- and age-dependent GABAergic synaptic plasticity in the developing rat hippocampus. *Eur. J. Neurosci.* 14:1937-1946.

Gummer AW and Mark RF (1994) Patterned neural activity in brain stem auditory areas of a prehearing mammal, the tammar wallaby (Macropus eugenii). *NeuroReport* 5:685–688.

Hanson MG and Landmesser LT (2003) Characterization of the circuits that generate spontaneous episodes of activity in the early embryonic mouse spinal cord. *J. Neurosci.* 23:587-600.

Hanson MG and Landmesser LT (2004) Normal patterns of spontaneous activity are required for correct motor axon guidance and the expression of specific guidance molecules. *Neuron* 43:687-701.

Helfert RH and Schwartz IR (1986) Morphological evidence for the existence of multiple neuronal classes in the cat lateral superior olivary nucleus. *J. Comp Neurol.* 244:533-549.

Hendry SH and Jones EG (1986) Reduction in number of immunostained GABAergic neurones in deprived-eye dominance columns of monkey area 17. *Nature* 320:750-753.

Hendry SH and Jones EG (1988) Activity-dependent regulation of GABA expression in the visual cortex of adult monkeys. *Neuron* 8:701-712.

Hensch TK, Fagiolini M, Mataga N, Stryker MP, Baekkeskov S, and Kash SF (1998) Local GABA circuit control of experience-dependent plasticity in developing visual cortex. *Science* 282: 1504-1508.

Hsieh CY, Cruikshank SJ, and Metherate R. (2000) Differential modulation of auditory thalamocortical and intracortical synaptic transmission by cholinergic agonist. *Brain Res.* 880:51-64.

Huang ZJ, Kirkwood A, Pizzorusso T, Porciatti V, Morales B, Bear MF, Maffei L, and Tonegawa S. (1999) BDNF regulates the maturation of inhibition and the critical period of plasticity in mouse visual cortex. *Cell* 98:739-755.

Hubel DH, Wiesel TN, and LeVay S (1977) Plasticity of ocular dominance columns in monkey striate cortex. *Philos. Trans. R. Soc. Lond B Biol. Sci.* 278:377-409.

Jackson H and Parks TN (1982) Functional synapse elimination in the developing avian cochlear nucleus with simultaneous reduction in cochlear nerve axon branching. *J. Neurosci.* 2:1736-1743.

Ji W, Gao E, and Suga N. (2001) Effects of acetylcholine and atropine on plasticity of central

auditory neurons caused by conditioning in bats. *J. Neurophysiol.* 86:211-25.

Jones MV and Westbrook GL (1995) Desensitized states prolong GABAA channel responses to brief agonist pulses. *Neuron* 15:181-91.

Jones TA, Jones SM, and Paggett KC (2001) Primordial rhythmic bursting in embryonic cochlear ganglion cells. *J. Neurosci.* 21:8129–8135.

Kakazu Y, Akaike N, Komiyama S, and Nabekura J (1999*)* Regulation of intracellular chloride by cotransporters in developing lateral superior olive neurons. *J. Neurosci.* 19:2843-2851.

Kandler K and Friauf E (1995a) Development of electrical membrane properties and discharge characteristics of superior olivary complex neurons in fetal and postnatal rats. *Eur. J. Neurosci.* 7:1773-1790.

Kandler K and Friauf E (1995b) Development of glycinergic and glutamatergic synaptic transmission in the auditory brainstem of perinatal rats. *J. Neurosci.* 15:6890-6904.

Kandler K, Givens RS, and Katz LC (1998) Imaging Neurons. *Cold spring harbor laboratory press* (eds. Yuste R, Lanni F and Konnerth A*)* pp. 271-279.

Kandler K, Kullmann PH, Ene FA, and Kim G (2002) Excitatory action of an immature glycinergic/GABAergic sound localization pathway. *Physiol. Behav.* 77:583-7.

Kano M (1995) Plasticity of inhibitory synapses in the brain: a possible memory mechanism that has been overlooked. *Neurosci. Res.* 21:177-182.

Kapfer C, Seidl AH, Schweizer H, and Grothe B (2002) Experience-dependent refinement of inhibitory inputs to auditory coincidence-detector neurons. *Nat. Neurosci.* 5:247-253.

Kasthuri N and Lichtman JW (2003) The role of neuronal identity in synaptic competition. *Nature* 424:426-430.

Katz LC and Shatz CJ (1996) Synaptic activity and the construction of cortical circuits. *Science* 274:1133–1138.

Kaufman L and Rousseeuw PJ (1990) Finding groups in data: An introduction to cluster analysis. *Wiley, New York.*

Kilman V, van Rossum MC, and Turrigiano GG (2002) Activity deprivation reduces miniature IPSC amplitude by decreasing the number of postsynaptic GABA(A) receptors clustered at neocortical synapses. *J. Neurosci.* 22:1328-1337.

Kim G and Kandler K (2003) Elimination and strengthening of glycinergic/GABAergic connections during tonotopic map formation. *Nat. Neurosci.* 6:282-90.

Kim J and Alger BE (2001) Random response fluctuations lead to spurious paired-pulse facilitation. *J. Neurosci.* 21:9608-9618.

Kirsch J and Betz H (1998) Glycine-receptor activation is required for receptor clustering in spinal neurons. *Nature* 392:717-720.

Kittler JT and Moss SJ (2003) Modulation of GABAA receptor activity by phosphorylation and receptor trafficking: implication for the efficacy of synaptic inhibition. *Curr. Opin. Neurobiol.*13:341-347.

Kitzes LM, Kageyama GH, Semple MN, and Kil J (1995) Development of ectopic projections from the ventral cochlear nucleus to the superior olivary complex induced by neonatal ablation of the contralateral cochlea. *J. Comp. Neurol.* 353:341-63.

Knott GW, Quairiaux C, Genoud C, and Welker E (2002) Formation of dendritic spines with GABAergic synapses induced by whisker stimulation in adult mice. *Neuron* 34:265-273.

Knudsen EI (2002) Instructed learning in the auditory localization pathway of the barn owl. *Nature* 417:322-328.

Korn H, Oda Y, and Faber DS (1992) Long-term potentiation of inhibitory circuits and synapses in the central nervous system. *PNAS* 89:440-443.

Kotak VC and Sanes DH (1996) Developmental influence of glycinergic transmission: regulation of NMDA receptor-mediated EPSPs. *J. Neurosci.* 16:1836-1843.

Kotak VC and Sanes DH (2000) Long-lasting inhibitory synaptic depression is age- and calcium-dependent. *J. Neurosci.* 20:5820-5826.

Kotak VC and Sanes, D. H. (1995) Synaptically evoked prolonged depolarizations in the developing auditory system. *J. Neurophysiol.* 74:1611–1620.

Kotak VC, DiMattina C, and Sanes DH (2001) GABA(B) and Trk receptor signaling mediates long-lasting inhibitory synaptic depression. *J. Neurophysiol.* 86:536-540.

Kotak VC, Korada S, Schwartz IR, and Sanes DH (1998) A developmental shift from GABAergic to glycinergic transmission in the central auditory system. *J. Neurosci.* 18:4646-4655.

Kraushaar U and Jonas P (2000) Efficacy and stability of quantal GABA release at a hippocampal interneuron-principal neuron synapse. *J. Neurosci.* 20:5594-607.

Kros CJ, Ruppersberg JP, and Rusch A (1998) Expression of potassium current in inner hair cells during development of hearing in mice. *Nature* 394:281–284.

Kullmann PH and Kandler K (2001) Glycinergic/GABAergic synapses in the lateral superior

olive are excitatory in neonatal C57Bl/6J mice. *Brain Res. Dev. Brain Res.* 131:143-7.

Kullmann PH, Ene FA. and Kandler K (2002) Glycinergic and GABAergic calcium responses in the developing lateral superior olive. *Eur. J. Neurosci.* 15:1093-1104.

Land PW, de Blas AL, and Reddy N (1995) Immunocytochemical localization of GABAA receptors in rat somatosensory cortex and effects of tactile deprivation. *Somatosens. Mot. Res.* 12:127-41.

Leao RN, Oleskevich S, Sun H, Bautista M, Fyffe RE, and Walmsley B (2004) Differences in glycinergic mIPSCs in the auditory brain stem of normal and congenitally deaf neonatal mice. *J. Neurophysiol.* 91:1006-1012.

Lichtman JW and Colman H (2000) Synapse elimination and indelible memory. *Neuron* 25:269-278.

Lohmann C, Ilic V and Friauf E (1998) Development of a topographically organized auditory network in slice culture is calcium dependent. *J. Neurobiol.* 34:97-112.

Lu T and Trussell LO (2000) Inhibitory transmission mediated by asynchronous transmitter release. *Neuron* 26:683-94.

Lu T and Trussell LO (2001) Mixed excitatory and inhibitory GABA-mediated transmission in chick cochlear nucleus. *J. Physiol.* 535:125-31.

Luebke AE and Foster PK (2002) Variation in inter-animals susceptibility to noise damage is associated with α9 acetylcholine receptor subunit expression level. *J. Neurosci.* 22:4241-4247.

Maccaferri G and Lacaille JC (2003) Interneuron diversity series: hippocampal interneuron classifications – making things as simple as possible, not simpler. *TINS* 26:564-571.

Maison SF, Luebke AE, Liberman MC, and Zuo J (2002) Efferent protection from acoustic injury is mediated via α9 nicotinic acetylcholine receptors on outer hair cells. *J. Neurosci.* 22:10838-10846.

Malinow R and Tsien RW (1990) Presynaptic enhancement shown by whole-cell recordings of long-term potentiation in hippocampal slices. *Nature* 346:177-80.

Marty S, Wehrle R, and Sotelo C (2000) Neuronal activity and brain-derived neurotrophic factor regulate the density of inhibitory synapses in organotypic slice cultures of postnatal hippocampus. *J. Neurosci.* 20:8087-8095.

May BJ, Prosen CA, Weiss D, Vetter D. (2002) Behavioral investigation of some possible effects of the central olivocochlear pathways in transgenic mice. *Hear. Res.* 171:142-157.

McBain CJ and Fisahn A (2001) Interneurons unbound. *Nat. Neurosci.* 2:11-23.

McLaughlin T, Torborg CL, Feller MB, and O'Leary DD (2003) Retinotopic map refinement requires spontaneous retinal waves during a brief critical period of development. *Neuron* 40:1147-60.

McLean HA, Caillard O, Ben-Ari Y, and Gaiarsa JL. (1996) Bidirectional plasticity expressed by GABAergic synapses in the neonatal rat hippocampus. *J. Physiol.* 496:471-7.

Meister M, Wong ROL, Baylor DA, and Shatz CJ (1991) Synchronous bursts of action potentials in ganglion cells of the developing mammalian retina. *Science* 252:939–943.

Micheva KD and Beaulieu C (1996) Quantitative aspects of synaptogenesis in the rat barrel field cortex with special reference to GABA circuitry. *J. Comp. Neurol.* 373:340-354.

Morales B, Choi SY, and Kirkwood A (2002) Dark rearing alters the development of GABAergic transmission in visual cortex. *J. Neurosci.* 22:8084-8090.

Mulders WH, Paolini AG, Needham K, and Robertson D. (2003) Olivocochlear collaterals evoke excitatory effects in onset neurones of the rat cochlear nucleus. *Hear. Res.* 176:113-21.

Muller M (1990) Quantitative comparison of frequency representation in the auditory brainstem nuclei of the gerbil, Pachyuromys duprasi. *Exp. Brain Res.* 81:140-9.

Nabekura J, Katsurabayashi S, Kakazu Y, Shibata S, Matsubara A, Jinno S, Mizoguchi Y, Sasaki A, and Ishibashi H (2004) Developmental switch from GABA to glycine release in single central synaptic terminals. *Nat. Neurosci.* 7:17-23.

Needham K and Paolini AG (2003) Fast inhibition underlies the transmission of auditory information between cochlear nuclei. *J. Neurosci.* 23:6357-6361.

O'Donovan MJ (1999) The origin of spontaneous activity in developing networks of the vertebrate nervous system. *Curr. Opin. Neurobiol.* 9:94–104.

Otis TS, De Koninck Y, and Mody I (1994) Lasting potentiation of inhibition is associated with an increased number of gamma-aminobutyric acid type A receptors activated during miniature inhibitory postsynaptic currents. *PNAS* 91:7698-7702.

Pedroarena CM and Schwarz C (2003) Efficacy and short-term plasticity at GABAergic synapses between Purkinje and cerebellar nuclei neurons. *J. Neurophysiol.* 89:704-15.

Pouzat C and Hestrin S (1997) Developmental regulation of basket/stellate cell-->Purkinje cell synapses in the cerebellum. *J. Neurosci.* 17:9104-9112.

Pratt KG, Watt AJ, Griffith LC, Nelson SB, and Turrigiano GG (2003) Activity-dependent remodeling of presynaptic inputs by postsynaptic expression of activated CaMKII. *Neuron* 39:269-81.

Purves D and Lichtman JW (1980) Elimination of synapses in the developing nervous system. *Science* 210:153-7.

Purves D and Lichtman JW (1985) Principles of neural development. *Sinauer Associates Inc.*, Sunderland

Rico B, Xu B, and Reichardt LF (2002) TrkB receptor signaling is required for establishment of GABAergic synapses in the cerebellum. *Nat. Neurosci.* 5:225-233.

Rietzel HJ and Friauf E (1998) Neuron types in the rat lateral superior olive and developmental changes in the complexity of their dendritic arbors. *J. Comp Neurol.* 390:20-40.

Rozas C, Frank H, Heynen AJ, Morales B, Bear MF, and Kirkwood A (2001) Developmental inhibitory gate controls the relay of activity to the superficial layers of the visual cortex. *J. Neurosci.* 21:6791-6801.

Russell FA and Moore DR (2003) Afferent reorganisation within the superior olivary complex of the gerbil: development and induction by neonatal, unilateral cochlear removal. *J. Comp. Neurol.* 352:607-25.

Ruthazer ES and Cline HT (2004) Insights into activity-dependent map formation from the retinotectal system: a middle-of-the-brain perspective. *J. Neurobiol.* 59:134-46.

Ruthazer ES, Akerman CJ, and Cline HT (2003) Control of axon branch dynamics by correlated activity in vivo. *Science* 301:66-70.

Rutherford LC, DeWan A, Lauer HM, and Turrigiano GG (1997) Brain-derived neurotrophic factor mediates the activity-dependent regulation of inhibition in neocortical cultures. *J. Neurosci.* 17:4527-4535.

Sanes DH and Chokshi P (1992) Glycinergic transmission influences the development of dendrite shape. *NeuroReport* 3:323-326.

Sanes DH and Friauf E (2000) Development and influence of inhibition in the lateral superior olivary nucleus. *Hear Res.* 147:46-58.

Sanes DH and Hafidi A (1996) Glycinergic transmission regulates dendrite size in organotypic culture. *J. Neurobiol.* 31:503-511.

Sanes DH and Rubel EW (1988) The ontogeny of inhibition and excitation in the gerbil lateral superior olive. *J. Neurosci.* 8:682–700.

Sanes DH and Siverls V (1991) Development and specificity of inhibitory terminal arborizations in the central nervous system. *J. Neurobiol.* 22:837-854.

Sanes DH and Takacs C (1993) Activity-dependent refinement of inhibitory connections. *Eur. J. Neurosci.* 5:570–574.

Sanes DH, Markiwitz S, Bernstein J, and Wardlow J (1992) The influence of inhibitory afferents on the development of postsynaptic dendritic arbors. *J. Comp. Neurol.* 321:637-644.

Sanes DH, Markowitz S, Bernstein J, and Wardlow J (1992) The influence of inhibitory afferens on the development of postsynaptic dendritic arbors. *J. Comp. Neurol.* 321:637–644.

Shatz CJ (1996) Emergence of order in visual system development. *PNAS* 93:602-8.

Simmons DD, Mansdorf NB, and Kim JH (1996) Olivocochlear innervation of inner and outer hair cells during postnatal maturation: evidence for a waiting period. *J. Comp. Neurol.* 370:551–562.

Smith AJ, Owens S, and Forsythe ID (2000) Characterisation of inhibitory and excitatory postsynaptic currents of the rat medial superior olive. *J. Physiol.* 529:681-98.

Stellwagen D, Shatz CJ, and Feller MB (1999) Dynamics of retinal waves are controlled by cyclic AMP. *Neuron* 24:673-85.

Stellwagen D and Shatz CJ (2002) An instructive role for retinal waves in the development of retinogeniculate connectivity. *Neuron* 33:357-367.

Stevens CF and Wang Y (1994) Changes in reliability of synaptic function as a mechanism for plasticity. *Nature* 371:704-707.

Stuart G, Spruston N, and Hausser M (2001) Dendrites. *Oxford University Press (New York).*

Takahashi T, Momiyama A, Hirai K, Hishinuma F, and Akagi H (1992) Functional correlation of fetal and adult forms of glycine receptors with developmental changes in inhibitory synaptic receptor channels. *Neuron* 9:1155-1161.

Taschenberger H and von Gersdorff H (2000) Fine-tuning an auditory synapse for speed and fidelity: developmental changes in presynaptic waveform, EPSC kinetics, and synaptic plasticity. *J. Neurosci.* 20:9162-9173.

Turrigiano GG and Nelson SB (2004) Homeostatic plasticity in the developing nervous system. *Nat. Rev. Neurosci.* 597-107.

Turrigiano GG, Leslie KR, Desai NS, Rutherford LC, and Nelson SB (1998) Activity-dependent scaling of quantal amplitude in neocortical neurons. *Nature* 391:892-896.

Vale C and Sanes DH (2002) The effect of bilateral deafness on excitatory and inhibitory synaptic strength in the inferior colliculus. *Eur. J. Neurosci.* 16:2394-404.

Vale C, Juiz JM, Moore DR, and Sanes DH (2004) Unilateral cochlear ablation produces greater loss of inhibition in the contralateral inferior colliculus. *Eur. J. Neurosci.* 20:2133-40.

Vetter DE, Liberman MC, Mann J, Barhanin J, Boulter J, Brown MC, Saffiote-Kolman J, Heinemann SF, and Elgoyhen AB (1999) Role of α9 nicotinic acetylcholine receptor subunits in the development and function of cochlear efferent innervation. *Neuron* 23:93–103.

von Gersdorff H and Borst JG (2002) Short-term plasticity at the calyx of held. *Nat. Rev. Neurosci.* 3:53-64.

Waldeck RF, Pereda A, and Faber DS (2000) Properties and plasticity of paired-pulse depression at a central synapse. *J. Neurosci.* 20:5312-20.

Walsh EJ and McGee J (1997) Does activity in the olivocochlear bundle affect development of the auditory periphery? Diversity in auditory mechanics (Lewis ER, Long GR, Lyon RF, Narins PM, Steele CR, and Hecht-Poinar E eds) *Singapore: World Scientific*, pp. 376–385.

Walsh EJ, McGee J, McFadden SL, and Liberman MC (1998) Long-term effects of sectioning the olivocochlear bundle in neonatal cats. *J. Neurosci.* 18:3859–3869

Warr WB (1992) Organization of olivocochlear efferent systems in mammals. The mammalian auditory pathway: neuroanatomy (Webster DB, Popper AN, and Fay RR eds.) New York: Springer, pp. 410–448.

Warr WB, Guinan JJ, and White JS (1986) Organization of the efferent fibers: the lateral and medial olivocochlear systems. Neurobiology of hearing: The cochlea (Altschuler RA, Bobbin RP, and Hoffman DW eds). New York: Raven press, pp. 333–348.

Weliky M (2000) Correlated neuronal activity and visual cortical development. *Neuron* 27:427–430.

White JS and Warr WB (1983) The dual origins of the olivocochlear bundle in the albino rat. *J. Comp. Neurol.* 219:203–214.

Wong RO, Meister M, and Shatz CJ (1993) Transient period of correlated bursting activity during development of the mammalian retina. *Neuron* 11:923-38.

Woodin MA, Ganguly K,, and Poo MM (2003) Coincident pre- and postsynaptic activity modifies GABAergic synapses by postsynaptic changes in Cl- transporter activity. *Neuron* 39:807-820.

Xu-Friedman MA and Regehr WG (1999) Presynaptic strontium dynamics and synaptic transmission. *Biophys. J.* 76:2029-42.

Zhang LI, Bao S, and Merzenich MM (2001) Persistent and specific influences of early acoustic environments on primary auditory cortex. *Nat. Neurosci.* 4:1123-30.